CRYSTAL STRUCTURES OF SOME TRANSITION METAL COMPLEXES CONTAINING NOVEL SULPHUR AND PHOSPHORUS LIGANDS

Upali Siriwardane

A Thesis
in
The Department
of
Chemistry

Presented in Partial Fulfilment of the Requirements
for the degree of Master of Science at
Concordia University
Sir George Williams Campus
Montreal, Quebec, Canada

April 1981

ABSTRACT

CRYSTAL STRUCTURES OF SOME TRANSITION METAL COMPLEXES CONTAINING NOVEL SULPHUR AND PHOSPHORUS LIGANDS

UPALI SIRIWARDANE

CONCORDIA UNIVERSITY

SIR GEORGE WILLIAMS CAMPUS, 1981

This thesis describes the results of X-ray crystallographic structure determinations on four transition metal organometallic complexes.

The first is a platinum complex, $(\mu_2\text{-}C_6H_5CH_2S)_2Pt_2(C_6H_5CH_2S)_2[CH_3(C_6H_5)_2P]_2$. It has two platinum atoms joined by two bridging benzylthiolate ligands. The remaining benzylthiolate and diphenylmethylphosphine ligands, one each on the two platinum atoms, are in a cis configuration. Each platinum atom is surrounded in an approximately square planar fashion. The mercaptide bridge is a folded ring with the two benzyl groups in an anti orientation.

The second is an iron complex, $[Fe_2(CO)_6]_2(SC_6H_4CS_2)$. It has two $Fe_2(CO)_6$ units joined by a novel o-mercaptobenzenedithiocarboxylate ligand acting as a tetradentate system, possessing a unique iron-carbon bond.

The third is a titanium complex, $Ti[\eta^5C_5(CH_3)_5]_2S_3$. It has two π bonded pentamethylcyclopentadienyl ligands and a novel four membered metallacycle containing three sulphur atoms. The ligands are arranged in a distorted tetrahedron around the titanium.

The last, a ruthenium complex, $(\mu_2\text{-}H_4)Ru_4(CO)_9\{[(C_6H_5)_2P]_3CH\}$, is a tetrahedral tetranuclear cluster. The tripod (trisdiphenylphosphenomethane) ligand is bonded to three ruthenium atoms in one face of the tetrahedron. Certain longer Ru-Ru bond lengths and the displacement of certain carbonyl groups suggested the position of hydrogen atoms bridging along the four edges of the tetrahedron. These were subsequently located and refined.

This Thesis is

Dedicated

to

my Parents

ACKNOWLEDGEMENTS

I wish to express my deep appreciation to Dr. P.H. Bird for his guidance and encouragement during the execution of this research work.

Thanks are also due to Prof. J.G. Dick and Dr. R.A. Westbury who served on my research committee.

The financial support in the form of a teaching assistanship from the Department of Chemistry, Concordia University is highly appreciated. I am also grateful to the Graduate Student's Association of Concordia University for partial financial support towards the differential fees.

I am specially appreciative to the fellow graduate students in the Department of Chemistry for their encouragement and help.

Finally, I would like to thank my wife, Nilanthi, for her patience and understanding.

TABLE OF CONTENTS

LIST OF TABLES

LIST OF FIGURES

SEGTION I. GENERAL INTRODUCTION

The objective of this thesis is to present the results of single crystal X-ray crystallographic structure determinations on four transition metal complexes. The four complexes are:

A) $(\mu_2\text{-}C_6H_5CH_2S)_2Pt_2(C_6H_5CH_2S)_2[CH_3(C_6H_5)_2P]_2$, named UNIQUE.

B) $[Fe_2(CO)_6]_2(SC_6H_4CS_2)$, named FESCO.

C) $Ti[\eta^5C_5(CH_3)_5]S_3$, named TICEP.

D) $(\mu_2\text{-}H_4)Ru_4(CO)_9\{[(C_6H_5)_2P]_2CH\}$, named RUSH.

The first three compounds were prepared by Dr. A. Shaver et al. at the McGill University, Montreal, Canada and the last compound at Université Louis Pasteur de Strasbourg, France, by Dr. J.A. Osborn et al.

The theoretical and instrumental aspects of single crystal X-ray crystallographic determination are discussed in the section II of the thesis. The experimental work carried out for all four structures described in this thesis is presented in section III. A common feature of the first three compounds is that they all contain sulphur ligands, a theme of Dr. Shaver's research. However, all four compounds are structurally different, thus the results and discussion are segregated as four separate parts in section IV of the thesis. Each part of the section IV consists

of an introduction to the problem being studied followed by a description of the results and the discussion.

SECTION II. CRYSTALLOGRAPHIC

1) DIFFRACTION OF X-RAYS BY CRYSTALS [1-3].

A crystal is built from regularly repeating unit structures, which are stacked side by side to form a three-dimensional lattice.

A unit cell can be defined in the lattice using three edges named a, b and c. The angles between them are α, β and γ, with α between b and c, β between a and c, and γ between a and b.

The X-rays diffracted from the 'planes' through the three-dimensional lattice obey the Bragg law given by equation:

$$2d_{hkl} \sin \theta = n \lambda \qquad \text{II-1-1}$$

Here, λ is the wavelength of the X-ray radiation and d_{hkl} is the spacing between the planes which are defined by the Miller indices (hkl). θ is the angle between the incident beam and the diffracting plane. Rearranging the equation II-1-1 gives:

$$\sin \theta = \frac{n\lambda}{2} \frac{1}{d_{hkl}} \qquad \text{II-1-2}$$

It is seen that sin θ is inversely proportional to the spacing of the planes. The interpretation of diffraction patterns will be easier if the sin θ-d relationship could be replaced by a direct one. This can be achieved by constructing a reciprocal lattice based on $1/d_{hkl}$ which varies directly with sin θ.

Figure II-1-1 illustrates the construction of a reciprocal cell belonging to a triclinic crystal system. The normals to the planes (100), (010) and (001) drawn from the origin of the unit cell of lengths 1/a, 1/b and 1/c will be the reciprocal axes a^*, b^* and c^*, respectively. By construction a^* must be perpendicular to the bc plane; similarly the b^*c^* plane of the reciprocal lattice must be perpendicular to a direct axis.

A graphical representation of the Bragg law can be visualized if a circle is drawn whose diameter is equal to $2/\lambda$. If a right triangle having $1/d_{hkl}$ as one of its legs is inscribed in this circle, the directions of incident and diffracted beams will be as shown in Figure II-1-2. The angle between these two beams is 2θ as given by the Bragg law.

If a crystal is mounted with the direct axis b perpendicular to a X-ray beam the a^*c^* plane of the crystal will be parallel to the X-ray beam. Applying the Bragg law to this situation, a graphical representation illustrated in Figure II-1-3 is obtained. Whenever a reciprocal lattice point coincides with the

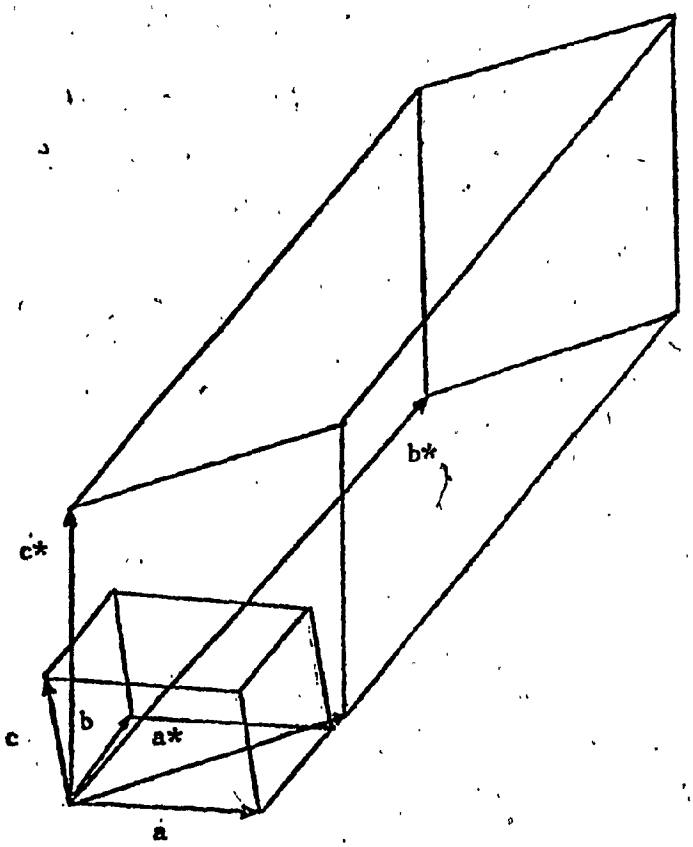

Figure II-1-1. An illustration of relationship between direct and reciprocal unit cell belonging to the triclinic crystal system.

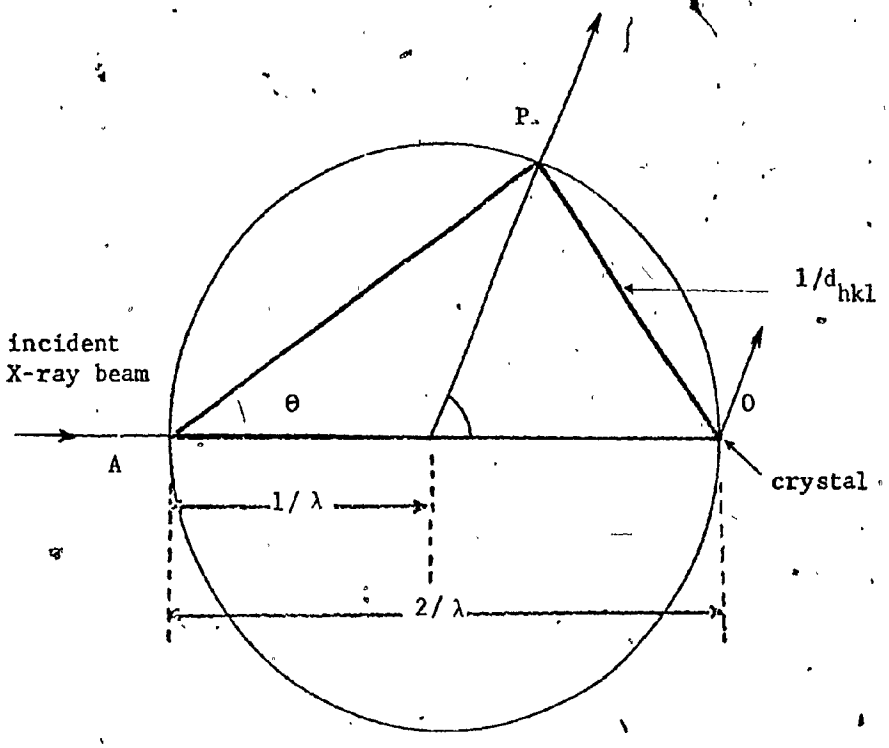

Figure II-1-2. A graphical representation of the Bragg law.

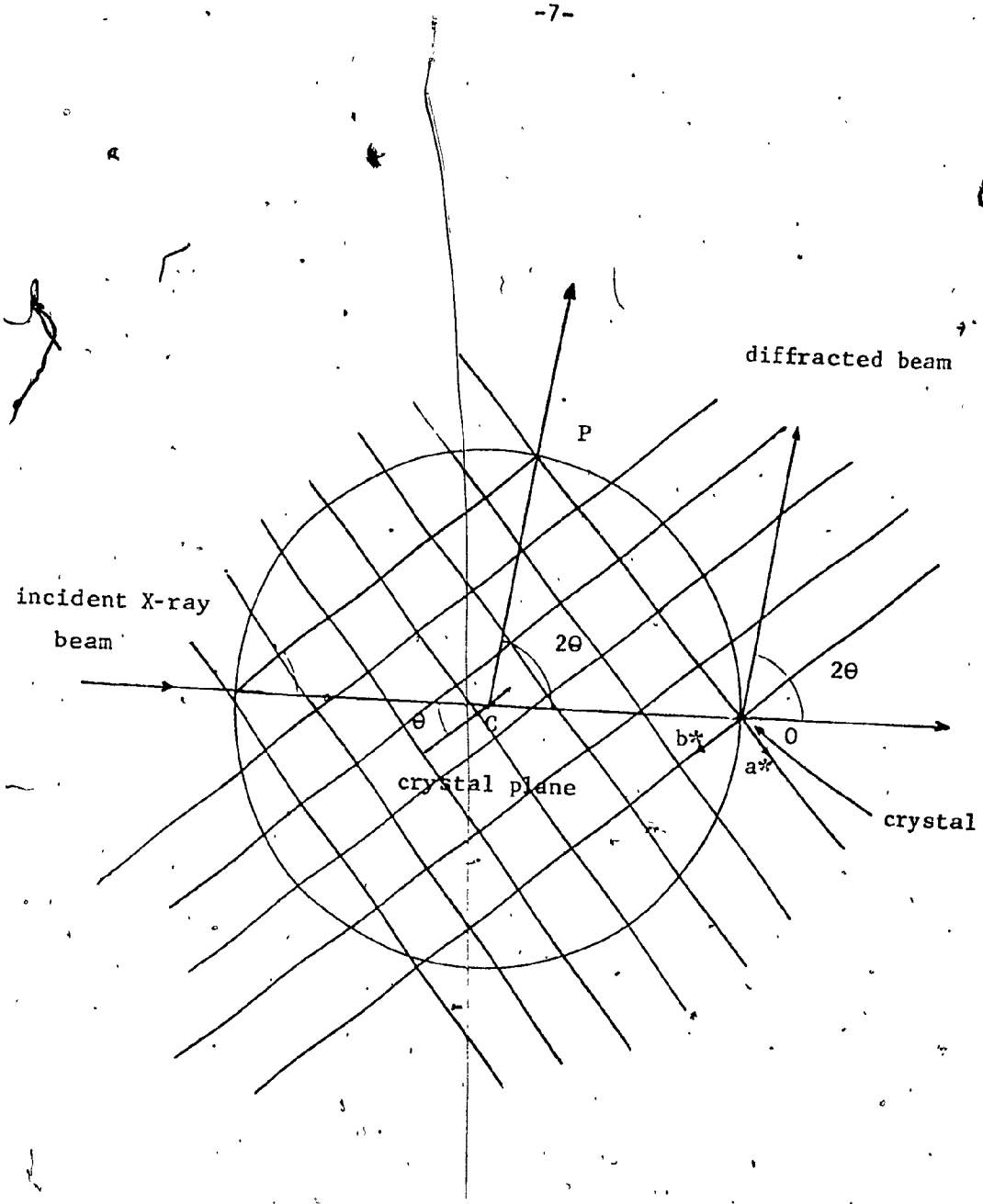

Figure II-1-3. A graphical representation of the Bragg law for the reciprocal lattice plane a^*c^*.

circle of reflections the Bragg condition is satisfied and reflection occurs. The origin of the reciprocal lattice is at the point O. The reflecting plane is perpendicular to OP and makes an angle θ with AO. Thus the direction of the diffracted beam can be taken as either CP or OD. This construction can be extended to a three-dimensional lattice: a sphere of reflections is obtained. Any point on the surface of the sphere will satisfy the Bragg condition.

The concept of the reciprocal lattice and the sphere of reflection is very useful in describing the rotation, Weissenberg and precession photographs.

2) SPACE GROUP DETERMINATION [4-6].

The first step of the X-ray structure investigation is the determination of the space group and the dimensions of the reciprocal lattice, often using photographic methods. The photographs that are normally used for this purpose are taken using rotation, Weissenberg and precession methods.

Rotation Photographs

Rotation photographs are useful in aligning a crystal on a goniometer head so that it rotates about one of its principal axes. This is necessary prior to taking Weissenberg photographs.

The rotation photographs also yield preliminary information about the crystal symmetry. These photographs are usually taken on a Weissenberg camera without moving the cassette holding the film. The crystal is mounted so that the X-ray beam will be perpendicular to a direct axis, thus parallel to the reciprocal lattice nets perpendicular to this direct axis. If the crystal is rotated through a small angle, some reciprocal lattice points will cut the sphere of reflections. The Bragg condition is satisfied and the diffracted rays will pass from the origin forming cones. Each cone represents a reciprocal lattice plane. These cones meet the cylindrical film and each two-dimensional plane is recorded as a layer line, Figure II-2-1. The length of the cell edges parallel to the axis of rotation can be calculated from the distance between the layer lines. The presence of mirror symmetry in the photograph indicates the presence of a mirror plane in the reciprocal lattice perpendicular to the rotation axis.

Weissenberg Photographs [4]

In a rotation photograph, all reflections from a two-dimensional lattice plane are condensed into a one-dimensional layer line. This disadvantage is overcome by using the Weissenberg moving film technique to obtain a photograph, where data from a reciprocal lattice plane is spread onto a entire sheet of film. Thus, a Weissenberg photograph is a rotation photograph taken using

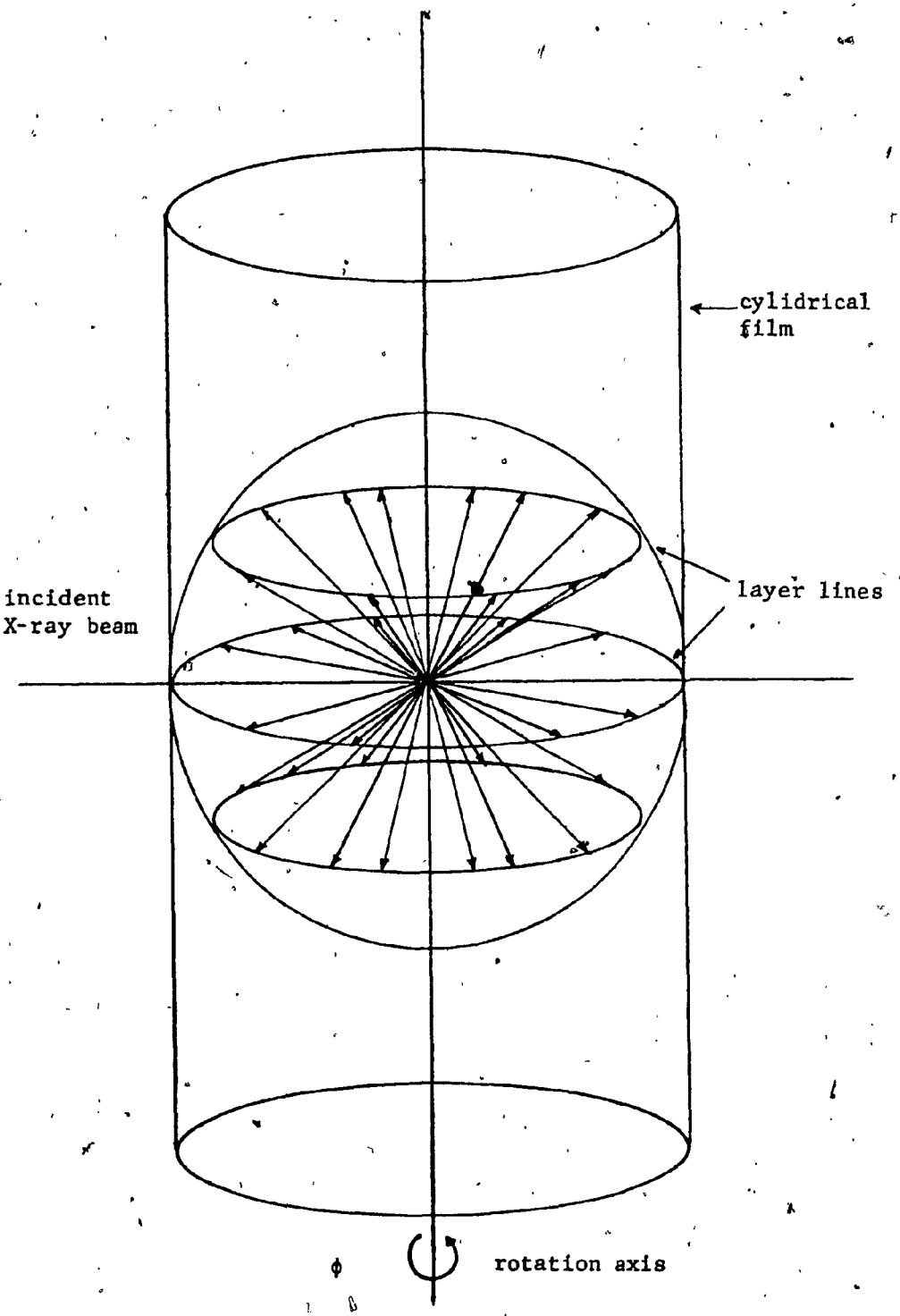

Figure II-2-1. An illustration of relationship between layer lines and cones of reflections in a rotation photograph.

a cylindrical metal screen that allows only one layer line at a time to reach the moving film. The film is shaped into a cylinder around the sphere of reflections and is translated parallel to the axis of rotation. The distance of a spot from the central line of the film is proportional to the angle 2θ of the diffracted beam. The camera is designed so that 1 mm in 2θ direction on the unrolled film is equal to 2^{o} in 2θ and 1 mm in sideways motion corresponds to a 2^{o} rotation of ϕ, Figure II-2-2. The limitations of the Weissenberg photographs are that they only provide a distorted record of the reciprocal lattice nets perpendicular to the rotation axis. The crystal has to be remounted on different axes to obtain full information.

Precession Photographs [5]

Precession photographs provide an undistorted record of the reciprocal lattice from which the angles and distances of the reciprocal lattice can be measured directly.

The crystal is oriented on the precession camera such that a direct lattice axis is parallel to the X-ray beam. The zero-level reciprocal lattice plane perpendicular to this axis will thus be tangent to the sphere of reflections. The reciprocal lattice plane will cut the sphere of reflections if the crystal is rotated through a small angle μ about an axis perpendicular to the X-ray beam.

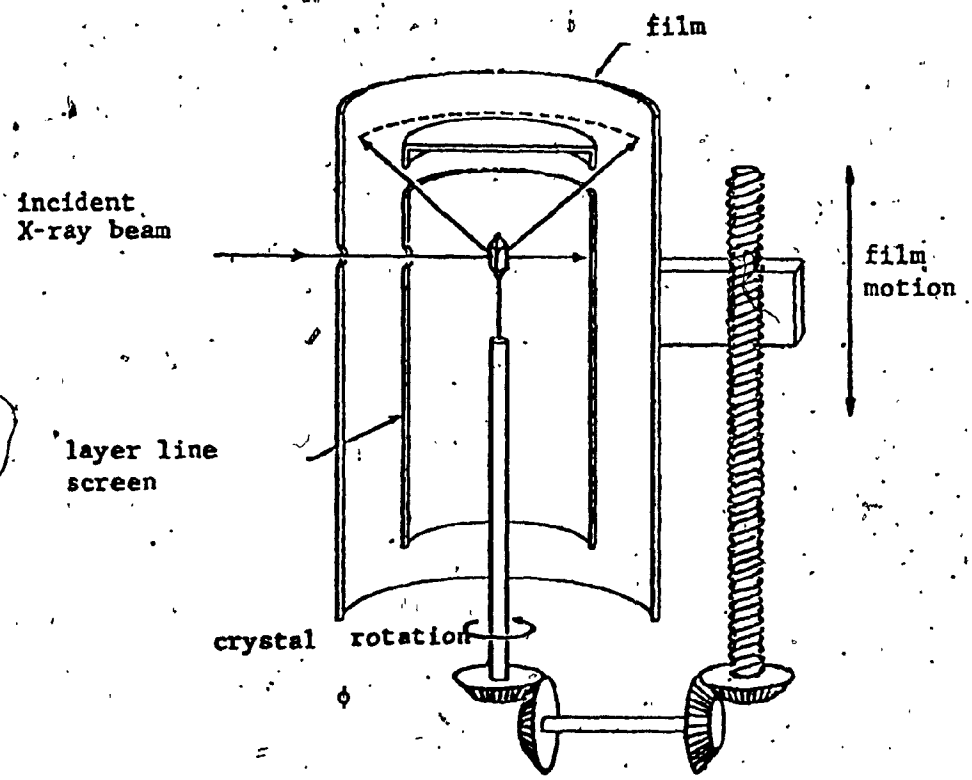

Figure II-2-2. An illustration of a Weissenberg camera.

The intercepted circle will revolve about the origin O if the crystal precesses about the direction of the X-ray beam so as to maintain the angle μ, Figure II-2-3. This motion is coupled to the film holder such that the reciprocal lattice will always be parallel to the film holder. A metal screen is used to select a particular layer while eliminating others. Thus the information on axes perpendicular to Weissenberg rotation axis can be obtained without remounting the crystal.

The choice of space group can be reduced to a few possibilities by carefully examining the symmetry information and systematic absences of reflections on the complementary Weissenberg and precession photographs.

3) DATA COLLECTION

This section deals with the collection of relative intensities of reflections which are used subsequently for the deduction of the electron density and finally the arrangement of the molecules in the unit cell.

The intensity of a reflection is a measure of the total number of photons of the characteristic wavelength diffracted in the proper direction as a reciprocal lattice point passes from outside to the inside of the sphere of reflection or vice versa.

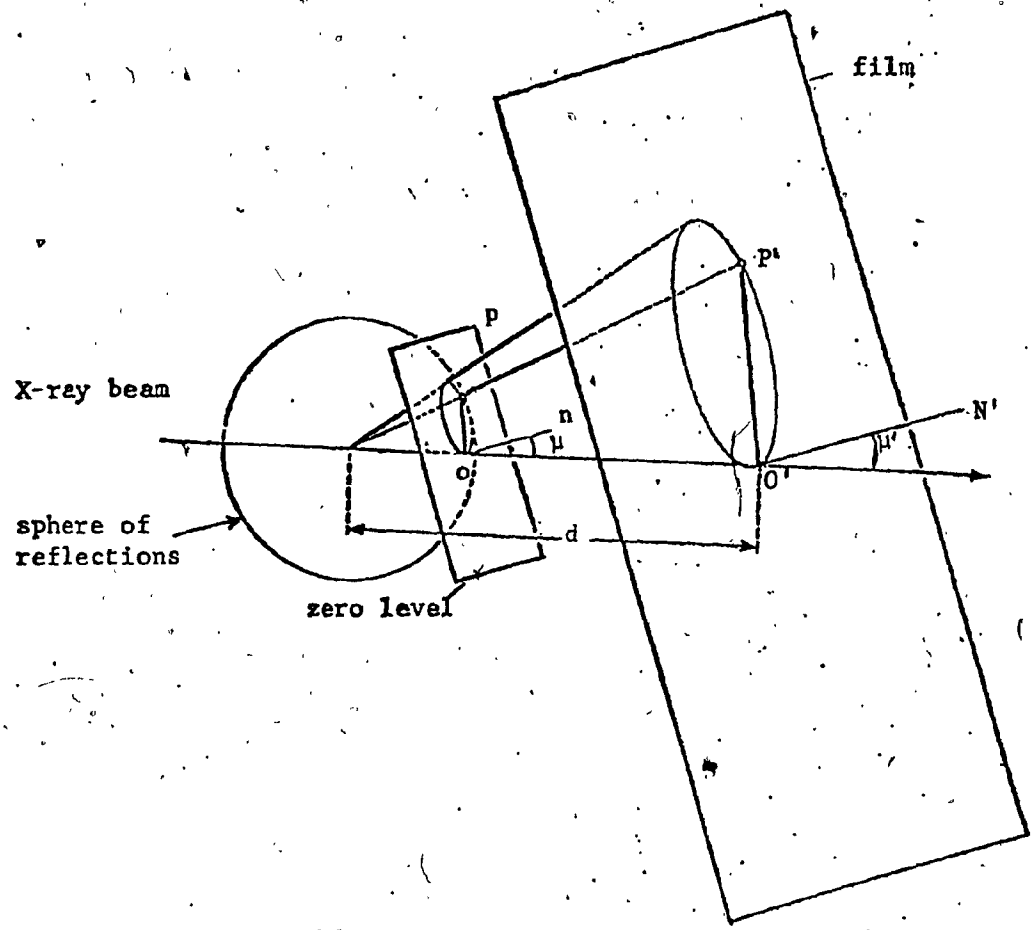

Figure II-2-3. An illustration of relationship between sphere of reflections and a zero-layer precession photograph.

Difficulties are encountered [7] in measuring intensities since they are usually accompanied by certain amount of other background radiation arising from the diffuse scattering of X-rays by all atoms in the crystal and also from the non-monochromaticity of the X-ray beam due to K_β line and the white radiation (continuum).

A four circle diffractometer [8] with a suitable counter to measure the intensities of the reflections is used in the data collection. Any crystal plane can be brought into the reflecting position by changing the angles of the four circles 2θ, ω, χ and ϕ, Figure II-3-1. A zero-level Weissenberg photograph is used to guide the alignment of the crystal on the diffractometer. A reflection, chosen from the zero-level, can be brought into the reflecting position by changing ϕ while keeping 2θ constant at the angle calculated from the Weissenberg photograph (the angles ω and χ are set to zero). An initial orientation martix is calculated using the angular values of two indexed reflections along with the unit cell dimensions calculated from the photographs.

A set of angular values obtained using the initial orientation matrix is optimized and used in a least squares refinement program to ensure that the crystal is oriented properly on the diffractometer and the final orientation matrix thus obtained is used to compute the positions of all reflections during the intensity data collection.

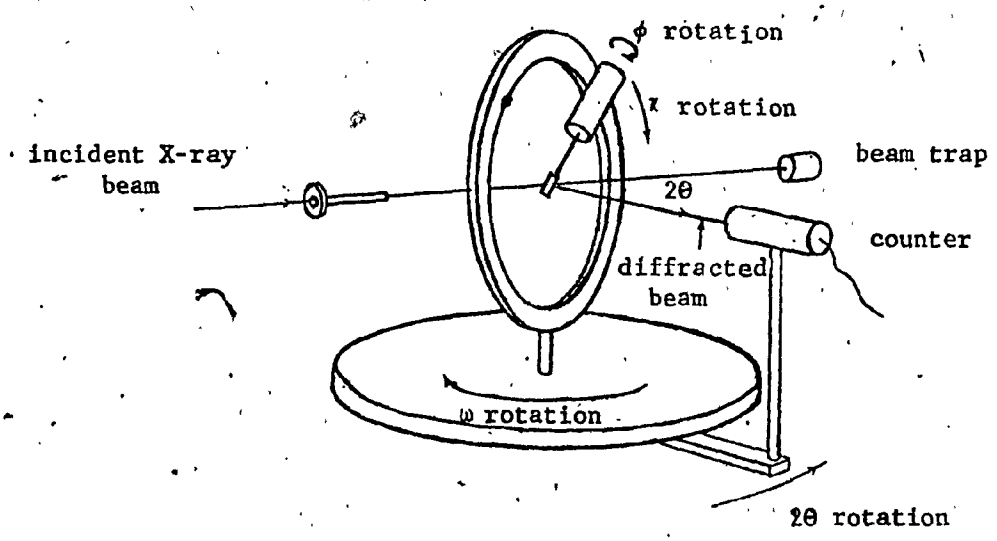

Figure II-3-1. An illustration of four circle diffractometer.

Three standard reflections are measured before the data collection and the stability of the system (ie. the crystal and electronics) is checked by remeasuring these standard reflections after every batch of fifty reflections.

The 2θ scanning method is normally used to record the integrated intensities of the reflections. The values of maximum and minimum 2θ, scan width, scan rate and the time for background measurements are specified depending on the size and the shape of the diffraction peaks based on a few trial scans. In this method the 2θ angle of a reflection is calculated using the least squares orientation matrix and the reflection is scanned for t_s seconds, as a function of the scan width and the dispersion factors. The backgrounds are measured at each end of the peak for t_b seconds. The NRC data collection package [9] uses, whenever possible, a special type of scan analysis called profile analysis. In this method, the reflection profile is examined to determine at which point the background is significantly flat. This point is taken to be the point at which the peak ends and the background begins. A significant amount of time otherwise required for counting backgrounds is saved by this procedure. The correction for backgrounds is done at the same time as the data is collected. In the case of reflections having very high intensities, Ni foils with known attenuator factors are used to reduce the intensity of radiation reaching the counter.

4) DATA REDUCTION

The conversion of the raw data into a more generally usable form is called data reduction. The subsequent development of the crystal structure solution depends on the skilled extraction of information contained within the observed data.

Removal of Background Intensity

The intensities corrected for backgrounds are calculated using the equation:

$$I = N - (B_1 + B_2)\, t_s / t_b \qquad \text{II-4-1}$$

where, N is the peak count in the scan time t_s seconds, B_1 and B_2 are the background counts on either side of the peak, each measured for t_b seconds. In the NRC data collection package this step is done at the same time data is collected.

Scaling of Intensities

After the application of attenuator factors, if necessary, the intensities are scaled in accordance with the variation of the three standard reflections during the data collection. A reflection is considered absent if the intensity computed is less than 0.0. The standard deviation $\sigma(I)$ of the intensity I is computed using

the equation:

$$\sigma(I) = [\, N + (\frac{B_1 + B_2}{2})\ (t_s / t_b) + P\, N^2]^{1/2} \qquad \text{II-4-2}$$

where, P is the instrumental constant (also called the "ignorance" factor) for which a value is chosen (usually 0.01 or 0.02) before the least squares refinement of atomic parameters. The reflection intensities less than $3\sigma(I)$ are usually rejected and along with the reflections which are systematically absent are omitted from the structure solution and refinement.

Lorentz-Polarization Correction

The intensities processed as described in the preceding sections are used to compute the relative structure factors, F_{rel}, using the equation:

$$F_{rel} = [\frac{I_{hkl}}{LP}] \qquad \text{II-4-3}$$

Here, LP represents the combined correction factors for the polarization of the X-ray beam, and for the specific geometry of the method used in the data collection. The correction for the polarization P of the X-ray beam is given separately by the equation:

$$1/P = \frac{\cos^2 2\theta_m + 1}{\cos^2 2\theta_m + \cos^2 2\theta_s} \qquad \text{II-4-4}$$

where θ_s and θ_m are the diffracting angles at the crystal and the monochromator, respectively. The Lorentz correction, L, arises from the differences in velocities with which reciprocal lattice points pass through the sphere of reflection. L for a reflection obtained using the Weissenberg geometry is given by the equation:

$$L = \frac{\sin \theta}{\sin 2\sqrt{\sin^2 \theta - \sin^2 \mu}} \qquad \text{II-4-5}$$

Here, μ is the equi-inclination angle. In the case of a reflection on the zero-level, equation II-4-5 reduces to:

$$L = \frac{1}{\sin 2\theta} \qquad \text{II-4-6}$$

The combined correction for L and P for Weissenberg zero-level or diffractometer geometry is given by the equation:

$$LP = \frac{\cos^2 2\theta_m + \cos^2 2\theta_s}{\sin 2\theta_s (\cos^2 2\theta_m + 1)} \qquad \text{II-4-7}$$

Absorption Correction [10-12]

The absorption of the incident and the diffracted X-ray beam by the crystal depends on the path length of the beam through the crystal. The intensities should be corrected for differential absorption if the path length is different for the beam

through various directions of the crystal. Absorption corrections are made by calculating the absorption for actual path lengths within the crystal to various summation points on a grid and integrating these results over the entire volume of the crystal. Precise measurement of crystal dimensions under a microscope is necessary for making a successful correction. The absorption can be minimized by selecting a crystal with fairly uniform thickness in all directions. Alternatively, it is possible to use crystals ground to a spherical shape. In this case an absorption correction can be computed analytically.

5) INTENSITY STATISTICS

Several useful pieces of information can be obtained by the statistical comparison of the corrected data with structure factors estimated theoretically, assuming a random distribution of atoms.

The observed average intensity, $\bar{I}_{rel}$, corrected for Lorentz-Polarization effects is given by the equation:

$$\bar{I}_{rel} = \langle F^2_{rel} \rangle_{av} \qquad \text{II-5-1}$$

The theoretical average intensity, $\bar{I}_{abs}$, for a unit cell containing N atoms is given by the equation:

$$\bar{I}_{abs} = \sum_{i=1}^{N} f_{oi}^2 \qquad \text{II-5-2}$$

where, f_{oi} is the scattering power [13] of the i^{th} atom. $\bar{I}_{abs}$ depends only on the type and the number of atoms assumed distributed randomly in the unit cell. The value of f_o for a stationary atom decreases with increasing $\sin\theta/\lambda$. The vibration of the electron cloud of an atom depends on the temperature [14,15], the mass of the atoms, and also the firmness with which it is held in place by covalent or other forces. The effect of thermal motion is to spread the electron cloud over a larger volume, reducing the scattering power of the real atom compared to a stationary atom. The atomic scattering factor corrected for thermal vibrations is given by the equation:

$$f_j = f_o \, e^{-B(\sin^2\theta/\lambda^2)} \qquad \text{II-5-3}$$

where, B is the thermal parameter which is related to the mean-square amplitude of atomic vibration as given by the equation:

$$B = 8\pi^2 \bar{\mu}^2 \qquad \text{II-5-4}$$

Thus the $\bar{I}_{abs}$ corrected for thermal vibrations is given by the equation:

$$\bar{I}_{abs} = \sum_{i=1}^{N} f_{oi}^2 \, e^{-2B(\sin^2\theta/\lambda^2)} \qquad \text{II-5-5}$$

if $\bar{I}_{rel} = C\,\bar{I}_{abs}$

$$\bar{I}_{rel} = C\, e^{-2B(\sin^2\theta/\lambda^2)} \sum_{i=1}^{N} f_{oi}^2 \qquad \text{II-5-6}$$

Where, C is a scale term. The equation II-5-6 is rearranged to:

$$\frac{\bar{I}_{rel}}{\sum_{i=1}^{N} f_{oi}^2} = C\, e^{-2B(\sin^2\theta/\lambda^2)} \qquad \text{II-5-7}$$

Taking natural logrithms:

$$\ln \frac{\bar{I}_{rel}}{\sum_{i=1}^{N} f_{oi}^2} = \ln C - (2B \sin^2\theta/\lambda^2) \qquad \text{II-5-8}$$

The plot, $\ln \dfrac{\bar{I}_{rel}}{\sum_{i=1}^{N} f_{oi}^2}$ vs $\sin^2\theta/\lambda^2$ is called a Wilson plot [16], where the extrapolated intercept at $(\sin^2\theta/\lambda^2) = 0$ is ln C and the slope is $-2B$. The C thus obtained is related to the scale constant K needed to correct $|F_{rel}|$ to $|F_{abs}|$.

If $K = 1/C$, then $|F_{abs}|$ is given by the equation:

$$|F_{abs}| = K |F_{rel}| \qquad \text{II-5-9}$$

The scale term, K, thus obtained, is used subsequently in the least squares refinement of atomic parameters.

6) STRUCTURE FACTOR CALCULATIONS AND FOURIER SYNTHESIS

Structure Factor Calculations [17-19]

The structure factors can be considered as the resultant of j waves scattered in the direction of reflection hkl by j atoms in the unit cell. The superposition of waves and the magnitude of the resultant amplitude, F is given by the basic equation:

$$|F|^2 = \left(\sum_j f_j \cos \delta_j\right)^2 + \left(\sum_j f_j \sin \delta_j\right)^2 \qquad \text{II-6-1}$$

where, f_j is the magnitude of the rotation vector and δ_j is the phase difference. The phase angle, ϕ is given by the equation:

$$\phi = \tan^{-1} \frac{\sum_j f_j \sin \delta_j}{\sum_j f_j \cos \delta_j} \qquad \text{II-6-2}$$

The amplitude of each reflection (hkl) is proportional to the scattering factors, f_j of the atoms in the unit cell and the phase differences can be expressed in terms of the positions of the atoms and the indices of the reflections by the equation:

$$\delta = 2\pi (hx + ky + lz) \qquad \text{II-6-3}$$

Substituting δ values in equation II-6-1, the following equation is obtained:

$$|F_{hkl}|^2 = \left[\sum_j f_j \cos 2\pi (hx_j + ky_j + lz_j) \right]^2 + \ldots\ldots$$

$$\ldots\ldots \left[\sum_j f_j \sin 2\pi (hx_j + ky_j + lz_j) \right]^2 \qquad \text{II-6-4}$$

A structure factor can be given as a complex number by the equation:

$$F_{hkl} = A_{hkl} - i B_{hkl} \qquad \text{II-6-5}$$

where,

$$A = \sum_j f_j \cos 2\pi (hx_j + ky_j + lz_j) \qquad \text{II-6-6}$$

$$B = \sum_j f_j \sin 2\pi (hx_j + ky_j + lz_j) \qquad \text{II-6-7}$$

The phase angle ϕ_{hkl} for a reflection (hkl) is given by the equation:

$$\phi_{hkl} = \tan^{-1} \frac{B_{hkl}}{A_{hkl}} \qquad \text{II-6-8}$$

The equation II-6-5 can also be expressed in an exponential form:

$$F_{hkl} = \sum_j f_j \, e^{2\pi i (hx_j + ky_j + lz_j)} \qquad \text{II-6-9}$$

Since, $f\, e^{i\delta} = f (\cos \delta + i \sin \delta)$

The f_j in the equation II-6-9 is the scattering factor of the j^{th} atom corrected for the thermal vibrations and related to the free atomic scattering factors given by the equation:

$$f_j = f_{oj} \, e^{-2B (\sin^2 \theta/\lambda^2)} \qquad \text{II-6-10}$$

Substituting f_j in II-6-10 to the equation II-6-9, the equation II-6-11 is obtained.

$$F_{hkl} = \sum_j f_{oj} \, e^{-2B (\sin^2 \theta/\lambda^2)} \cdot e^{2\pi i (hx_j + ky_j + lz_j)} \qquad \text{II-6-11}$$

Structure Factors in terms of Electron Density

The structure factors can also be calculated considering the sum of the wavelets scattered from all infinitesimal elements of electron density in a unit cell. If the number of electrons in any volume element dV is equal to $\rho(x,y,z)\,dV$, where ρ is the electron density at the point with coordinates x,y,x, the resultant amplitude of all the wavelets scattered by the electrons in the unit cell is given by the equation:

$$F_{hkl} = \int_V \rho(x,y,z)\, e^{2\pi i\,(hx_j + ky_j + lz_j)}\, dV \qquad \text{II-6-12}$$

Fourier Synthesis [20]

The electron density of a crystal is a periodic function which can be expressed, by means of a fourier series, as a sum of sine and cosine terms with appropriate coefficients. The electron density distribution thus calculated is the fourier transform of the structure factors and related to F_{hkl} by the equation:

$$\rho(x,y,z) = 1/V \sum_h \sum_k \sum_l F_{hkl}\, e^{2\pi i\,(hx+ky+lz)} \qquad \text{II-6-13}$$

where, V is the unit cell volume.

An electron density distribution in the unit cell calculated by fourier synthesis using observed structure factors is called an "observed" fourier map. A "difference" fourier map which is very useful in locating atoms in the unit cell in a partially solved structure, is calculated using the difference between the observed and calculated structure factors.

7) THE PHASE PROBLEM [21]

The electron density distribution in the unit cell can be calculated using structure amplitudes, $|F_{hkl}|$, and their phases using a fourier synthesis. Unfortunately, the intensity data is proportional to F^2_{hkl}. The complex F_{hkl} can not be used to calculate the electron density distribution until the phases are known.

In the case of a centrosymmetric crystal, an atom at x,y,z, is related to a another at $\bar{x},\bar{y},\bar{z}$, and the equation II-6-5 reduces to the equation:

$$F_{hkl} = A_{hkl} + i\,0 \qquad \text{II-7-1}$$

where, $A_{hkl} = 2\sum f_j \cos 2\pi\,(hx_j + ky_j + lz_j)$ II-7-2

The phase angle ϕ_{hkl} is either 0 or π for

centrosymmetric structures and the structure factors need only a sign (+ or -) to be determined.

The phase angle can have any value from 0 to 2π in the cases of noncentrosymmetric structures. However, for some F_{hkl} the phase may have special restricted values depending on the space group. The problem of assigning values to the phases is known as the "phase problem".

Patterson Synthesis [22-24]

The fourier series using $|F_{hkl}|^2$ as coefficients instead of F_{hkl} as in the equation II-6-13 is called the Patterson function, equation II-7-3. This function is very useful in finding the position of heavy atoms and allows the calculation of approximate phases for each F_{hkl} based on the location of heavy atoms. The position of other atoms in the unit cell can be located from the difference fourier map phased by these heavy atoms.

$$P(u,v,w) = 2 / V \sum_h \sum_k \sum_l F^2_{hkl} \cos 2\pi (hu+kv+lw) \quad \text{II-7-3}$$

The peaks P (u,v,w) in the Patterson map correspond to each interatomic vector between a pair of atoms in the unit cell. A unit cell containing N atoms will have $N^2 - N/2$ independent Patterson peaks excluding the intence peak at the origin. There is considerable

overlap between the peaks due to the diffuse nature of the atoms in space. This can be minimized using "sharpened structure factors", where the atoms are considered as point scatterers calculated using the equation:

$$(F_{sharp})^2_{hkl} = \frac{[\,0.1667 + \sin^2\theta/\,^2]\,[\,F_{obs}]_{hkl}}{[\sum_{j=1}^{N} f_{oj}\, e^{-B(\sin^2\theta/\lambda^2)}]} \qquad \text{II-7-4}$$

where, f_{oj} is the mean atomic scattering factor of the j^{th} atom. The positions of "heavy" atoms can be deduced from the location of the major peaks on the Patterson map since the peak heights are proportional to the product of the scattering power of the atoms defining the vector. If an asymmetric unit of the unit cell contains few heavy atoms their location is straightforward. However, if the structure is more complex with or without heavy atoms it will be difficult to assign peaks to specific vectors.

Direct Methods

Direct methods, where phases for the observed structure factors are assigned directly, have been particularly successful in the case of centrosymmetric crystals. However, the phase solution of noncentrosymmetric crystals by direct methods is now becomming quite common. The basis for the direct methods has been extensively developed [25-26] since the appearance of the original papers by Sayre [27].

The basis of this method is given in the equation II-7-5, which states that the phase angle ϕ_{hkl} of a strong reflection hkl is approximately equal to the sum of the phase angles $\phi_{h'k'l'}$ and $\phi_{h-h',k-k',l-l'}$ of strong reflections whose indices add to give hkl.

$$\phi_{hkl} \approx \phi_{h'k'l'} + \phi_{h-h',k-k',l-l'} \qquad \text{II-7-5}$$

The three reflections involved in this relationship are called a triple.

In the first stage of phase solution by direct methods, normalized structure factors, E_{hkl}, are calculated using the equation:

$$E^2_{hkl} = \frac{F^2_{hkl}}{\varepsilon} \frac{1}{\sum_{j=1}^{N} f_j^2} \qquad \text{II-7-6}$$

where, N is the total number of atoms in the unit cell and f_j is the atomic scattering factor for the j^{th} atom at 2θ value of the reflection hkl. ε is a integer which is used to adjust the data at a symmetrical location in reciprocal space, for example in the space group $P\,2_1/c$, $\varepsilon = 2$ for h0l and 0k0 reflections and $\varepsilon = 1$ for the rest. E's are scaled such that $< E^2 > = 1$. The strong reflections, with E's greater than a specified minimum (usually 1.8), are selected along with the weakest reflections, which are to be used for the

PSI ZERO test described later. All the triples, h,k,l ; h',k',l' ; h-h',k-k',l-l' (called $\sum^2$ relationships) are sorted out, including those where hkl is a weak PSI ZERO reflection and the other two are stronger reflections. All strong reflections among the $\sum^2$ reflections are tested for their usefulness in the phase solution using a quantity "$< \alpha_h^2 >$" defined by the equation:

$$< \alpha_h^2 > = \sum_{h'} K_{hh'}^2 + \sum_{h'} \sum_{h''} K_{hh'} \, K_{hh''} \cdot X \qquad \text{II-7-7}$$

where, $$X = \frac{I_1(K_{hh'})}{I_0(K_{hh'})} \cdot \frac{I_1 (K_{hh''})}{I_1 (K_{hh''})}$$

I_0 and I_1 are Bessel functions and $< \alpha_h^2 >$ means the expectation value of α_h^2. K is given by the equation:

$$K_{hh'} = 2 \sigma_3 \sigma_2^{-3/2} \left| E_h E_{h'} , E_{h-h'} \right| \qquad \text{II-7-8}$$

where, σ_2 and σ_3 are given by the equations:

$$\sigma_2 = \sum_i^N n_i^2 \qquad \text{II-7-9}$$

$$\sigma_3 = \sum_i^N n_i^3 \qquad \text{II-7-10}$$

and $$n_i = \frac{f_i}{\sum_i^N f_i} \qquad \text{II-7-11}$$

where, f_i and f_j are scattering powers of i^{th} and j^{th} atom, respectively.

The next stage of the phase determination uses the special case of triples where,

$$h' = h-h'$$

$$k' = k-k'$$

$$l' = l-l'$$

In the case of centrosymmetric crystals and for special reflections of noncentrosymmetric crystals where, the phase is either - or + (0 or π), the sign of $E_{2h,2k,2l}$ is positive regardless of the phase of the $E_{h,k,l}$, provided both $E_{h,k,l}$ and $E_{2h,2k,2l}$ are strong:

$$S\{E_{2h,2k,2l}\} = S\{E^2_{h,k,l} - 1\} \qquad \text{II-7-12}$$

where, S means the sign of the Es involved. The relationships which are obtained by equation II-7-12 are called $\sum_s^1$ relationships.

The following steps lead to the definition of the origin and the construction of the most suitable path for phase determination for the whole data set. As an example, three reflections are necessary for a crystal in the space group $P\bar{1}$. They are selected such that none have even,even,even indices, each belong to a different parity

group and the parity of the vector sum of any two is different from the third. In the case of more symmetric space groups fewer reflections are required for the origin definition and the parity groups may be different.

The reflection with smallest α_h is eliminated from the starting set together with all the phase relationships in which the reflection is involved. This process is repeated and the remaining reflections form a group with stronger phase relationships. This process is called convergence mapping. The phases of up to three reflections (depending on the space group) can be arbitarily assigned in order to specify the origin position. This procedure continues until the origin can no longer be defined by the remaining reflections. Then, the one just eliminated becomes one of the origin fixing reflections. Thus all the reflections necessary for the origin definition are selected at the end of convergence.

The starting set of the reflections for the tangent formula calculations comprises the origin fixing reflections which are assigned arbitary phases, reflections from $\sum^1$ relationships whose phases have been determined and a reflection to fix the enantiomorph if the crystal is noncentrosymmetric. In addition some more reflections can be included in the starting set, but their starting phases are given several values depending on the space group. As an example, for a crystal belonging to $P_{2_1/c}$, three reflections

are necessary for the origin definition, but there will be eight starting sets if three additional reflections are included in the starting set (in this case additional reflections can have either 0 or π as phases since the space group is centrosymmetric).

In the tangent formula calculations, new phases are assigned to other reflections related by triples to those in the starting set. Unit weights are given to the origin fixing reflections and those from $\sum^{1}$ relationships, while zero weights are given to new phases. The phases are refined using a weighted tangent formula [28]:

$$\tan\phi_h = \frac{T_h}{B_h} = \frac{\sum_{h'} \omega_{h'}\omega_{h-h'} |E_{h'} E_{h-h'}| \sin(\phi_{h'}+\phi_{h-h'})}{\sum_{h'} \omega_{h'}\omega_{h-h'} |E_{h'} E_{h-h'}| \cos(\phi_{h'}+\phi_{h-h'})} \qquad \text{II-7-13}$$

where, ω_h is the weight associated with the phase ϕ_h.

$$\omega_h = \tanh(1/2\ \alpha_h) \qquad \text{II-7-14}$$

and $$\alpha_h = |E_h| (T_h^2 + B_h^2) \qquad \text{II-7-15}$$

The weights are increased as the number of further phase determinations involving them increases. At the end of the tangent formula calculations, phasing information is summerized for each

starting set in terms of three figures of merits called ABS FOM, PSI ZERO and RESID.

The first figure of merit, ABS FOM is a measure of the interhal consistancy of the phases of the starting set and it is related to the α_h defined in the equation II-7-15. ABS FOM is usually maximum for a correct phase solution.

The second figure of merit, PSI ZERO is related to the approximate E's calculated for the weakest reflections using the phase information of strong reflections by the equation:

$$\psi_o = \sum_h \left| \sum_{h'} E_{h'} \cdot E_{h-h'} \right| \qquad \text{II-7-16}$$

The terms in the inner summation are all those for which phases are known. The outer summation is over all the reflections selected for the PSI ZERO test ie. weakest reflections. ψ_o is usually minimum for a correct phase solution.

The third figure of merit, RESID is the residual for the equations:

$$E_h = k \langle E_h , E_{h-h'} \rangle_{h'} \qquad \text{II-7-17}$$

here, k is a scale factor. RESID is usually minimum for a correct

phase solution. The best solution set is selected using ABS FOM, PSI ZERO and RESID. This set is used to calculate an E-map from which some or all atoms of the structure are located.

8) LEAST SQUARES REFINEMENT OF ATOMIC PARAMETERS [29-32]

Structure factors can be calculated for a particular reflection hkl using the equation:

$$F_c = \sum_j f_{oj}\, e^{-2B_j (\sin^2\theta/\lambda^2)}\, e^{2\pi i (hx_j+ky_j+lz_j)} \quad \text{II-8-1}$$

where, F_c, f_{oj}, B_j and x,y,z are calculated structure factor, free atom scattering factor, thermal parameter and three positional coordinates, respectively. The thermal parameter B_j is called the iosthermal parameter since the vibration is considered spherical. In the anisotropic case the thermal parameter is replaced by six parameters which take into account the amplitude and directions of vibration as an ellipsoid. Thus the atomic scattering factor corrected for anisotropic thermal vibration is given by the equation:

$$f = f_{oj}\, e^{-(\beta_{11}h^2+\beta_{22}k^2+\beta_{33}l^2+2\beta_{12}hk+2\beta_{13}hl+2\beta_{23}kl)} \quad \text{II-8-2}$$

The mean square amplitude of atomic vibration, $\overline{\mu}^2 = U$ is more useful than β, therefore, the exponent in the equation II-8-2 takes the following form if the $\overline{\mu}^2$ are used.

$$[\ -2\pi^2(U_{11}h^2a^* + U_{22}k^2b^* + U_{33}l^2c^* + 2U_{12}hka^*b^* + 2U_{12}kla^*c^* + 2U_{23}klb^*c^*)] \quad \text{.... II-8-3}$$

Free electron scattering factors are corrected for relativistic effects before using in the stucture factor calculations. Thus, due to the fast movement of core electrons, the scattered X-ray photons are out of phase with the incident photons, ie. the scattering is inelastic to a significant degree. These corrections are significant in the case of 'heavy atoms', and take the form of a real $\Delta f'$ and imaginary part $\Delta f''$.

The positional and thermal parameters are refined using conventional non-linear least squares methods to minimize the difference, D between the observed $|F_o|$ and the calculated, $|F_c|$ structure factors.

$$D = \sum_{hkl} \omega_{hkl} \left(|F_o| - |k\,F_c| \right)^2 \quad \text{II-8-4}$$

where, k is a scale factor for F_c and ω_{hkl} is given by the equation;

$$\omega_{hkl} = 1/\sigma^2 \qquad \text{II-8-5}$$

where, σ is the standard deviation of F.

The derivative of the expression in the equation II-8-4 with respect to each parameter is set to zero. The resulting equations are expanded as a Taylor series neglecting terms higher than first power. The new equations are solved for shifts x_j in the parameters p_j according to the matrix equation:

$$\begin{pmatrix} a_{11} & a_{12} & \cdots & a_{1n} \\ a_{21} & a_{22} & \cdots & a_{2n} \\ \vdots & \vdots & & \vdots \\ a_{n1} & \cdots & & a_{nn} \end{pmatrix} \begin{pmatrix} x_1 \\ x_2 \\ \vdots \\ x_n \end{pmatrix} = \begin{pmatrix} v_1 \\ v_2 \\ \vdots \\ v_n \end{pmatrix} \qquad \text{II-8-6}$$

where,

$$a_{ij} = \sum_{hkl} \omega_{hkl} \frac{\partial \left|F_{cal}\right|_{hkl}}{\partial p_i} \cdot \frac{\partial \left|F_{cal}\right|_{hkl}}{\partial p_j} \qquad \text{II-8-7}$$

$$x_i = \Delta p_j \qquad \text{II-8-8}$$

$$v_i = \sum_{hkl} \omega_{hkl} \left(\Delta F_{hkl} \right) \frac{\partial \left| F_{cal} \right| hkl}{\partial p_i} \qquad \text{II-8-9}$$

The estimated standard deviation of parameter $p_j (\sigma p_j)$ is calculated using the equation:

$$\sigma (p_j) = \sqrt{b_{jj} \left[\sum_{hkl} \omega_{hkl} \Delta F^2_{hkl} \right] / (m-n)} \qquad \text{II-8-10}$$

where, b_{jj} is the j^{th} diagonal element of the inverse matrix from equation II-8-6. m and n are the numbers of observations and parameters, respectively.

The correctness of the atomic positions and hence the degree of correctness of the structure at any stage of the refinement is related to R factors (also called the the descrepancy indices, residual factors or reliability factors) which can be computed from the equations:

$$R_{unweighted} \ (R_F) = \frac{\sum_{hkl} \left| \left| F_{obs} \right| hkl - \left| F_{cal} \right| hkl \right|}{\sum_{hkl} \left| F_{obs} \right| hkl} \qquad \text{II-8-11}$$

$$R_{weighted}\ (R_{WF}) = \left[\frac{\sum_{hkl} \omega_{hkl} \left(|F_{obs}|_{hkl} - |F_{cal}|_{hkl} \right)^2}{\sum_{hkl} \omega_{hkl} |F_{obs}|^2_{hkl}} \right] \quad \text{II-8-12}$$

The goodness of fit index (GOF) is defined by the equation:

$$\left[\sum_{hkl} \frac{\omega_{hkl} \left(|F_{obs}|_{hkl} - |F_{cal}|_{hkl} \right)^2}{n - m} \right] \quad \text{II-8-13}$$

The GOF represents the deviation in an observation of unit weight. This index should approach 1.0, if the weights are chosen correctly.

The least squares procedures for the refinement of atomic parameters use either full-matrix or block diagonal methods depending on the number of variables used. The number of variables are usually determined by adding four variables for each atom treated as vibrating isotropically, nine variables for each atom treated as vibrating anisotropically, plus one variable for the scale factor.

On the PDP8/A minicomputer, the full matrix method is used if the number of variables is less than eighty. In SFLS and

NUCLS, least squares programs which are used on the CDC 172 computer, close to 200 hundred variables can be accomodated.

The least squares program NUCLS is a special program which can treat phenyl groups as rigid idealized phenyl rings with C-C distances, 1.39Å. This reduces the number of variables required for the refinement of a ring to twelve, including three coordinate parameters defining the ring centroids (x_c, y_c, z_c), three angles (θ, ρ, ϕ) to fix the orientation of the ring and six isothermal parameters. If the rings are refined using SFLS, treating each atom separately, twenty four variables are required. Several least squares cycles are usually required to complete the refinement starting with approximate values derived from the preceding calculation. The refinement is considered complete when there is no significant change in the parameters between two successive cycles.

Broadly speaking structures having R less than 10.0% are said to be adequate to be sure that the gross structure is correct and R less than 5.0% is considered fairly accurate; the atomic parameters can be used to calculate the bond angles and lengths.

SECTION III EXPERIMENTAL

1) CRYSTAL MOUNTING AND SPACE GROUP DETERMINATION:

A single crystal of suitable dimensions, chosen under a Bausch and Lomb stereo-zoom microscope, was mounted on a borosilicate capillary tube so that it would rotate about one of the principal crystal axes. This tube was in turn fixed to a goniometer.

Rotation and Weissenberg photographs were taken using a Charles Supper Co. Weissenberg camera. Precession photographs were taken using a precession camera made by the same manufacturer. A Dunlee Mo target tube was used as X-ray source: it was operated at 40 KV and 20 mA, powered by a Picker Nuclear X-ray generator and control (model 8093). Most of the photographs were taken using Kodak "No Screen" film. Polaroiod films (type 57, high speed) were used to take some of the precession photographs.

The crystals were first aligned using rotation photographs to determine the changes to be made on the goniometer arcs. Two unit cell axes were identified using the Weissenberg photographs, and the reciprocal angle between these axes was measured. Precession photographs were taken, each including one of the axes already identified, and the remaining reciprocal axis. The lengths of all three reciprocal cell edges, and the two remaining reciprocal

angles were measured. All the measurements of angles and distances on the photographs were carried out using a Charles Supper Co. film measuring device. Angles and distances thus obtained were subsequently used in computing the approximate direct unit cell dimensions.

The space group of the crystal was deduced using the symmetry and the systematic absences appearing on the Weissenberg and precession photographs.

2) DATA COLLECTION, STRUCTURE SOLUTION AND REFINEMENT.

The goniometer head, with arcs set to Weissenberg positions, was fixed to a Picker Nuclear FACS-1 four circle diffractometer having an Elliot Mo target tube as the X-ray source. The power to the X-ray tube was supplied by a Picker Nuclear constant potential diffraction generator (model 6238E), stable within 0.19 kV and 0.029 mA. The X-ray tube was operated at 20 mA and 40 kV, in the case of the first structure (UNIQUE) and 30 mA and 40 kV for the other three structures (FESCO, TICEP, RUSH). The take-off angle for the direct beam was 3.0° and the $K_{\alpha 1}$ / $K_{\alpha 2}$ peak was isolated with a graphite "crystal" (reflection from the 002 face). A 1 mm pinhole collimator was used for the incident beam. A receiving apperture with vertical and horizontal slits, was located 23 cm from the crystal and 20 mm from the scintillation counter. A series of nickel foil attenuators, fixed to a rotating disc, was placed between the aperture and the

detector to attenuate reflections having intensity greater than 10,000 cps. The detector was operated at 1,000 volts and the pulse height analyser was set to receive 100% of the K_α X-ray radiation.

The crystals were visually centered using a microscope attached to the diffractometer. Two reflections selected from a zero-level Weissenberg photograph were manually brought into their reflecting positions.

From this point the procedures used in the data collection, structure solution and refinement were different for the first structure (UNIQUE) and the other three structures (FESCO, TICEP, RUSH) since the data collection and the subsequent steps were carried out using different computers and programs. The description will be continued for two cases separately. The numerical data related to the crystal, structure solution and refinement for the four structures are collected in Table III-1 at the end of this section.

UNIQUE

Two reflections identified on the Weissenberg zero-level were centered, and the angular values thus obtained were used, along with the unit cell dimensions from the photographs, to calculate the initial orientation matrix. The Picker Nuclear crystal alignment program was used in centering the reflections and other computations

involved. Twelve reflections, evenly distributed over the reciprocal lattice, having fairly high intensities and $2\theta \approx 20^{\circ} - 30^{\circ}$, were chosen and centered at both $+2\theta$ and -2θ (hkl and -h-k-l). The two seta of angular values ($2\theta, \omega, \chi, \phi$) thus obtained were averaged, and used as observations in the least-squares optimization of the six approximate cell constants and the initial orientation matrix and based on ω, χ, ϕ for primary and secondary reflections. (These were chosen such that their χ angles were close to 0° and their ϕ angles were separated by about 90°). The least-squares program used was supplied by Picker Nuclear Co. as a part of their alignment package.

The data collection was carried out using the Picker Nuclear data collection package. The θ-2θ scan method was used to record the integrated intensity of the reflections. The attenuation factors used in the collection of intensities greater than 10,000 cps, were 2.781, 7.959 and 38.190. Minimum and maximum values of 2θ and the limits for h, k and l were given to specify the portion of the sphere of reflections to be collected. The time specified for the background measurements on either side of the reflection was 20 seconds. The data were recorded on a punched tape and a print out of hkl, scan time, intensity and the two background intensities for each reflection hkl was also available. All the steps from the computation of the initial orientation matrix to the end of the data collection were carried out using a PDP8/S minicomputer interfaced to the four circle diffractometer. This computer has a 4K memory

and programs were loaded from paper tapes. The data on the punched tape was transferred to a magnetic tape using a Hewlett Packard 2114 A computer.

After this point all the computations necessary for the structure solution and refinement were carried out on a CDC Cyber 172 computer using the data transferred via the magnetic tape. Data reduction and absorption corrections were carried out using programs PREP [33] and GNABS [34], respectively. An instrumental constant of 0.02 was used (see section II-4, equation II-4-2). The observed structure factors thus obtained were used to calculate a 'sharpened' Patterson function using the fourier program FORDAP [35]. The two platinum atoms located using a Patterson-map were assigned arbitary isothermal parameters (3.0). Their positional and thermal parameters were used, along with the absolute scale factor obtained from the Wilson plot section of PREP, as input to the least-squares program SFLS [36], which calculated the partial factors. The structure factors thus obtained were used to calculate a difference fourier map using FORDAP. Some more non-hydrogen atoms were located from this map. After several cycles of SFLS including the new atoms, followed by the calculation of an improved difference fourier map, all the non-hydrogen atoms had been located. From this point the phenyl groups of the molecule were treated as idealized rigid bodies. Three coordinate parameters, three orientation angles and an isothermal parameter for each phenyl group were thus

calculated using a program RIGID [37], and the refinement was completed using the program NUCLS [38].

FESCO, TICEP AND RUSH

The NRC crystallographic programs [9] running on a new PDP8/A minicomputer interfaced to the four circle diffractometer were used in the crystal alignment, structure solution and refinement. This computer has 32K of memory and a floating point processor. It is equipped with 4.8 million words of disc storage and a 120 character/sec. printer.

The calculation of the initial orientation matrix was similar to that described for UNIQUE. A set of angular values 2θ, ϕ, ω and χ for twenty five reflections obtained using the initial orientation matrix, were optimized by centering these reflections. The final angular values thus obtained were used in a least-squares program to calculate the accurate direct cell dimensions. A line profile analysis was carried out for certain reflections to ensure that the refined matrix is properly defined. Three reflections were measured and specified as standard reflections. The 2θ limits and space group were input to specify the portion of the sphere of reflections to be collected and the systematic absences. The total intensity of each reflection was collected using the profile analysis mode and the background corrections were made

simultaneiously. The intensity data collected was recorded (the DA file) on a magnetic disc. It was also available as a print out.

A crystal data file (the CD file) was created to provide the information (cell parameters, symmetry, scattering factors etc.) necessary for the subsequent steps in the structure solution and refinement. The data reduction step was carried out using the NRC data reduction program which reduces the intensity data from the DA file. The attenuator factors 1.00, 2.85, 8.04 and 38.03 were applied and the data from the DA file was scaled according to the variation of the three standard reflections during the data collection. Finally the observed structure factors (F_{obs}) were recorded onto a fundamental reflection file (the RE file). In a last step all $|F_{obs}|$ on the RE file were normalized and an overall thermal parameter was calculated using a Wilson plot.

The phase problem was solved by direct methods using the program MULTAN [39] adapted for PDP8/A minicomputer. Eight solution sets were obtained for each structure and the best set was selected using the three figures of merit. The phase information thus obtained was used to calculate an E-map from which most of the 'heavy' atoms were located. The atoms thus located were assigned arbitary isothermal parameters (U) and refined using the NRC least-squares program LSTSQ. Remaining non-hydrogen atoms were located from the difference fourier maps drawn using the NRC fourier program

FOURR. The positional and thermal parameters of all the atoms were refined using LSTSQ.

The NRC program DISPOW was used to calculate the distances and angles quoted for the refined structures. The diagrams of structures UNIQUE, FESCO, TICEP and RUSH were drawn on a Bausch and Lomb DP-1, X-Y plotter interfaced to a Hewlett Packard 2114 A computer using the program ORTEP [40], run on the CDC Cyber 172 computer.

Table III-1 The experimental data for X-ray diffraction studies (crystal, data collection and refinement).

A) Crystal parameters at 20°C, with λ (Mo K_α) = 0.71069

	UNIQUE	FESCO	TICEP	RUSH
1. a, Å	10.856(3)	16.042(2)	8.842(8)	17.046(2)
2. b, Å	19.938(5)	10.71 (1)	30.91 (2)	16.347(5)
3. c, Å	12.202(4)	9.05 (9)	8.852(9)	17.870(3)
4. α, deg	82.52(2)	59.57(9)	90.00	90.00
5. β, deg	105.18(2)	85.2 (1)	122.32 (7)	87.02(1)
6. γ, deg	92.35(2)	105.6 (1)	90.00	90.00
7. Crystal system	triclinic	triclinic	monoclinic	monoclinic
8. Space group	$P\bar{1}$	$P\bar{1}$	$P2_1/C$	$P2_1/n$
9. Molecular weight	1282.00	743.82	294.44	1228.81
10. Z	2	2	4	4
11. V, $Å^3$	2527.41	1245.82	2044.52	4972.76
12 ρ_{calcd}, g,cm^{-3}	1.684	1.982	1.298	1.755
13 ρ_{obsd}, g,cm^{-3}	1.696	1.962	1.288	1.761

Table cont'd.....

Table III-1, CONT'D

	UNIQUE	FESCO	TICEP	RUSH
14. μ, cm^{-1}	61.14	26.45	7.26	14.20
15. Crystal dimensions				
$(100) \rightarrow (\bar{1}00)$	0.10	0.15	0.40	0.10
$(010) \rightarrow (0\bar{1}0)$	0.12	0.14	0.20	0.12
$(001) \rightarrow (00\bar{1})$	0.25	0.15	0.50	0.15
16. Estimated transmission factors %	23-55	———	———	———
B) Parameters related to data collection				
1. Radiation	Mo K_α	Mo K_α	Mo K_α	Mo K_α
2. Scan type	coupled θ-2θ 2.0°/ min	- profile analysis of θ / 2θ scan		1 min/reflection -
3. Rotation axis	010	010	010	010
4. Reflections measured	$\pm h \pm k$ 1	$\pm h \pm k$ 1	$\pm h$ k 1	$\pm h$ k 1
5. Min 2θ, deg	3.5	3.5	3.5	3.5
6. Max 2θ, deg	40.0	40.00	40.00	40.00
7. Std. reflections (after 50 cycles)	6 0 $\bar{1}$ 0 6 0 0 0 4	$\bar{2}$ 4 3 3 4 2 $\bar{6}$ 4 2	0 0 $\bar{6}$ 0 6 0 9 0 0	6 0 $\bar{2}$ 6 4 $\bar{6}$ $\bar{7}$ 1 $\bar{3}$

Table cont'd.....

Table III-1 CONT'D

	UNIQUE	FESCO	TICEP	RUSH
8. variation of Std. %	±4	±3	±4	±3
9. Total of reflections collected	6078	3255	1319	4618
10. Reflections where $I<3\sigma(I)$	4444	2292	867	2785
C) Parameters related to the refinement				
Isotropic Refinement				
Cycles to converge	5	4	5	7
R_F	0.076	0.067	0.145	0.061
R_{FW}	0.097	0.078	0.120	0.071
GOF	3.679	0.967	13.60	4.01
Final Refinement				
Cycles to converge	4	5	5	5
R_F	0.052	0.050	0.126	0.047
R_{FW}	0.066	0.086	0.107	0.0416
GOF	2.168	0.523	10.69	3.525

SECTION IV

PART A THE CRYSTAL AND MOLECULAR SRUCTURE OF CIS-$(\mu_2\text{-}C_6H_5CH_2S)_2Pt_2$-$(C_6H_5CH_2S)_2[CH_3(C_6H_5)P]_2$.

1) INTRODUCTION

Sulphur bonding to transition metal organometallic complexes can be described in terms of a σ bonding interaction involving s and p valence electrons with metal orbitals of appropriate symmetry.

Monoalkyl and aryl mercaptans (SR, R= alkyl and aryl) are found bonded to one, two or three metal atoms using one, three or five electrons, respectively. Complexes with two mercaptide bridges can have either a planar or a folded M_2S_2 ring. Two isomers 1 are possible [41] in the planar case owing to the pyramidal stereochemistry of the sulphur atom.

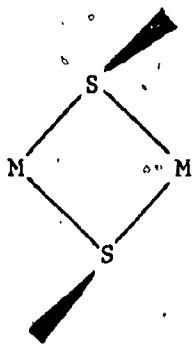

Anti

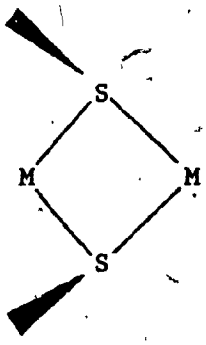

Syn

1

In the folded M_2S_2 rings three geometrical isomers 2 are conceivable although the syn-exo form has not been observed.

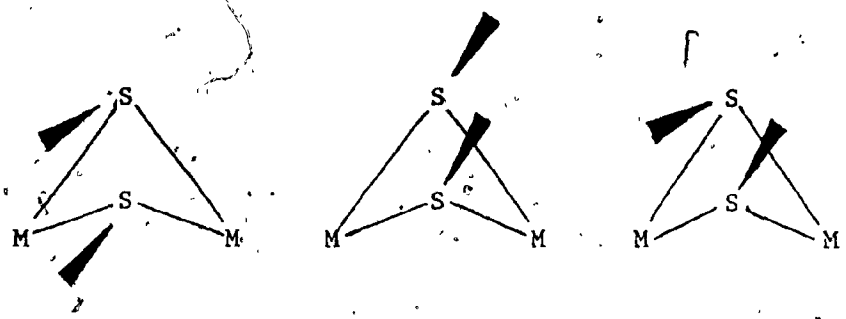

syn-endo syn-exo anti

2

In the past few years many binuclear transition metal complexes with S or SR (R= H, alkyl or aryl) as bridging groups have been prepared and investigated [41-72]. The thio-bridged binuclear complexes are interesting [68] since they exist as cis 3 or trans 4 isomers if there are two different ligands, X and Y, attached to each platinum atom.

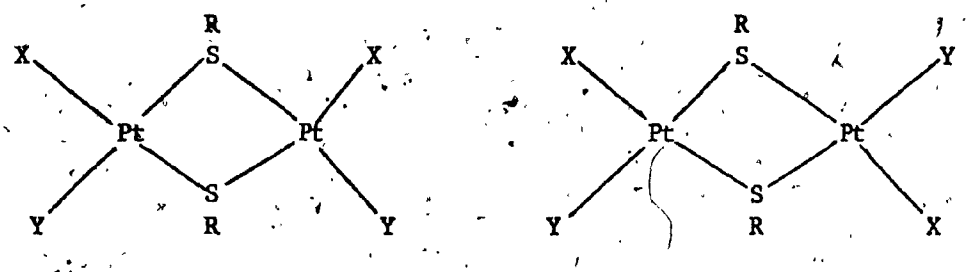

Cis Trans

3 4

In the case of thio-bridged binuclear platinum complexes, the cis configuration seems to be more stable, despite the large amount of associated electrostatic energy (indicated by the high dipole moment of the solutions containing these complexes). Among binuclear platinum complexes bridged by different bridging groups such as chloro-Cl [71], thiocyanato-CNS [71], phosphido-PR_2 and arseno-AsR_2 [69], cis isomers are not known. The stability of cis isomers of thio-bridged platinum complexes are explained in terms of the trans influence of the ligands involved. In cis-$(\mu_2\text{-SEt})_2Pt_2Cl_2(PPr_3)$ [72] the platinum atoms are bridged by SEt groups and the remaining Cl and PPr_3 groups are arranged in the cis configuration 5.

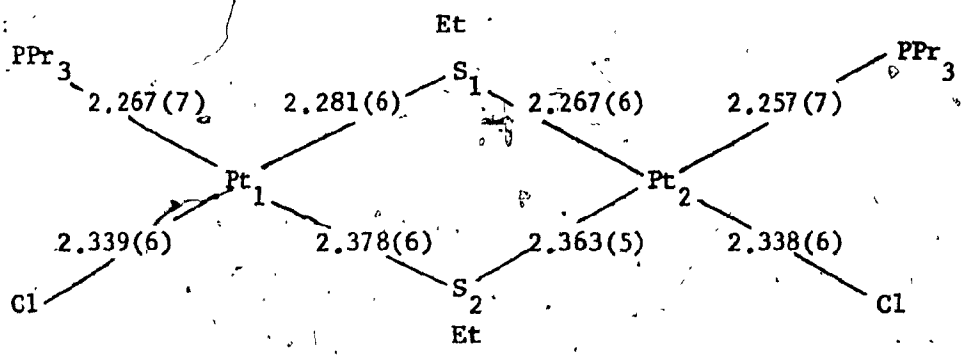

The stronger, hence shorter, Pt-S_1 bonds are formed trans to Cl groups due to lesser trans weakening influence of Cl. In the cis configuration two platinum atoms are held together by two stronger bonds involving the SEt group and the binuclear species is stabilized as shown by the predominance of this configuration in

aqueous solutions. If the molecule adopts the trans configuration the two platinum atoms are held by a weaker and a stronger bond such that the molecule easily dissociates into the mononuclear species.

There is considerable crowding of groups on the two phosphorus atoms and the sulphur atom S_1 as shown by several short non-bonded distances in the molecule. It seems that the stabilization due to the electronic effects in the cis configuration is large enough to overcome the destabilization resulting from this steric crowding. However, the steric effects might overcome the electronic effects if the molecule contains significantly bulkier groups on both the sulphur and phosphorus atoms.

The binuclear platinum complex, $(\mu_2\text{-}C_6H_5CH_2S)_2Pt_2(C_6H_5CH_2S)_2[CH_3(C_6H_5)_2P]_2$ was prepared [73] by vacuum distillation of molten cis-$(C_6H_5CH_2S)_2Pt[CH_3(C_6H_5)_2P]_2$. The X-ray crystallographic studies were undertaken to determine which configuration the complex adopts with these bulky groups.

2) RESULTS AND DISCUSSION

The molecular configuration and the numbering scheme for UNIQUE is shown in Figure IV-A-2-1. The principal molecular distances and angles are listed in Table IV-A-2-1. The positional and thermal parameters of the atoms are listed in Table A-1 of the Appendix A. A packing diagram of the triclinic unit cell containing two molecules of UNIQUE is shown in Figure IV-A-2-2.

The complex is dimeric with two square planar platinum units joined by two mercaptide bridges, Figure IV-A-2-3. The dihedral angle between the two square planes is 138.83°. The deviations of the atoms of the two square planes from the least-squares planes through them are listed in IV-A-2-2. Two benzyl groups, one on each bridging sulphur atom, are arranged in an anti configuration. The most significant feature is the arrangement of the remaining two benzylthiolate and diphenylmethylphosphine groups around the folded Pt_2S_2 ring: this was found to be cis. Thus, in spite of the bulky ligands in UNIQUE, the cis configuration seems to remain stable. The structure of the molecule is similar to cis-$(\mu_2\text{-SEt})_2Pt_2(PPr_3)_2Cl_2$ [72].

In other known planar complexes, $[Pd(SPr)_2]_6$ [61], $[Pd(SC_2H_4OH)_2]_6$ [62], $[Ni(SC_2H_4OH)_2]_6$ [62] and $[Ni(SEt)_2]_6$ the

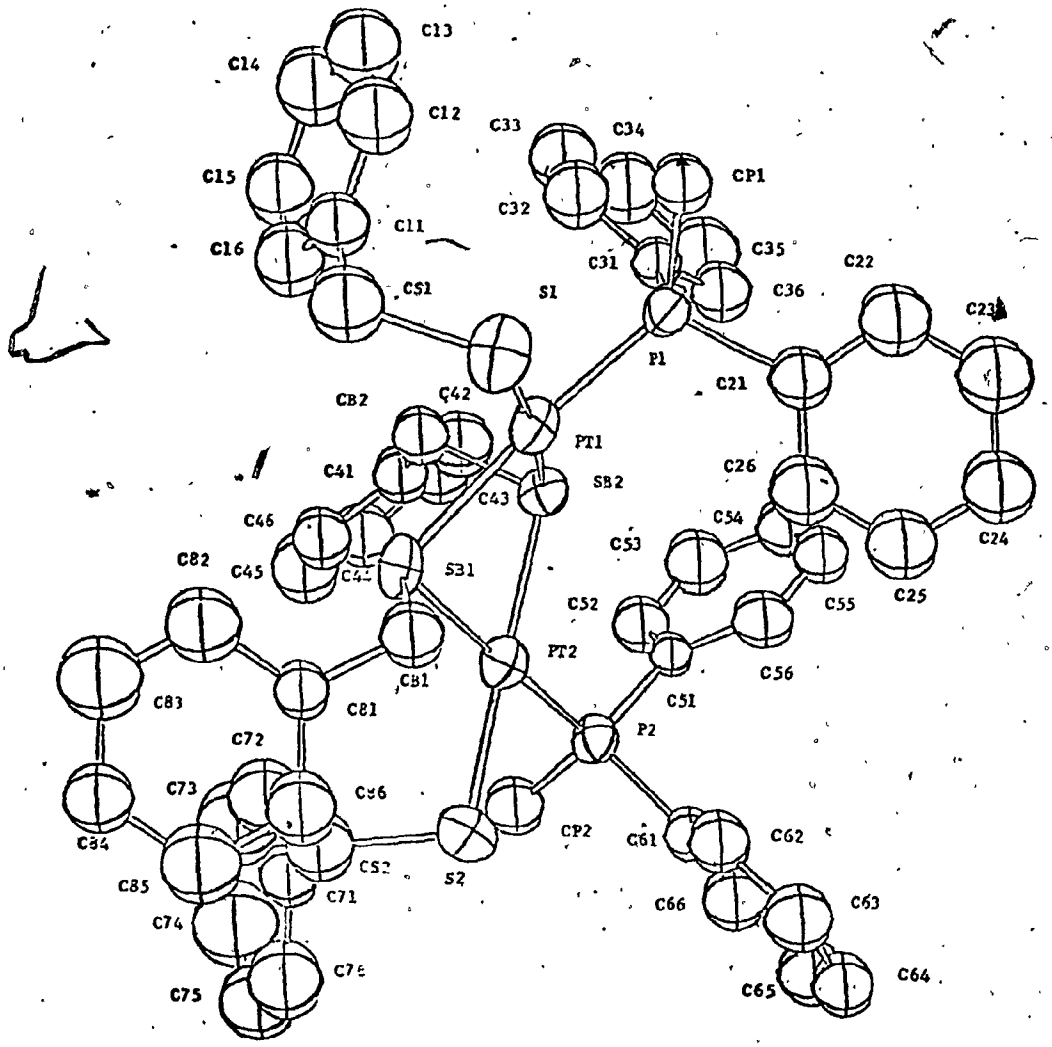

Figure IV-A-2-1. The molecular configuration and the numbering scheme for UNIQUE.

Table IV-A-2-1

Principal Bond Lengths(Å) and Angles(deg) for UNIQUE

Bond Lengths

Pt_1-P_1	2.250(4)	P_1-CP_1	1.84(2)	SB_1-CB_1	1.82(2)
Pt_2-P_2	2.245(4)	P_2-CP_2	1.88(2)	SB_2-CB_2	1.85(2)
Pt_1-S_1	2.342(5)	P_1-C_{21}	1.82(1)	CB_1-C_{81}	1.53(2)
Pt_2-S_2	2.317(5)	P_1-C_{31}	1.82(1)	CB_2-C_{41}	1.48(2)
Pt_1-SB_1	2.380(4)	P_2-C_{51}	1.83(1)	CS_1-C_{11}	1.52(2)
Pt_2-SB	2.380(4)	P_2-C_{61}	1.83(1)	CS_2-C_{71}	1.48(2)
Pt_1-SB_2	2.322(4)	S_1-CS_1	1.88(2)		
Pt_2-SB_2	2.323(4)	S_2-CS_2	1.84(2)		

Bond Angles

Pt_1-SB_1-Pt_2	89.3(1)	Pt_1-SB_1-CB_1	106.5(6)
Pt_1-SB_2-Pt_2	92.2(1)	Pt_2-SB_1-CB_1	109.9(5)
		Pt_1-SB_2-CB_2	98.7(5)
P_1-Pt_1-SB_2	91.3(2)	Pt_2-SB_2-CB_2	106.9(5)
P_2-Pt_2-SB_2	97.0(1)		
P_1-Pt_1-SB_1	170.8(2)	SB_1-CB_1-C_{81}	113(1)
P_2-Pt_2-SB_1	177.3(2)	SB_2-CB_2-C_{41}	111.8(1)
S_1-Pt_1-SB_1	94.5(2)	Pt_1-P_1-CP_1	117.9(5)
S_2-Pt_2-SB_1	96.5(2)	Pt_1-P_1-C_{21}	110.8(4)
S_1-Pt_1-SB_2	173.1(2)	Pt_1-P_1-C_{31}	112.2(4)
S_2-Pt_2-SB_2	174.4(2)	Pt_2-P_2-CP_2	112.8(5)
		Pt_2-P_2-C_{51}	115.2(4)
P_1-Pt_1-S_1	94.1(2)	Pt_2-P_2-C_{61}	114.1(4)
P_2-Pt_2-S_2	86.2(2)		
SB -Pt -SB	80.4(1)	S -CS -C	111(1)
SB -Pt -SB	80.2(1)	S -CS -C	113(1)

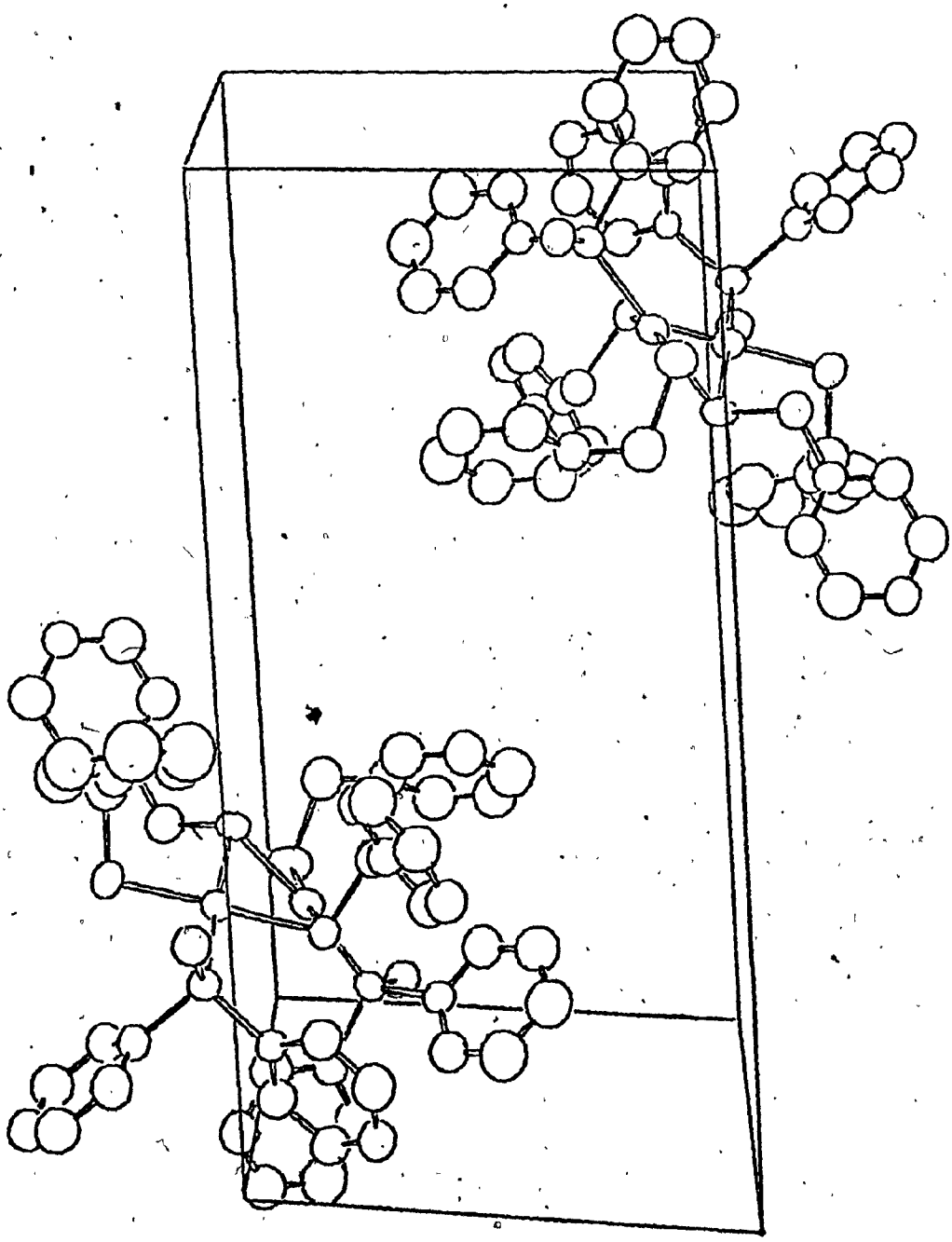

Figure IV-A-2-2. An illustration of the unit cell packing diagram containing two molecules of UNIQUE as viewed down the b axis.

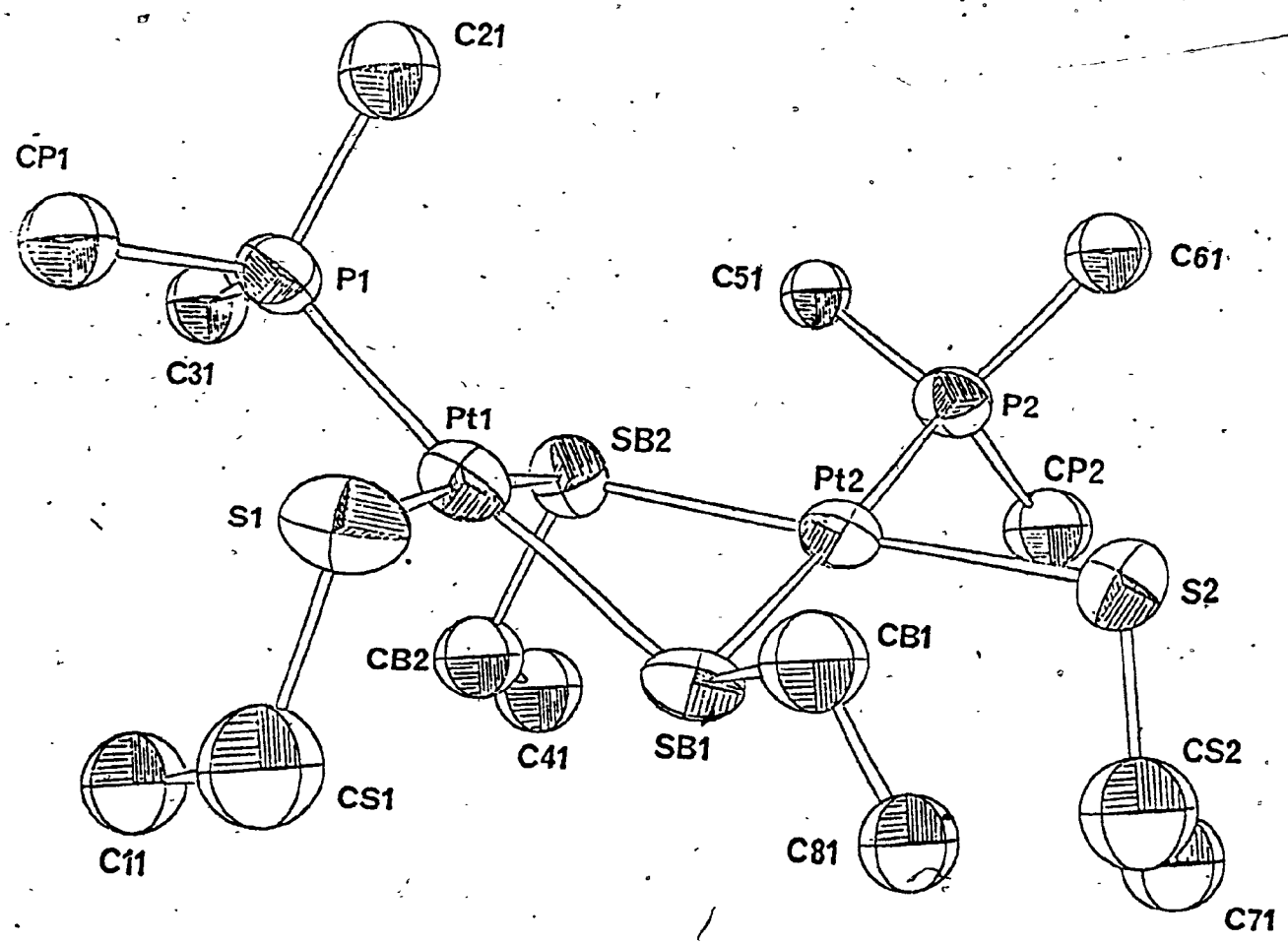

Figure IV-A-2-3. The configuration of UNIQUE excluding phenyl rings.

Table IV-A-2-2 The deviations of the atoms forming two square planes in UNIQUE from the least-squares planes through them.

Atoms defining the planes	Deviations (Å) of atoms from the plane				
	Pt_1	S_1	P_1	SB_1	SB_2
Pt_1, S_1, P_1, SB_1, SB_2	-.00795	.07661	-.07707	-.08096	.08938
	Pt_2	S_2	P_2	SB_1	SB_2
Pt_2, S_2, P_2, SB_1, SB_2	-.03866	.052816	-.03383	-.03580	.05468

dihedral angle is constrained to be 120° by the cyclic hexameric structures and in $[Ru(SC_6H_5)CO\ P(CH_3)_3]_2$ [64], $[Pt(SEt)\ (PPr_3)\ Cl]_2$ [72], $[RhCl(CO)(PMe_2Ph)]_2$ [64] and $C_8H_{12}Rh_2Cl_2[P(OPh)_3]$ [65], the dihedral angles are 113°, 130°, 123°, and 122°, respectively. The large value of the dihedral angle, 138.38°, in UNIQUE can be attributed to the steric hindrance due to the bulkier phenyl groups on phosphine and thiolate ligands.

In additon, angles in the two square planes P_1-Pt_1-SB_2, P_2-Pt_2-SB_2, S_1-Pt_1-SB_1 and S_2-Pt_2-SB_2 are increased to 91°, 92°, 94° and 96°, respectively, to accomodate the bulky phenyl groups.

The adoption of the anti configuration in the distribution of two bridging benzylthiolate ligands minimizes the crowding. The angles at the bridging sulphur atoms, Pt_1-SB_1-Pt_2 and Pt_1-SB_2-Pt_2 are 89° and 92°, respectively. In $cis(\mu_2\text{-}SEt)_2Pt_2(PPr_3)_2Cl_2$ similar angles were 85° and 89°, respectively. The increase in these angles again shows the results of steric effects.

Two stronger hence shorter Pt-S bonds, Pt_1-SB_2 (2.322Å) and Pt_2-SB_2 (2.323Å) are formed compared to two longer Pt-S bonds, Pt_1-SB_1 (2.380Å) and Pt_2-SB_1 (2.380Å). This is expected since the trans influence of PR_3 ligands is weaker than that from sulphur ligands [66]. Similar observations have been made in the complex, $cis(\mu_2\text{-}SEt)_2Pt_2(PPr_3)_2Cl_2$, where the average shorter and longer Pt-S bonds are found to be 2.274Å and 2.371Å, respectively.

The Pt-P distances, 2.250(4) and 2.245(4)Å, were similar to the Pt-P bond distances found in cis-$(\mu_2\text{-SEt})_2Pt_2(PPr_3)_2Cl_2$ but were longer than those observed for complexes with bridging chlorine atoms [71].

The P-C, S-C and C-C single bond distances, 1.82-1.88, 1.82-1.88 and 1.48-1.53Å, respectively, found in phosphine and benzylthiolate ligands are all in the range reported [67] for similar ligands.

PART B THE CRYSTAL AND MOLECULER STRUCTURE OF $Fe_4(CO)_{12}[S(C_6H_4)CS_2]$

1) INTRODUCTION

The complex, $Fe_4(CO)_{12}[S(C_6H_4)CS_2]$ - FESCO, is a cluster of four iron atoms which are held by iron-iron bonding and bridging sulphur and carbon atoms. The bonding mode adapted by the dithiocarboxylate part of the $S(C_6H_4)CS_2$ ligand in the molecule is unusual and it seems to be the first dithiocarboxylate complex to have such a bonding mode. In this molecule sulphur exemplifies its varied [74] ability to coordinate with transition metals giving rise to clustered species. The interest in these cluster species has been increased during the past few years due to the presence of similar species in biological systems [75]. A great deal of attention has been focused recently on the synthesis and structural characterization of metal cluster compounds because of their potential application as models for the active sites in non-heme iron proteins such as ferrodoxins. In this section, brief introductions to the sulphur ligands, and the nature of the transition metal-carbon bond are presented to define the terms involved in the discussion of the molecule.

Dithiolates

The bidentate unsaturated sulphur donor chelating ligands such as 1,1 dithiols 6 and 1,2 dithiols 7 are found to form complexes with transition metals. More emphasis will be given

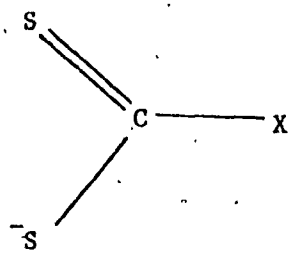

6

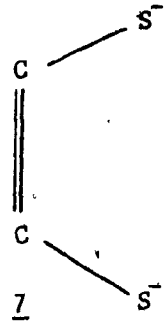

7

to the former since the title compound FESCO has o-mercaptodithiobenzoate 8 as one of the ligands.

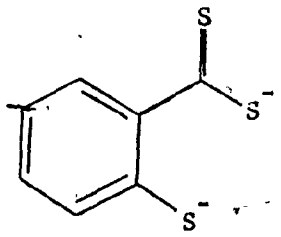

8

The formation of four membered rings 9 are common in transition metal 1,1 dithiolate complexes.

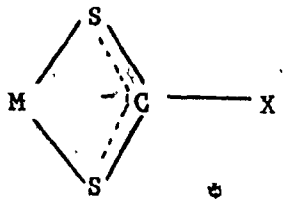

9

X may be $SCNR_2$- dithiocarbamate, S_2COR- xanthate and $S_2CC_6H_5$- dithiobenzoate.

The π molecular orbitals of the 1,1 dithiolate ligand are perpendicular to the plane containing C-CS_2 unit 10.

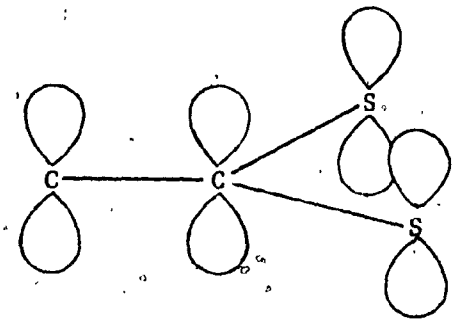

10

These molecular orbitals are delocalized over the chelating part of the ligand and they could overlap with the metal dπ orbitals of appropriate symmetry. Nevertheless, π bonding in 1,1 dithiolate system is found to be less important than in analogous 1,2 dithiolate systems [76] and the metal-sulphur distances are longer than those in 1,2 dithiolates.

The literature concerning the chemistry of transition metal 1,1 dithiolate complexes has been reviewed up to 1968 by Coucouvanis [76] and recently (up to 1979) by McCullogh [77]. Two iron complexes with dithiocarboxylate complexes of iron (III) are $Fe(C_6H_5CS_2)_3$, the dithiobenzoate, and $Fe(p\text{-}MeC_6H_4CS_2)_3$, the dithiotoluate. "Sulphur rich" $Fe(PhCS_3)_2(PhCS_2)$ and $Fe(p\text{-}MeC_6H_4CS_3)(p\text{-}MeC_6H_4CS_2)_2$ 11 have also been prepared [79]. The crystal structure of the latter shows that the coordination around the iron atom is a distorted octahedron with six sulphur atoms.

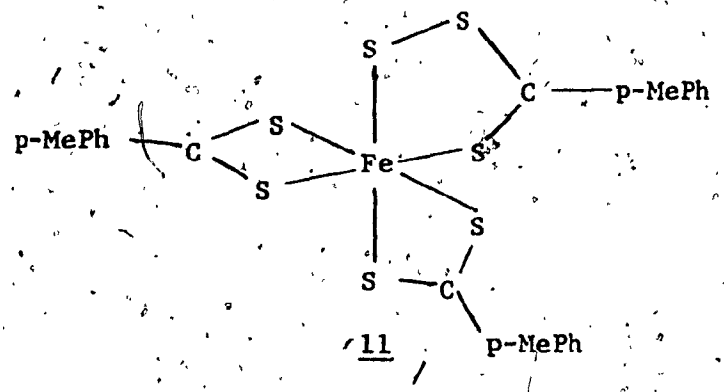

11

Usually 1,1 dithiolate ligands are bidentate. However, some tridentate bridging CS_2 units of the type 12 [80] and 13 [81] have also been reported.

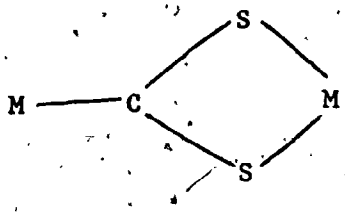

12

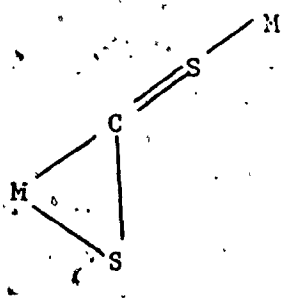

13

Bridging Mercaptides

Bridging mercaptans are found bonded to two and three iron atoms in $(\mu_2\text{-}SCH_3)_2Fe_2(CO)_4[PMe_3]_2$ [82] and $Fe_3(CO)_9(\mu_3\text{-}SPr^i)(\mu_2\text{-}SPr^i)$ [84], respectively. In doubly bridged complexes the Fe_2S_2 core has the typical butterfly configuration 14.

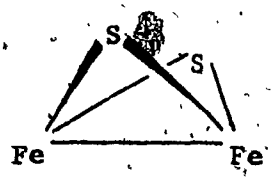

14

Three conformations 15, axial equatorial (ae), axial axial (aa) and equatorial equatorial (ee) are possible[94] for two R groups of the bridging mercaptide ligands in the core Fe_2S_2.

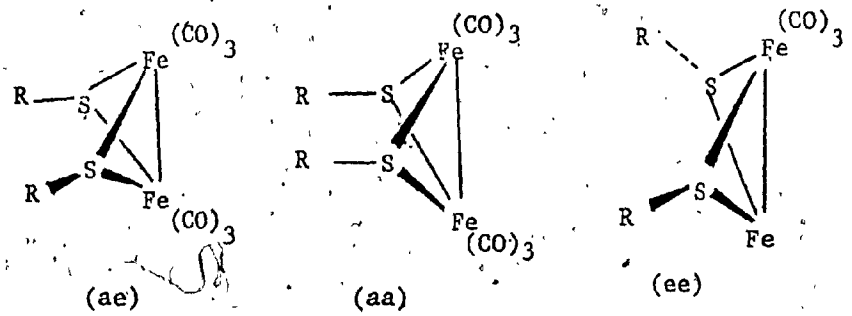

15

The triply bridging SPr^i group has been identified [84] in the complex $Fe_3(CO)_3(\mu_3\text{-}SPr^i)(\mu_2\text{-}SPr^i)$ 16 using the mass, ^1H NMR and IR spectra.

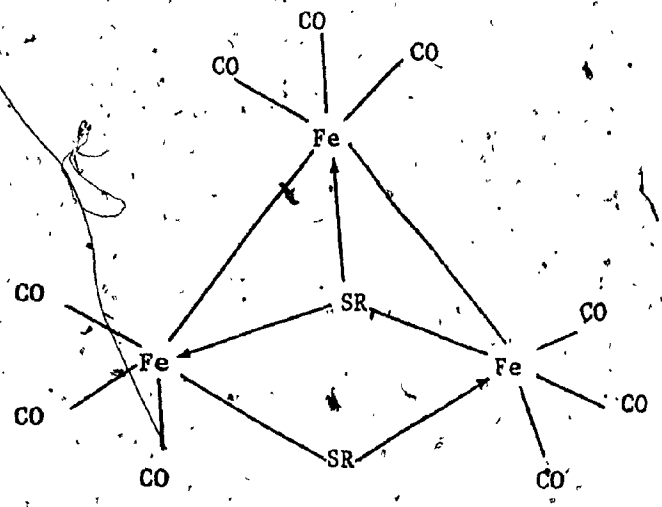

16

Metal-Carbon σ Bonding

Transition metal-carbon σ bonds are less stable than metal-carbon bonds of analogous main group elements. One reason given for this behaviour is the low ionic resonance energy available for the stabilization compared to main group organometallic compounds. This instability may also be due to the availability [85] of several low energy pathways for the decomposition of transition metal-carbon σ bonds. One of the important decomposition pathways is the β elimination giving olefins and the metal hydrides.

The stabilization of the metal-carbon bond in alkyl and aryl containing compounds is found to be different: the greater stability of the aryl metal-carbon bond is explained in terms of π^* interaction of vacant orbitals of the aryl groups with the d electrons of the metal. The involvement of π backbonding makes the metal-carbon bond stronger. The importance of this effect is clearly shown in the case of transition metal carbonyls which are more stable with respect to oxidation and thermal decomposition.

An iron-carbon bond (2.11Å) is found in the complex $(\pi\text{-}C_5H_5)Fe(CO)_2C_5H_5$ [89], where one of the cyclopentadienyl ligands are bonded to the Fe atom through a single carbon atom. The iron-carbon bond lengths reported in the literature vary [89] from 1.89 to 2.16Å giving a average value of 2.078Å.

The complex $Fe_4(CO)_{12}[S(C_6H_4)CS_2]$ - FESCO was prepared[87] as a part of the synthetic investigations directed towards the development of catanated polysulphur ligands, using the reaction:

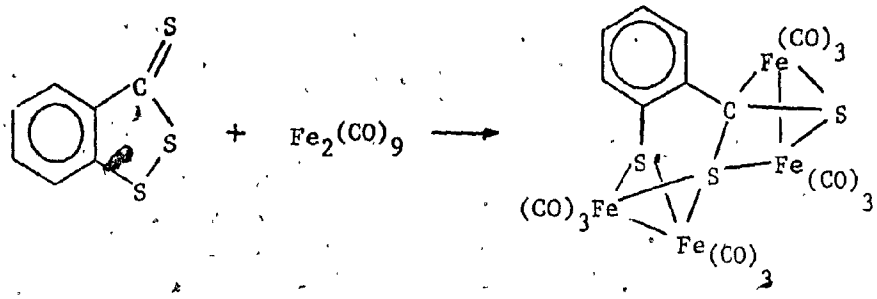

The X-ray crystallogrphic studies on FESCO was undertaken since the structure of the molecule seemed to be too difficult to deduce by conventional spectral techniques.

2) RESULTS AND DISCUSSION

The molecular configuration and the numbering scheme for the complex, $Fe_4(CO)_{12}(SC_6H_4CS_2)$- FESCO, is shown in Figure IV-B-2-1. The principal molecular distances and angles are listed in Table IV-B-2-1. The deviations of atoms Fe_1, Fe_2, Fe_3, Fe_4, S_1, S_2, S_3 and C_1 from the least squares plane through the phenyl ring are listed in Table IV-B-2-2. The positional and thermal parameters for the non-hydrogen atoms of the molecule are listed in Table A-2 of the Appendix A. A packing diagram of the triclinic unit cell containing two FESCO molecules as viewed down a axis is shown in Figure IV-B-2-2. The molecule consists of two $Fe_2(CO)_6$ sub units held together by the $SC_6H_4CS_2$ ligand: the central skeleton is shown in Figure IV-B-2-3.

Sulphur Bridging

The sulphur atom S_2 acts as a triply bridging mercaptide sulphur with Fe-S distances 2.211(3), 2.216(3) and 2.289(3)Å for Fe_1-S_2, Fe_2-S_2 and Fe_4-S_2, respectively. It connects the two $Fe_2(CO)_6$ units. The three iron atoms Fe_1, Fe_2, Fe_4 and carbon C_1 form a tetrahedral array around the S_1. The Fe_3-S_2 distance of approximately 3.0Å is essentially non-bonding.

The other two sulphur atoms S_1 and S_3 behave as doubly bridged mercaptide groups across Fe_1-Fe_2 and Fe_3-Fe_4, respectively.

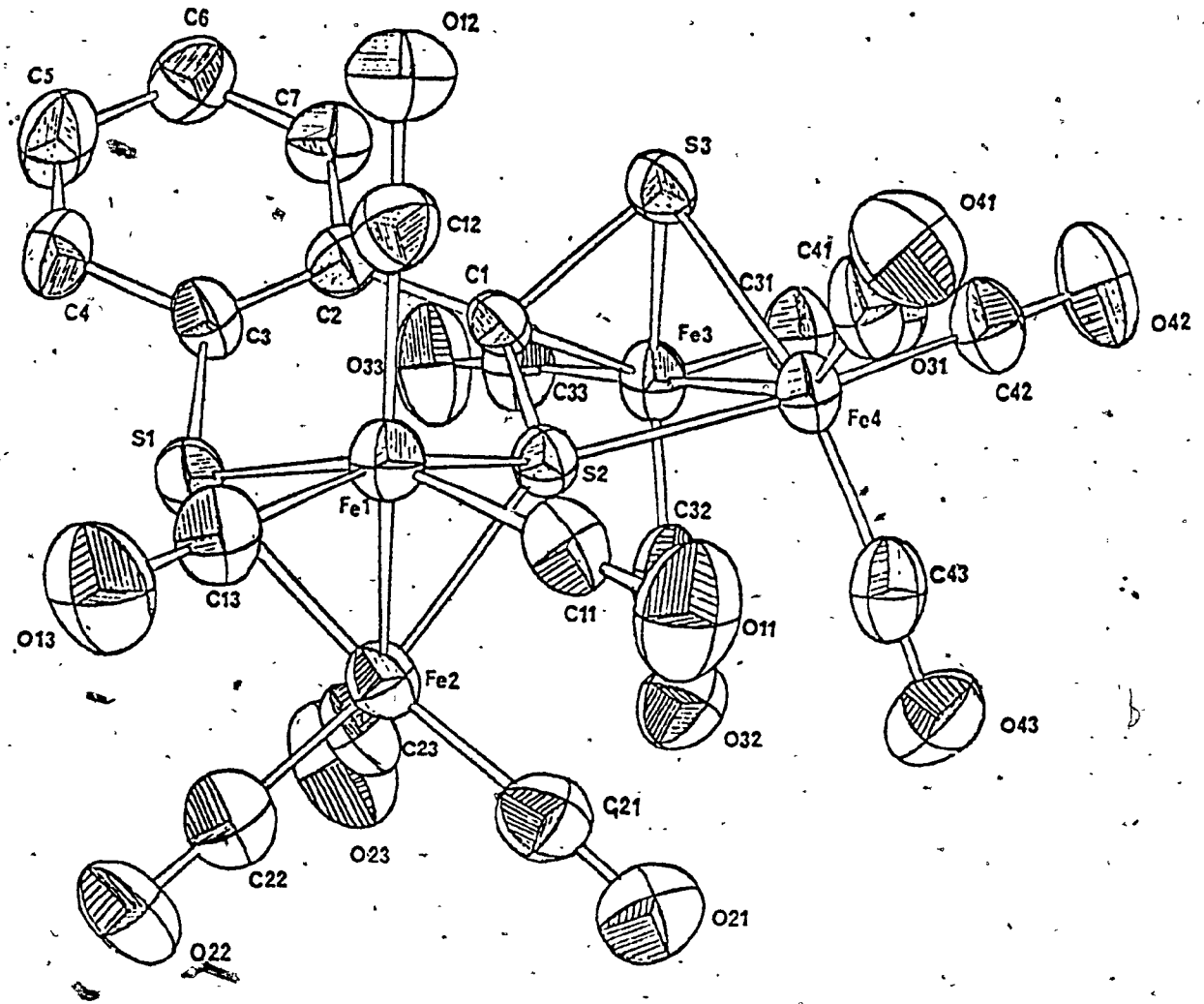

Figure IV-B-2-1. The molecular configuration and the numbering scheme for FESCO.

Table IV-B-2-1 The principal bond distances(Å) and angles(deg) for FESCO.

Bond Distances

Fe_1-Fe_2	2.510(4)	Fe_1-C_{11}	1.769(9)	C_{21}-O_{21}	1.15(1)
Fe_2-Fe_3	2.632(5)	Fe_1-C_{12}	1.807(9)	C_{22}-O_{22}	1.12(1)
		Fe_1-C_{13}	1.790(8)	C_{23}-O_{23}	1.11(1)
Fe_1-S_1	2.250(5)				
Fe_1-S_2	2.211(3)	Fe_2-C_{21}	1.769(9)	C_{31}-O_{31}	1.14(1)
Fe_2-S_1	2.262(5)	Fe_2-C_{22}	1.814(9)	C_{32}-O_{32}	1.17(1)
Fe_2-S_2	2.216(3)	Fe_2-C_{23}	1.804(9)	C_{33}-O_{33}	1.15(1)
Fe_3-C_1	2.055(7)	Fe_3-C_{31}	1.802(8)	C_{41}-O_{41}	1.13(1)
Fe_3-S_3	2.183(4)	Fe_3-C_{32}	1.740(10)	C_{42}-O_{42}	1.11(1)
		Fe_3-C_{33}	1.772(9)	C_{43}-O_{43}	1.16(1)
Fe_4-S_2	2.289(3)				
Fe_4-S_3	2.266(6)	Fe_4-C_{41}	1.816(9)	C_2-C_3	1.38(1)
		Fe_4-C_{42}	1.811(8)	C_2-C_7	1.40(1)
C_1-S_2	1.766(8)	Fe_4-C_{43}	1.765(10)	C_3-C_4	1.42(1)
C_1-S_3	1.791(7)			C_4-C_5	1.36(1)
C_3-S_1	1.780(8)	C_{11}-O_{11}	1.15 (1)	C_5-C_7	1.39(1)
C_1-S_2	1.47 (1)	C_{12}-O_{12}	1.12 (1)	C_6-C_7	1.38(1)
		C_{13}-O_{13}	1.14 (1)		

Bond Angles

Fe_3-C_1-S_2	103.0 (4)	C_3-C_2-C_7	89.7 (5)
Fe_3-C_1-C_2	126.1 (5)	C_2-C_3-C_4	120.7 (7)
Fe_3-C_1-S_3	68.8 (3)	C_3-C_4-C_5	119.2 (8)
S_2-C_1-C_2	122.5 (5)	C_4-C_5-C_6	121.4 (8)
S_2-C_1-C_3	104.6 (4)	C_5-C_6-C_7	118.9 (8)
C_3-C_1-C_2	118.6 (5)	C_2-C_7-C_6	121.4 (8)

IV-B-2-1 Cont'd.

Bond Angles

C_{11}-Fe_1-Fe_2	99.0 (3)	C_{31}-Fe_3-Fe_4	104.0 (3)
C_{11}-Fe_1-C_{12}	100.5 (4)	C_{31}-Fe_3-C_{33}	94.0 (4)
C_{11}-Fe_1-S_2	90.9 (3)	C_{31}-Fe_3-S_3	103.0 (3)
C_{11}-Fe_1-C_{13}	92.7 (4)	C_{31}-Fe_3-C_2	99.1 (4)
C_{12}-Fe_1-S_2	99.5 (3)	C_{32}-Fe_3-Fe_4	87.3 (3)
C_{12}-Fe_1-S_1	105.0 (3)	C_{32}-Fe_3-C_{33}	96.1 (5)
C_{12}-Fe_1-C_{13}	99.6 (4)	C_{32}-Fe_3-C_1	107.3 (4)
C_{13}-Fe_1-Fe_2	103.6 (3)	C_{33}-Fe_3-S_3	115.9 (4)
C_{13}-Fe_1-S_1	86.6 (3)	C_{33}-Fe_3-C_1	93.0 (4)
S_1-Fe_1-Fe_2	56.4 (7)	C_1 -Fe_3-S_3	49.9 (2)
S_1-Fe_1-S_2	81.32(1)	S_3-Fe_3-Fe_4	55.2 (1)

C_{21}-Fe_2-Fe_1	103.5 (3)	C_{41}-Fe_4-S_2	95.4 (3)
C_{21}-Fe_2-C_{22}	90.7 (4)	C_{41}-Fe_4-S_3	99.9 (3)
C_{21}-Fe_2-S_2	93.0 (3)	C_{41}-Fe_4-C_{42}	95.4 (4)
C_{21}-Fe_2-C_3	98.8 (5)	C_{41}-Fe_4-C_{43}	102.6 (4)
C_{22}-Fe_2-S_1	85.5 (3)	C_{42}-Fe_4-Fe_3	91.9 (3)
C_{22}-Fe_2-Fe_1	96.9 (3)	C_{42}-Fe_4-S_3	93.7 (3)
C_{22}-Fe_2-C_{23}	99.9 (4)	C_{42}-Fe_4-C_{43}	89.5 (4)
C_{23}-Fe_2-S_1	102.9 (4)	C_{43}-Fe_4-Fe_3	104.7 (3)
C_{23}-Fe_2-S_2	106.9 (3)	C_{43}-Fe_4-S_2	96.3 (3)
S_1 -Fe_2-Fe_1	56.0 (1)	Fe_3-Fe_4-S_3	52.3 (2)
S_1 -Fe_2-S_2	81.0 (1)	Fe_3-Fe_4-S_2	74.8 (1)

Table IV-B-2-2.

The least squares plane through the phenyl ring containing C_2, C_3, C_4, C_5, C_6 and C_7 in FESCO and the deviations of Fe_1, Fe_3, Fe_4, S_1, S_2, S_3 and C_1 atoms from this plane.

Atom	Fe_1	Fe_2	Fe_3	Fe_4	S_1	S_2	S_3	C_1
Deviation from the plane (Å)	-1.53004	.958382	1.242219	-.610070	-.061007	-.270646	-.90685	.008571

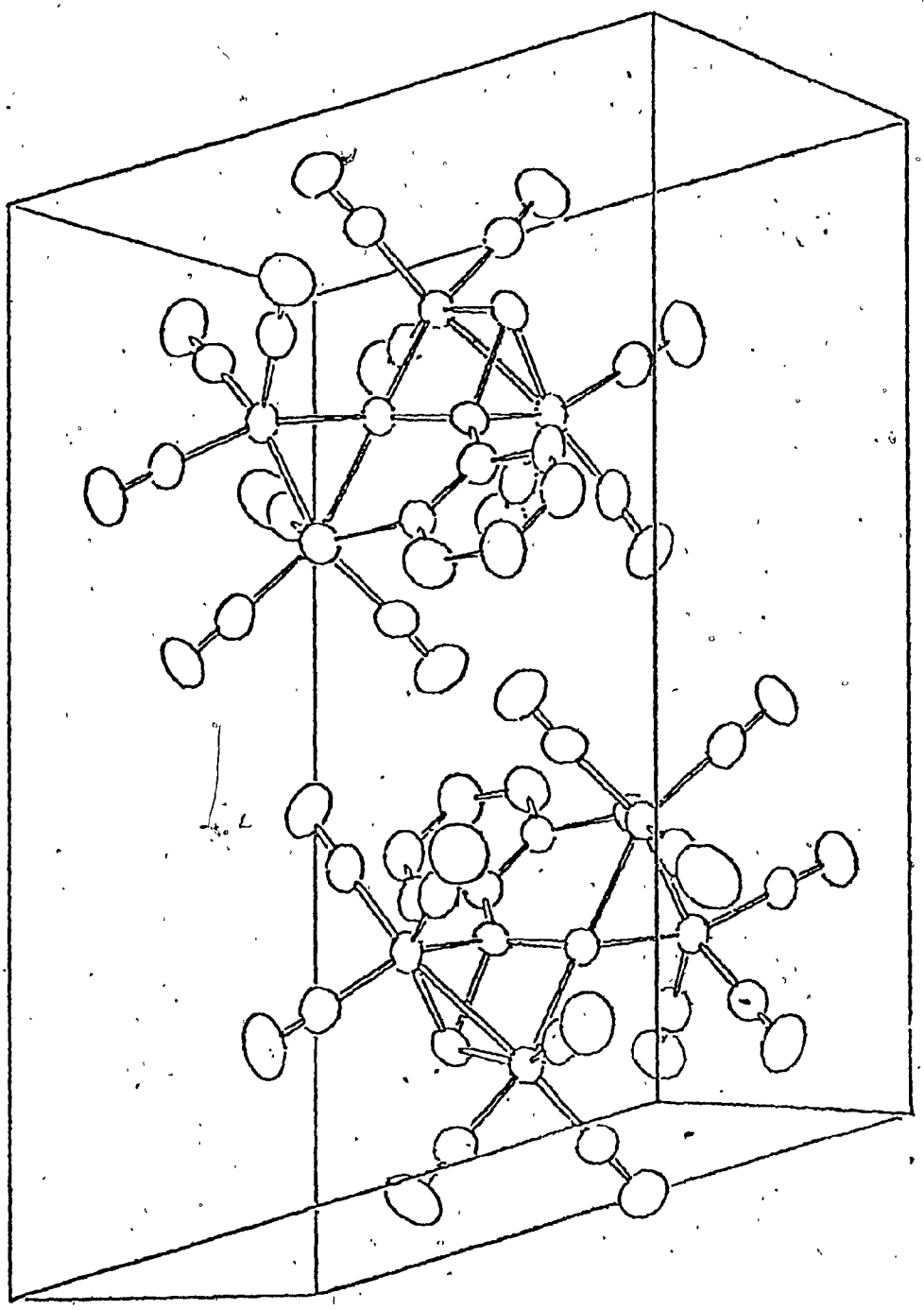

Figure IV-B-2-2. The triclinic unit cell packing diagram containing two FESCO molecules as viewed down a axis.

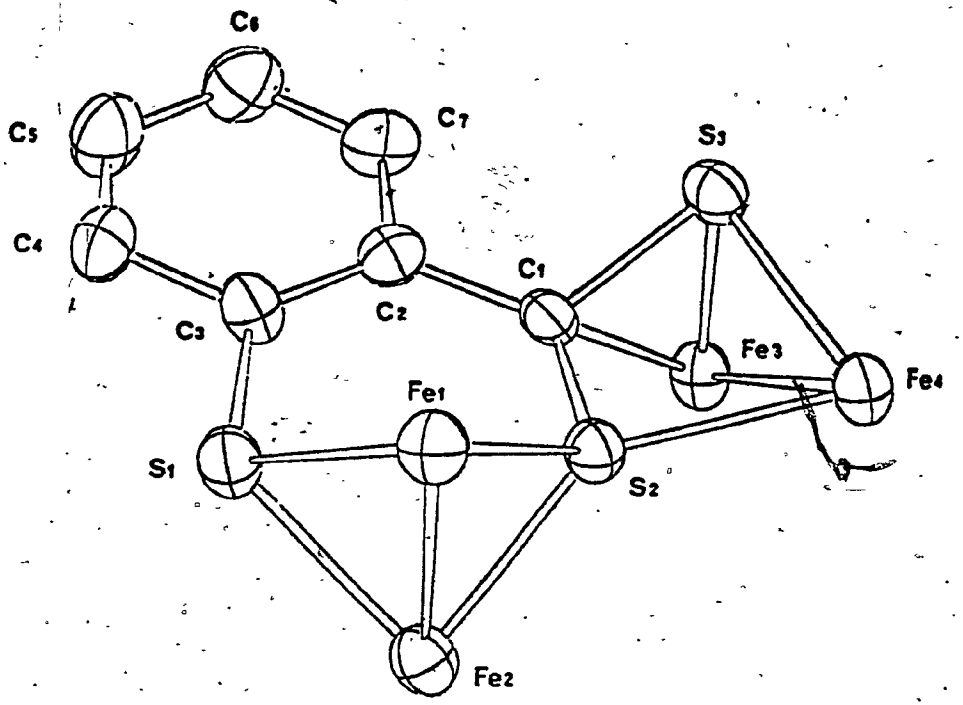

Figure IV-B-2-3. An illustration of the central skeleton of FESCO excluding carbonyl groups.

The Fe_1-S_1 (2.250), Fe_2-S_1 (2.262) and Fe_3-S_3 (2.266Å) bond lengths are within normal range [82]; however, the Fe_3-S_3 distance is a little shorter than expected.

Fe-Fe Bonding

The Fe_1-Fe_2 bond distance, 2.510(4)Å, is within the normal range [83] of 2.485-2.552Å for similar Fe-Fe distances found in the butterfly Fe_2S_2 core. The Fe_3-Fe_4 bond distance (2.623(5)Å) is slightly longer perhaps due to the unusual bonding shown by the carbon atom C_1 described below.

Coordination Around C_1

The most interesting feature of the molecule is the attachment of C_1 to Fe_3 atom, Figure IV-B-2-4-a and Figure IV-B-2-4-b. The Fe_3-C_1 distance (2.055(7)Å) is within the range (1.89-2.13Å) of a single Fe-C bond [97]. The C_1-S bond distances are somewhat shorter than expected (1.82-1.85Å) for C-S single bond distances and yet longer than those measured (1.69-1.71Å) in dithiocarboxylate complexes [88], where a delocalized π system over the three atoms of the CS_2 unit has been postulated.

The $S(C_6H_4)CS_2$ ligand is not planar as expected, but S_3 and S_2 are displaced (Table IV-B-2-1) by 0.91 and 0.27Å

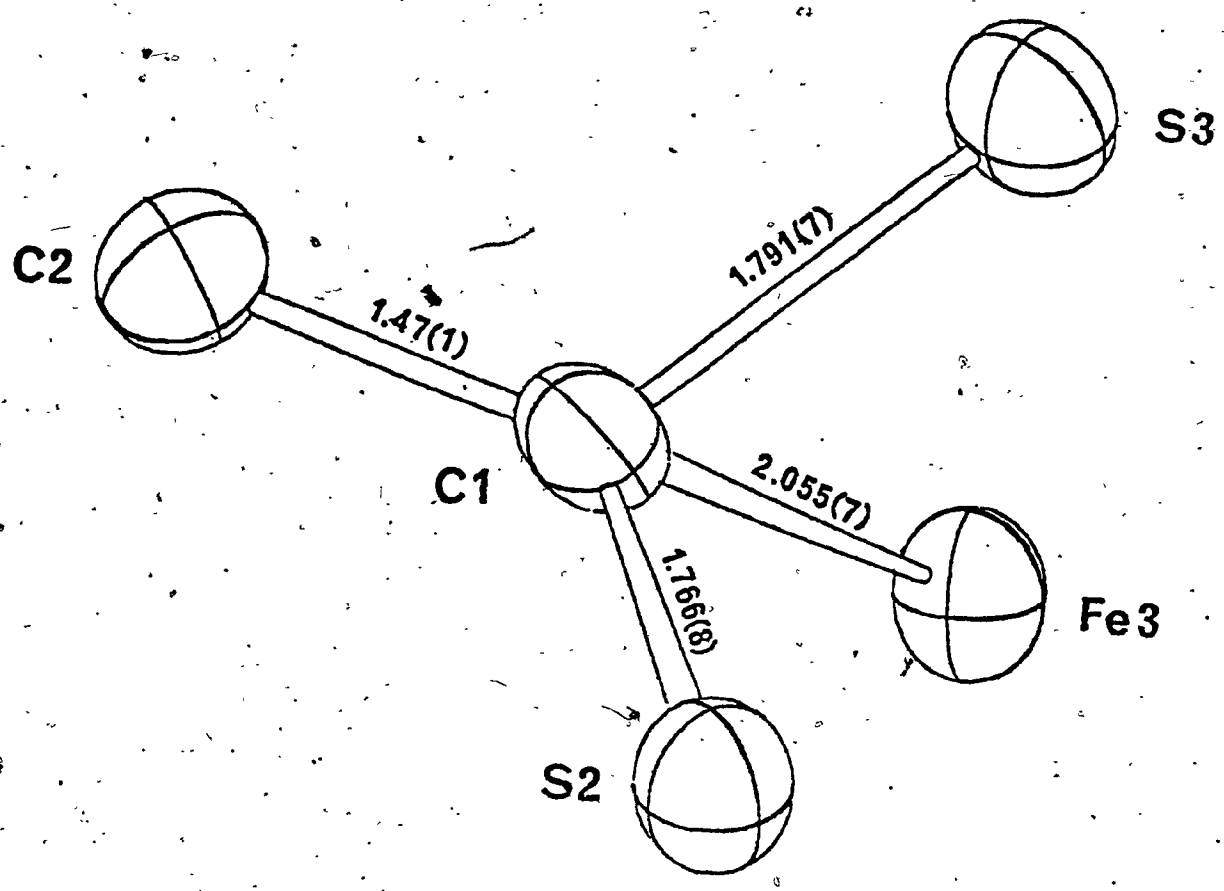

Figure IV-B-2-4-a. An illustration of coordination around C_1 atom and bond distances (Å).

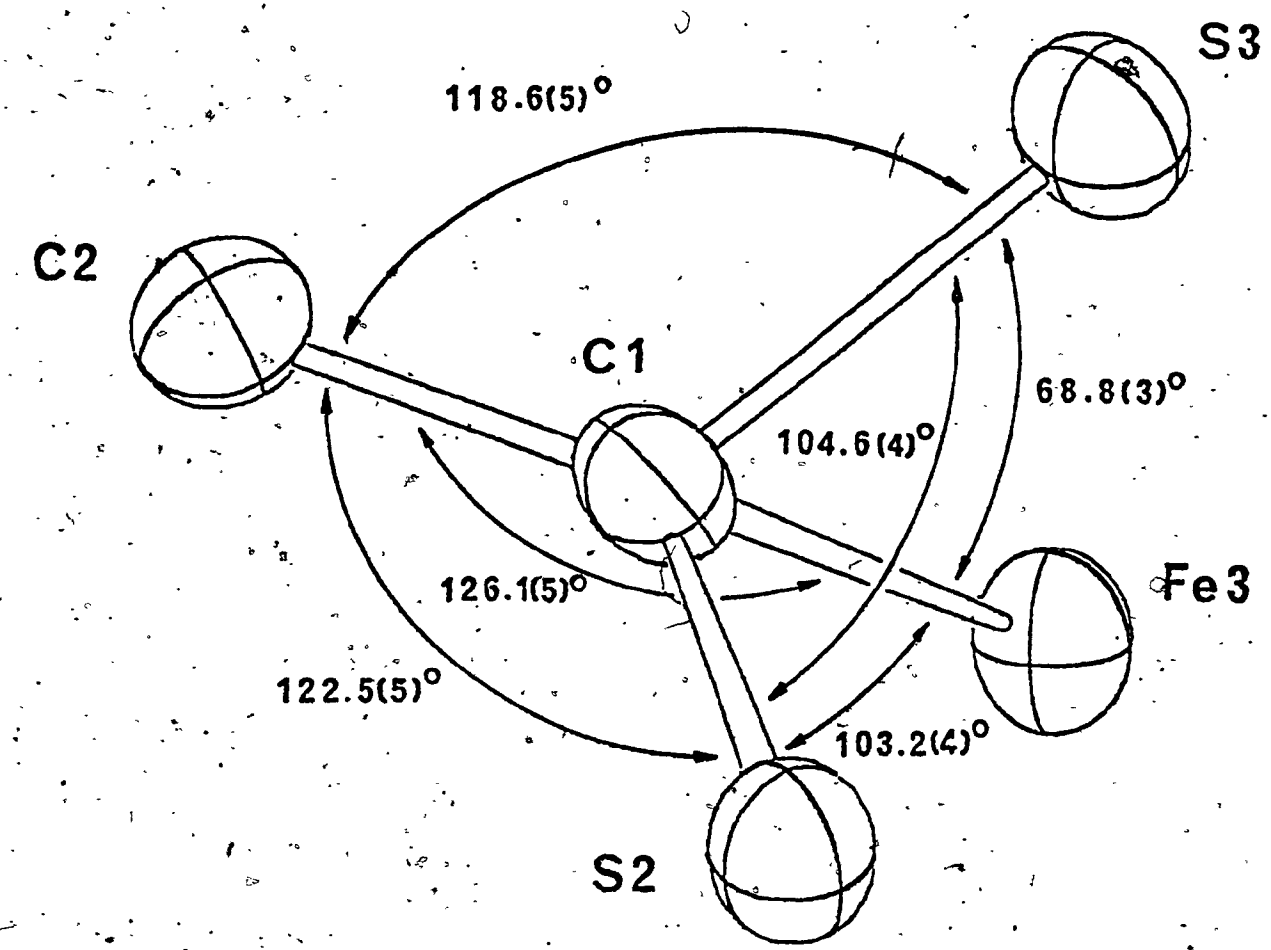

Figure IV-B-2-4-b. An illustration of coordination around C_1 and the bond angles (deg).

respectively, from the plane formed by the phenyl ring. The S-C distance (1.780(8)Å) and the phenyl C-C distances (1.36-1.42Å) of the phenyl mercaptide part of the ligand is in the same range observed, 1.745-1.790 and 1.35-1.46Å distances, respectively, for a similar ligand in the complex $[Rh(SC_6H_5)(CO)PMe_3]_2$ [64].

The carbon atom C_1 can be regarded as an alkyl group with respect to Fe_3 completing its coordination sphere with three other bonds to S_3, C_2 and S_2, Figure IV-B-2-4. The dithiocarboxylate part of the $S(C_6H_4)CS_2$ is tetradentate and attached to four metal atoms whereas this type of ligand is usually bidentate. This novel form of bonding seems to have affected the Fe_3-Fe_4 bond which is slightly longer than expected; Fe_3-S_3 which is a little shorter and Fe_4-S_2 which is a little longer than usual.

PART C THE CRYSTAL AND MOLECULAR STRUCTURE OF $[\eta^5C_5(CH_3)_5]_2TiS_3$

1) INTRODUCTION

The complex, $[\eta^5C_5(CH_3)_5]_2TiS_3$- TICEP belongs to a class of compounds which have bent metal bis-cyclopentadienyl fragment as a common feature. The trisulphide ligand of the molecule acts as a bidentate ligand forming a four membered metallacycle with the titanium, a fragment previously undescribed. This section, therefore, consists of a general introduction to the nature of bonding in bent bis-cyclopentadienes and the stereochemistry of both sulphur homocycles and heterocycles. Sulphur homocycles are included because of their close remsemblance to the heterocycles containing a transition metal.

Sulphur Rings

Although elemental sulphur has been extensively studied, the factors that determine chain length and ring size are poorly understood [90-91]. Pure sulphur rings with n= 6,7,8,10,12,18 and 20 are known [90]. They are fairly unstable compounds and readily form equilibrium mixtures of various chain lengths. The sulphur rings and chains are in a zig-zag arrangement since each sulphur atom has two pairs of electrons preventing the free rotation around the S-S bond. The torsion angle γ of a S_1-S_2-S_3-S_4 fragment is defined

as the angle between two planes 17 containing $S_1S_2S_3$ and $S_2S_3S_4$:

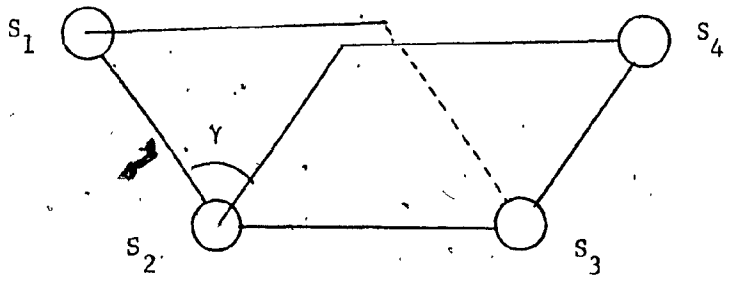

17

In disulphane H_2S_2, there is practically no steric hindrance between the two hydrogen atoms. The torsion angle γ is about 100°. In S_8 [90] which is the most stable of the sulphur homocycles, γ is about 98° and the eight sulphur atoms are arranged in a crown shaped molecule 18.

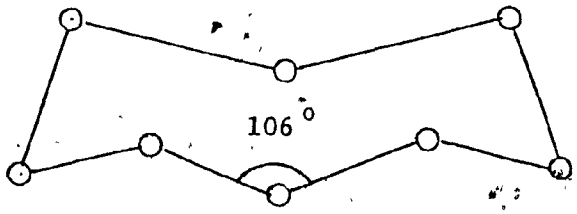

18

The relative stability of S_8 compared to other sulphur homocycles can be attributed to the favourable torsion angles and S-S-S bond angles. Similar γ and S-S-S angles are found in S_{12} [91] which is comparable to S_8 in stability.

A few transition metal complexes containing a poly-sulphur metallacycle MS_n, where n = 4 or 5 have been reported.

Surprisingly these sulphur heterocycles containing a transition metal are stabilized relative the sulphur homocycles. The relative stability of these sulphur heterocycles by contrast with the instability of pure sulphur rings such as S_6 still requires a convincing explanation.

Sulphur Heterocycles

Polysulphide ions acting as bidentate ligands have been structurally characterized in complexes such as Cp_2MoS_4 [93] Cp_2WS_4 [94], PtS_{15}^{-2} [95], $(PPh_3)_2PtS_4$ [96], Cp_2TiS_5 [97], $CpCo(PMe_3)S_5$ [98] and Cp_2VS_5 [97]. Thus only MS_4 and MS_5 rings have been reported.

The complex $[\eta^5C_5(CH_3)_5]TiS_3$ - TICEP was prepared [99] from $[C_5(CH_3)_5]_2TiCl_2$ and LiS_3. The variable temperature ^1H NMR of TICEP at room temparature in $CDCl_3$ solution has one sharp peak for methyl protons on cyclopentadienyl rings indicating the fluxional behaviour of the molecule. The broadening of the hydrogen peak and the appearence of the double peak of the ratio 1:1 and finally the resolution of the double peak into different methyl resonance frequencies have been observed at -75°, -90° and -130°C, respectively.

Several polymeric structures were proposed for TICEP using the results from elemental analysis. A monomeric structure with four membered metallacycle was the least expected due to the non-exsistance of such species in the literature. The X-ray crystallo-

graphic studies were undertaken on TICEP to assign a unique structure.

Bent Bis-Cyclopentadienes

The bonding in bis-cyclopentadienyl transition metal complexes has been described [100] in terms of the variation of the energy levels of normal or parallel bis-cyclopentadienyl complexes as the angle between two cyclopentadiene rings departs from 180° to form a bent structure 19.

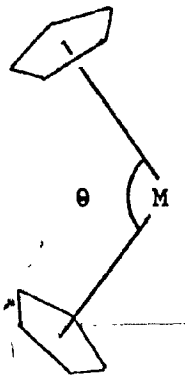

19

The bonding in normal bis-cylopentadienes is well understood [100]. In a D_{5d} geometry where the two $C_5H_5^-$ ligands are in a staggered conformation, the π orbitals of the ligands interact to form three sets of degenerate orbitals which in turn interact with the d orbitals of a transition metal. A schematic interaction diagram of a normal Cp_2M ($C_5H_5^-$ abbreviated as Cp) complex is shown in Figure IV-C-1-1. Ferrocene (Fe^{+2}- d^6) is by far the most stable D_{5d} metallocene since it has the ideal number of eighteen electrons filling the bonding

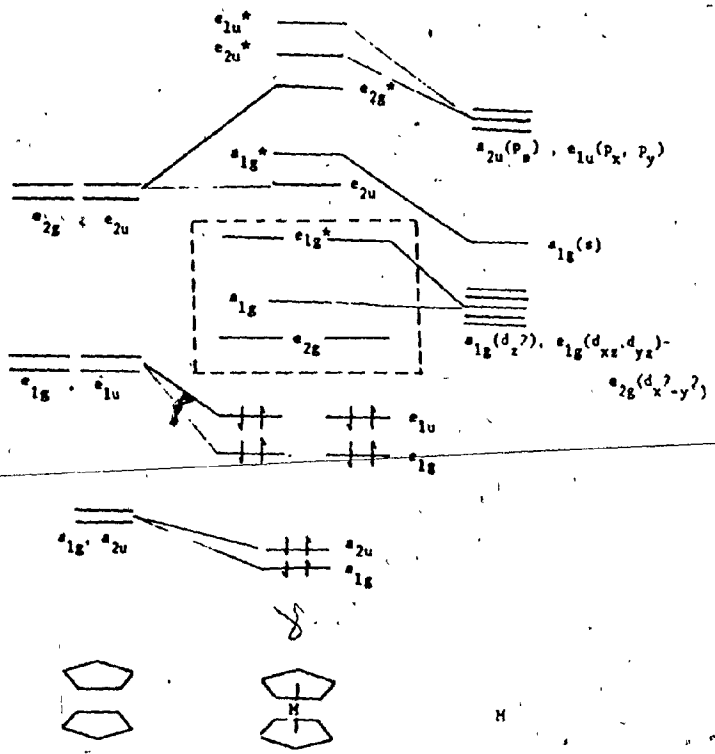

Figure IV-C-1-1. A schematic interaction diagram for a D_{5d} metallocene.

frontier orbitals (a_{1g} and e_{2g}). Cobaltacene and nikelacene are nineteen and twenty electron complexes, respectively, adding electrons to the anti-bonding e^*_{1g} orbital. Addition of extra electrons to the anti-bonding orbitals in these complexes is reflected in their readiness to undergo oxidation. On the other extreme, complexes such as vanadacene (d^3- 15 electrons) and chromocene (d^4- 16 electrons) are electron deficient.

Electron deficient normal bis-cyclopentadienyl complexes can achieve the more stable eighteen electron configuration by combining with additional ligands. The normal Cp_2M unit bends back to accomodate extra ligands. The angle θ between the normals to the Cp_2 unit is less than 180° and the symmetry of the unit changes from D_{5d} to lower symmetry depending on the positions of rings, to C_{2v} if the rings are eclipsed and to C_s if they are staggered. The variation of energy of the $TiCp_2$ orbitals as a function of θ can be computed using the extended Huckle procedure [102]. The basic trend noted as θ departs from 180° is shown in Figure IV-C-1-2. The orbitals a and b descended from e^*_{1g} set are stabilized because of a decrease in the overlap of the metal d orbitals with the filled ligand orbitals, and more importantly, in the C_s symmetry, the d_{xy} and d_{xz} orbitals are now of proper symmetry to interact with two of the empty anti-bonding orbitals of the ligand. The orbitals $1a_1$, b_2 and $2a_1$ descended from a_{1g} and e_{2g} are destabilized as a result of increased anti-bonding as θ departs from 180°. The orbitals $1a_1$, b_2 and

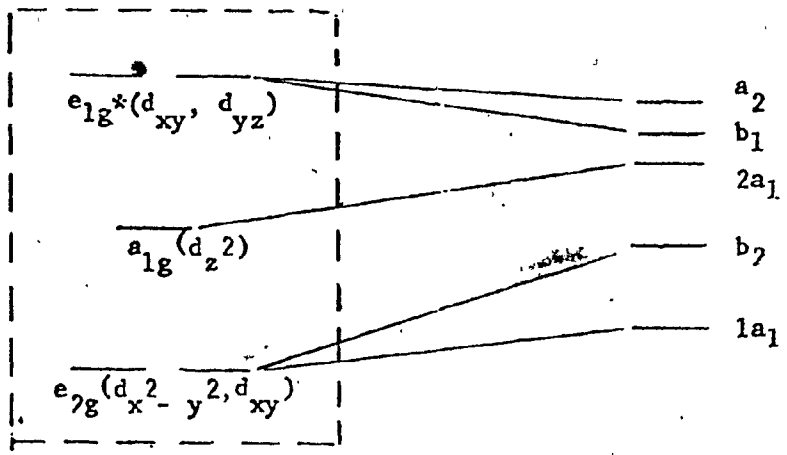

Figure IV-C-1-2. An illustration of relationship between energy levels of a normal and bent MCp_2 unit.

$2a_1$ will play a prime role since the electron deficient Cp_2M systems such as $TiCp_2$, $ZrCp_2$ and VCp_2 have four or fewer electrons. The contour diagram of $2a_1$, b_2 and $1a_1$ orbitals and the interaction diagram of bent Cp_2M orbitals with two donor ligands are shown in the figure IV-C-1-3.

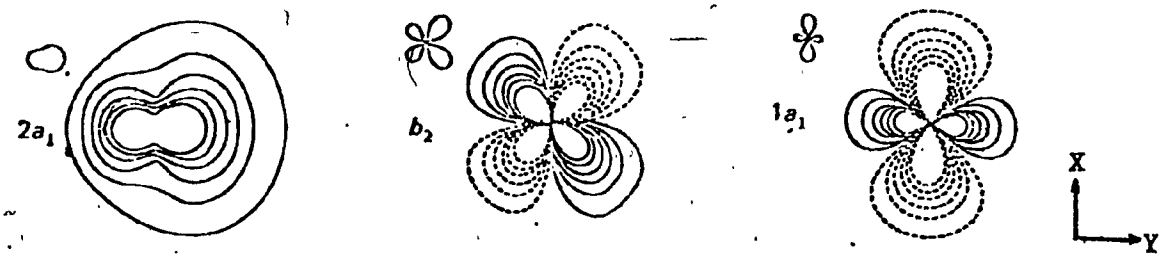

(a)

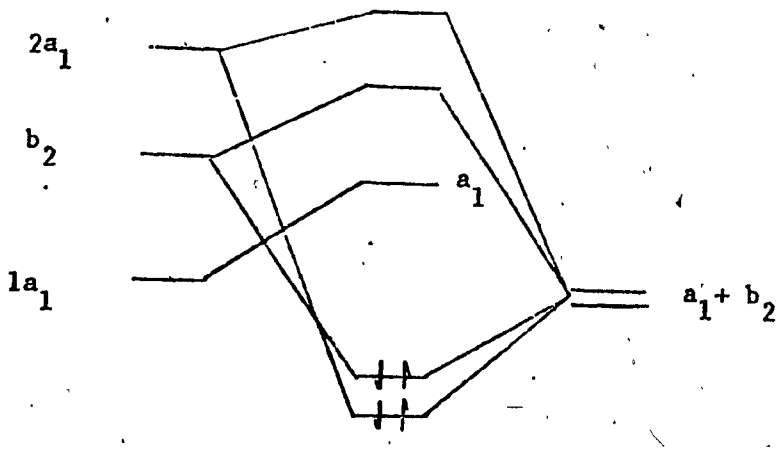

(b)

Figure IV-C-1-3. (a) Contour diagram [100] of $2a_1$, b_2 and $1a_1$ orbitals of bent MCp_2 unit.

(b) Interaction diagram of a bent MCp_2 orbitals with two σ donor ligands.

2) RESULTS AND DISCUSSION

The configuration of the molecule, TICEP and the numbering scheme is shown in Figure IV-C-2-1. The principal molecular distances and angles are listed in Table IV-C-2-1. A packing diagram of the monoclinic unit cell containing four TICEP molecules is shown in Figure IV-C-2-2. The positional and thermal parameters of all non-hydrogen atoms are listed in Table A-3 of the Appendix A.

Ti Tetrahedron

The molecule has a four membered heterocyclic ring in a bent conformation with the bis-η^5pentamethylcyclopentadienyl metal moeity as the heterospecies. The arrangement of the two terminal sulphur atoms (S_1 and S_3) from the trisulphide ligand, and the two centroids (D_1 and D_2) of the cyclopentadienyl rings is a distorted tetrahedron around the titanium atom, Figure IV-C-2-3. The molecule does not have C_{2v} or C_s symmetries since the S_1, S_2 and S_3 atoms are not symmetrically disposed with respect to a mirror plane passing through the mid points of two cyclopentadienyl rings and the metal atom. The deviations of S_1, S_2 and S_3 from the least-squares plane containing Ti, D_1 and D_2 are 1.46, 0.22 and 1.79Å, respectively. The angle between the mid points D_1D_2 and S_1S_3 at the metal atom is 173.82°, Figure IV-C-2-4.

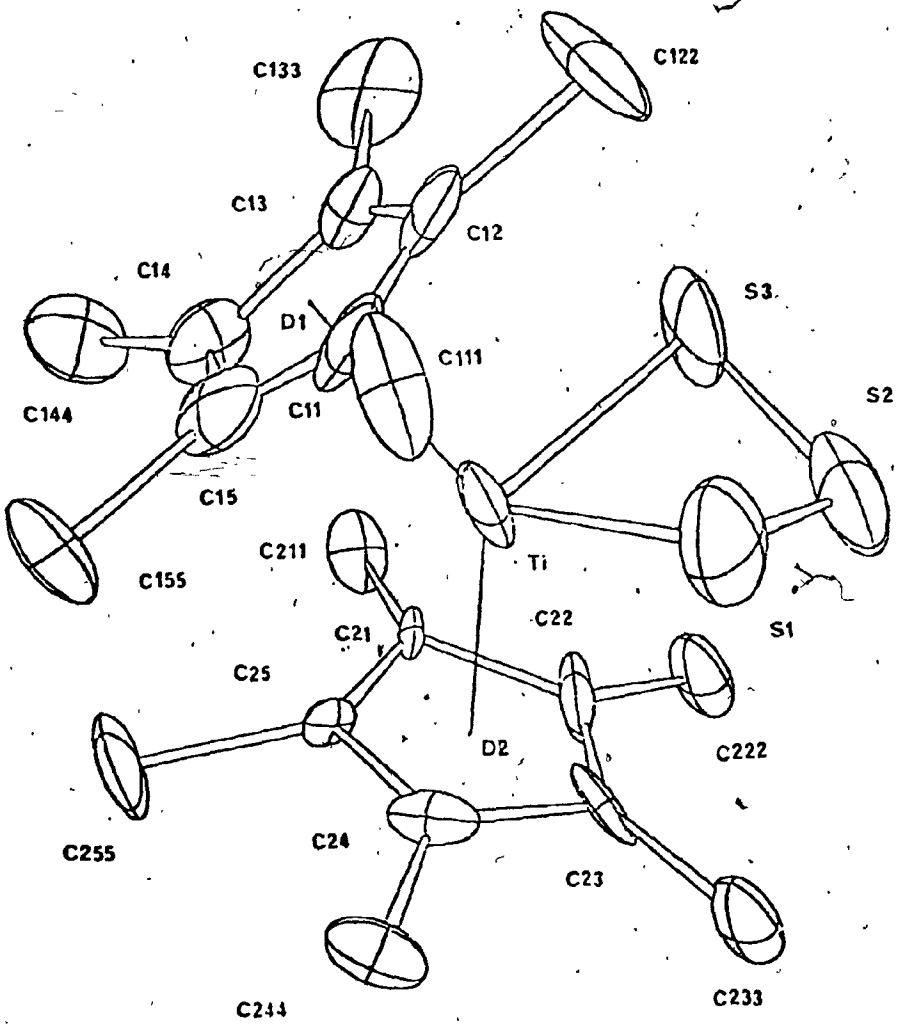

Figure IV-C-2-1. The molecular configuration and the numbering scheme for TICEP.

Table IV-C-2-1 The principal bond distances (Å) and angles(deg) for TICEP.

Bond Distances

$Ti-S_1$	2.491(9)	$C_{11}-C_{111}$	1.46 (4)
$Ti-S_3$	2.492(10)	$C_{12}-C_{122}$	1.60 (3)
$Ti-C_{11}$	2.56 (3)	$C_{13}-C_{133}$	1.50 (4)
$Ti-C_{12}$	2.44 (3)	$C_{14}-C_{144}$	1.55 (3)
$Ti-C_{13}$	2.46 (2)	$C_{15}-C_{155}$	1.68 (3)
$Ti-C_{14}$	2.43 (2)	$C_{21}-C_{211}$	1.38 (2)
$Ti-C_{15}$	2.37 (2)	$C_{22}-C_{222}$	1.50 (3)
$Ti-C_{21}$	2.51 (2)	$C_{23}-C_{233}$	1.50 (4)
$Ti-C_{22}$	2.51 (2)	$C_{24}-C_{244}$	1.62 (3)
$Ti-C_{23}$	2.58 (2)	$C_{25}-C_{255}$	1.71 (3)
$Ti-C_{24}$	2.38 (2)		
$Ti-C_{25}$	2.36 (2)	S_2-S_3	2.04 (1)
$Ti-D_1$	2.125(1)	S_2-S_1	2.04 (1)
$Ti-D_2$	2.150(1)		

Bond Angles

$C_{11}-C_{12}$	1.42 (3)		
$C_{12}-C_{13}$	1.50 (3)	S_1-Ti-S_3	84.79 (7)
$C_{13}-C_{14}$	1.50 (3)	S_1-Ti-D_1	101.87 (5)
$C_{14}-C_{15}$	1.40 (4)	S_1-Ti-D_2	109.86 (6)
$C_{15}-C_{11}$	1.39 (4)	S_3-Ti-D_1	106.78 (4)
$C_{21}-C_{22}$	1.49 (3)	S_3-Ti-D_2	104.92 (6)
$C_{22}-C_{23}$	1.38 (4)	D_1-Ti-D_2	139.86 (6)
$C_{23}-C_{24}$	1.43 (3)		
$C_{24}-C_{25}$	1.46 (3)	$S_1-S_2-S_3$	106.3 (5)
$C_{25}-C_{21}$	1.40 (3)	$Ti-S_1-S_2$	76.0 (4)
		$Ti-S_3-S_2$	75.8 (3)

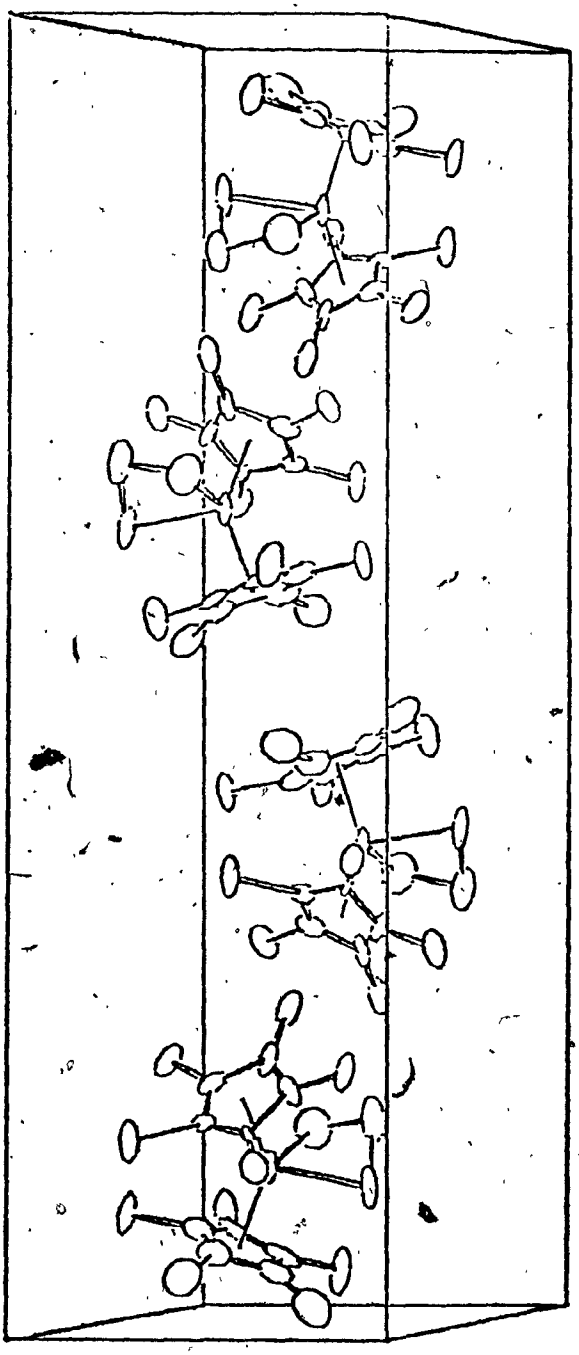

Figure IV-C-2-2 The monoclinic unit cell packing diagram containing four TICEP molecules as viewed down the a axis.

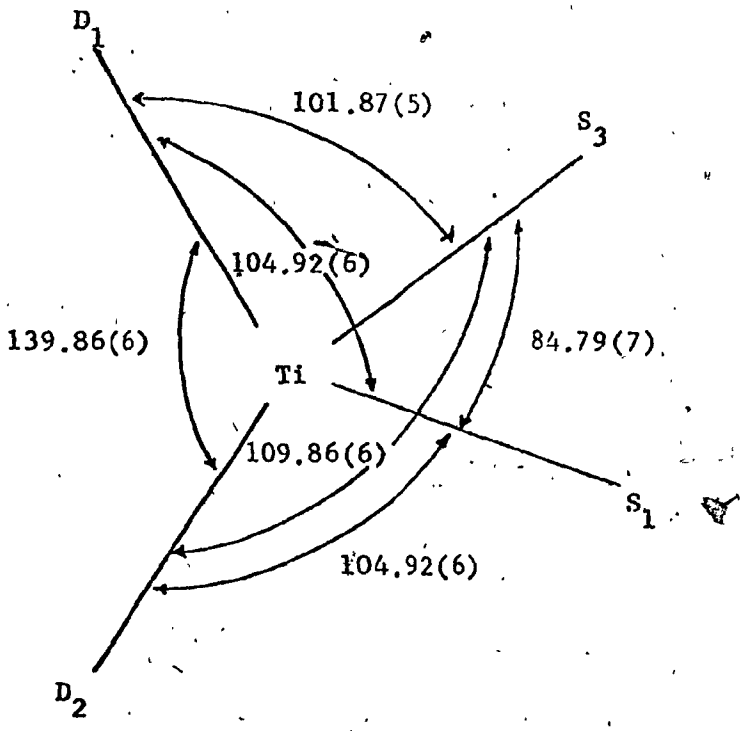

Figure IV-C-2-3. An illustration of coordination around Ti atom showing bond angles (deg).

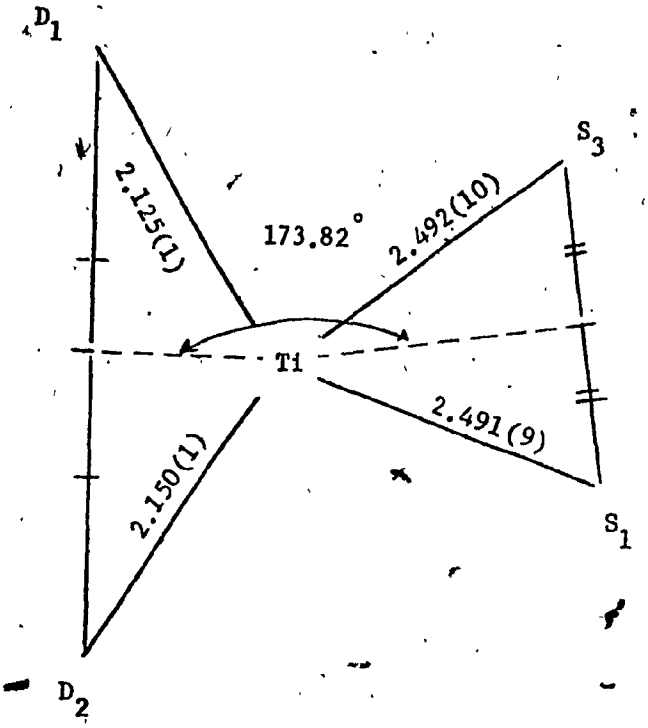

Figure IV-C-2-4. An illustration of the angle between S_1S_3 and D_1D_2 mid point and the bond distances (Å).

In contrast to these observations, in Cp_2TiS_5 [97] and Cp_2MoS_5 [93] the six and five membered rings, respectively, have C_s symmetry with a mirror plane passing through the mid point between the two terminal sulphur atoms bonded to the metal.

The Four Membered Metallacycle

The Ti-S distances 2.491(9) and 2.492(10)Å of the four membered metallacycle in TICEP are comparable to 2.441(2) and 2.410(3)Å found in the six membered metallacycle in the complex Cp_2TiS_5. The S-S distance in the rings TiS_3, MoS_4 and TiS_5 are in the range 2.03 to 2.09Å. The torsion angles and the bond angles are shown in Figure IV-C-2-5.[4] The following features are noteworthy: the S-M-S angle deceases as the ring become smaller and the tortion angles of the ring TiS_5 indicate smaller ring strain compared to rings TiS_3 and MoS_4. It was not possible to compare the angular strain in TiS_3 and MoS_4 since the tortion angles along M-S bonds in MoS_4 were smaller whereas the tortion angles along S-S bonds in TiS_3 were smaller. It is possible that both rings have similar angle strain. However, all the rings have more angle strain and intermolecular interactions compared to the S_8 homocycle, where the tortion angles and the bond angles [90] were 98° and 108°, respectively. Firm conclusions on the absolute or relative stabilities of the rings MS_3, MS_4 and MS_5 could not be drawn since the rings compared had different transition metals in them.

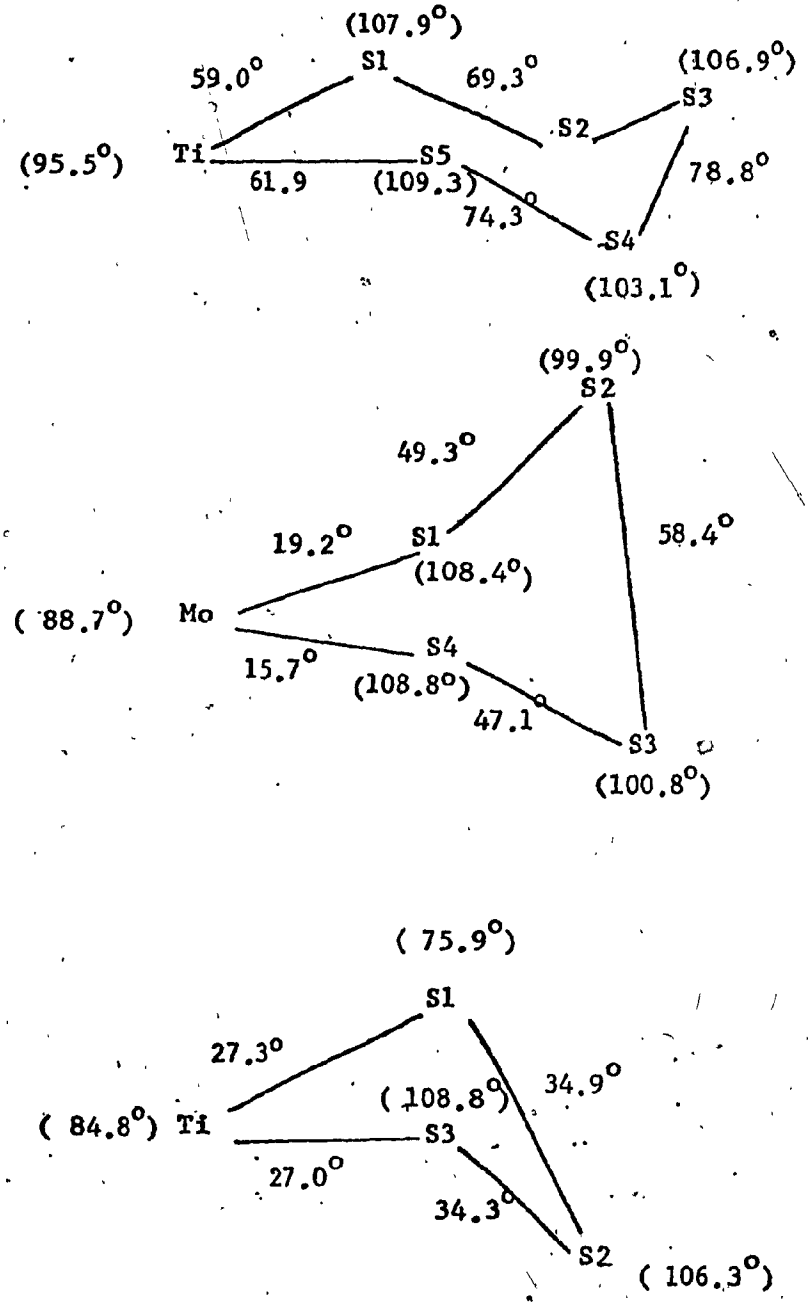

Figure IV-C-2-5. An illustration of torsion angles and bond angles (with in brackets) in TiS_5, MoS_4 and TiS_3.

MCp_2 Fragment

The two π bonded pentamethylcyclopentadienyl rings are staggered with centroid-Ti distances 2.125(1) and 2.150(1)Å. The average Ti-cyclopentadienyl carbon distances of 2.46Å is comparable to those found for similar complexes [95-98] of the type $(\eta^5\text{-}C_5H_5)_2TiX_2$ (X= Cl, S). The Cp-M-Cp angle in TICEP is 137.86°. In previous structure determinations these angles were found to be 132.7°, 134.0°, 134.1°, 135.1° and 137.4° in Cp_2TiS_5, Cp_2MoS_4, Cp_2VS_5, Cp_2WS_4 and $[\eta^5\text{-}C_5(CH_3)_5]_2TiCl_2$ [103], respectively. The increase in the Cp-M-Cp angle in TICEP and $[\eta^5\text{-}C_5(CH_3)_5]_2TiCl_2$ can be attributed to the methyl-methyl contacts of Cp rings in the bent structure. The cyclopentadienyl carbon atoms of each ring are coplanar as shown by the small deviations within 0.02-0.04Å from the least-squares plane through each ring, Table IV-C-2-2. The methyl groups on two cyclopentadienyl rings deviate between 0.07-0.58Å, from the least-squares plane through five carbon atoms of the rings. The largest deviations (see Table IV-C-2-2) are shown by C_{144} (0.39), C_{155} (0.28) and C_{255} (0.58Å), as expected, since the non-bonded distances between these atoms are about 3.33Å which is smaller than the methyl-methyl Van der Walls contact of 3.5Å. Similar observations have been made in the complex $[\eta^5\text{-}C_5(CH_3)_5]_2\text{-}TiCl_2$.

Several C-S distances (ie. $S_3\text{-}C_{13}$ (2.91), $S_3\text{-}C_{12}$ (3.18),

Table IV-C-2-2. The deviations of cyclopentadienyl ring carbon atoms from the least-squares plane through them and the deviations of methyl groups of the rings from these planes.

Atom	deviaton (Å)	Atom	deviation (Å)
C_{11}	0.01154	C_{21}	0.02487
C_{12}	0.00325	C_{22}	0.00432
C_{13}	-0.04280	C_{23}	-0.02828
C_{14}	0.01236	C_{24}	0.04481
C_{15}	-0.01611	C_{25}	-0.04572
C_{111}	0.07406	C_{211}	-0.08873
C_{122}	0.11816	C_{222}	-0.27937
C_{133}	0.19164	C_{233}	-0.22649
C_{144}	0.38934	C_{244}	-0.57621
C_{155}	0.28434	C_{255}	-0.57621

S_1-C_{111} (3.09), S_1-C_{12} (3.17), S_1-C_{11} (3.26), S_1-C_{23} (3.39), S_1-C_{233} (3.18), S_2-C_{22} (3.11), S_2-C_{23} (3.38), S_2-C_{222} (3.28) and S_2-C_{223} (3.33Å) are smaller than carbon sulphur Van der Waals contacts of 3.4Å indicating a steric crowding in this part of the molecule. However, firm conclusions could not be drawn since the positions of the carbon atoms of the two cyclopentadienyl rings were not well refined.

The disposition of two cyclopentadienyl rings relative to the four membered metallacycle in TICEP is of particular interest in the light of the two sets of nonequivalent methyl protons on the two cyclopentadienyl rings as shown by two peaks in the variable temperature ^{1}H NMR spectrum below -75°C. The coalescencence of these peaks can be attributed to the fluxional behaviour of the molecule involving a conformational averaging in solution between two folded TiS_3 ring conformations:

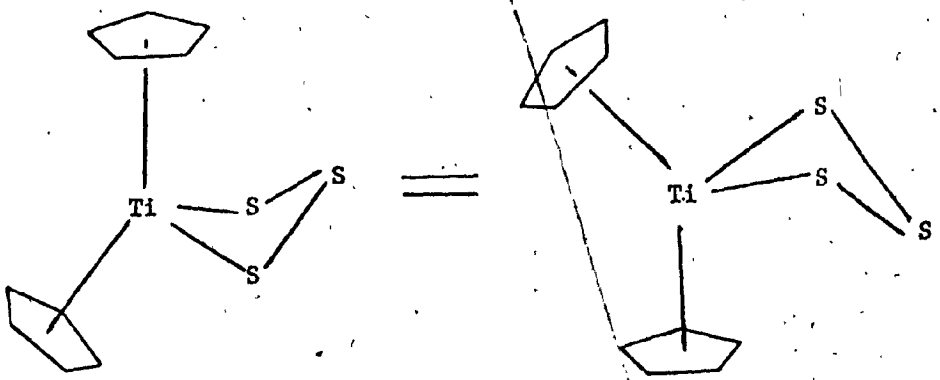

PART D THE CRYSTAL AND MOLECULAR STRUCTURE OF $(\mu_2\text{-}H_4)Ru_4(CO)_9\{[(C_6H_5)_2P]_3CH\}$.

1) INTRODUCTION

The complex, $(\mu_2\text{-}H_4)Ru_4(CO)_9\{[(C_6H_5)_2P]_3CH\}$- RUSH is a transition metal carbonyl cluster hydride, with a tripod ligand linked to a face of a tetrahedron formed by four ruthenium atoms. In this section brief introductions to catalysis, to the nature of the bonding in phosphine ligands, and to hydrides involving polynuclear clusters are presented, to explain the terms and the structural patterns encountered.

Catalysis

The structural investigations of transition metal cluster hydride complexes are important since they seem to be the closest model [104] of a metal's surface involved in heterogeneous catalysis. In several instances such complexes themselves are found to be catalytically active [105], for example in reactions such as isomerisation and hydrogenation of 1,alkenes to internal alkenes. Some intermediates in these reactions have been isolated [105] which may provide insight into the mechanism. Unlike most of the heterogeneous catalytic systems that have been used in industry, transition metal cluster catalytic reactions are carried out

homogeneouly. Homogeneous catalysts are more specific with respect to products formed and are in direct contact with the substrates in one phase. However, heterogeneous systems present significant advantages in an engineering and economic context since the costly separation of the catalyst and products is not involved. Recently, studies [106] have been carried out to combine the best features of homogeneous and heterogeneous catalysts. The homogeneous catalyst organometallic complexes are chemically bonded to specific groups on a solid support. The most common method that has been used is to attach the homogeneous catalyst to a solid organic or inorganic support containing group VB donors such as P, As and Sb by covalent or ionic bonding. The commonest supports that have been used are polystyrene and silica which have been modified to contain phosphine groups. In this context, phosphine complexes of transition metals show potent catalytic activity.

Phosphine Ligands

Transition metal complexes containing phosphorus ligands are stable since phosphorus can act as a σ donor and a π acceptor. The bonding capability of phosphorus results from the vacant 3d orbitals which can interact with filled non-bonding d orbitals of a transition metal. The strength of the M-P bond depends on the other groups X attached to the phosphorus unit PX_3. More electronegative groups increase the strength of the bond by increasing the π bonding contribution.

A series of alkyl and aryl phosphines can be prepared by changing X in the PX_3 unit with appropriate alkyl or aryl groups. Some of the most commonly used alkyl and aryl groups are methyl, ethyl, isopropyl, normal butyl, isobutyl and phenyl. The PX_3 unit is monodentate in binding with transition metals. Bidentate and tridentate phosphine ligands have been prepared [107-109] where two and three phosphine groups, respectively, are attached to the same ligand. Examples of bidentate and tridentate ligands of the general formula $R_2P(CH_2)_nPR_2$ 20 and $RC(CH_2)_nPR_2$ 21 are $Ph_2PCH_2PPh_2$ (bisdiphenylphosphinomethane) and $(Ph_2P)_3CH$ (trisdiphenylphosphinomethane-tripod) [110], respectively.

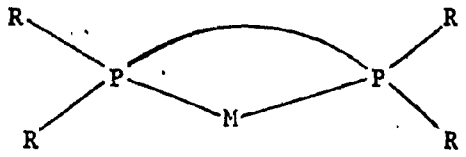

20

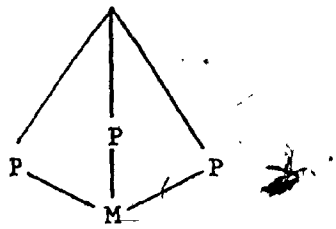

21

The tridentate ligand may bond to one, two or three metals. Their chelating power depends on the size of the ring formed with the metal. The tripod ligand belongs to an unusual class of ligands which will bind three metals simultaneouly in a triangular array. J.A. Osbourn's group in France has been trying to construct trinuclear clusters from mononuclear starting materials [110] using the tripod ligand.

Tetradentate and hexadentate phosphines have been synthesized [111] and the reactions of these multidentate systems with transition metals have resulted in a variety of novel transition metal complexes [111].

Transition Metal Hydrides

In simple terminal hydrides, the hydrogen occupies a distinct coordination site and the M-H distance is approximately the sum of the covalent radii. The early attempts to locate hydrogens by X-ray data were indirect. The missing hydrogen positions were deduced by examining the geometry of the rest of the molecule. For example, X-ray analysis of $HMn(CO)_5$ [112] revealed a square pyramidal geometry, indicating octahedral coordination with a "vacant" site presumably occupied by a terminally bonded hydrogen atom. The bonding in mononuclear hydrides are fairly well understood, being more straightforward than the bonding involved in bridging hydrogen atoms in binuclear and polynuclear cluster complexes. The location of hydrogen positions in complex structures by X-ray analysis is difficult since the X-ray cross section of hydrogen is small compared to other 'heavy atoms' in the structure. This problem becomes more severe in the cases where hydrogens are found embedded among the metal nuclei in clusters.

In the past few years an increased accuracy has been achieved [113-114] in locating hydrogen positions on the difference

fourier maps by eliminating high angle data. However, even when direct location is possible, their positions are of low precision. Moreover, metal-hydrogen distances measured by X-ray diffraction methods, are often 0.1-0.2A° shorter than their true values, because the hydrogen electron density is somewhat perturbed from the hydrogen nucleus towards metal-hydrogen σ bond.

Neutron diffraction has been successfully used [115] to locate the position of hydrogen atoms with more accuracy. Hydrogen atoms scatter with about the same frequency as do most other elements, eliminating the distinction between heavy and lighter atoms. However, two major drawbacks to the neutron diffraction are the necessity of large single crystals and the relative inaccessibility of the facilities required ie. a nuclear reactor.

Tetranuclear Cluster Hydrides

Structures with local T_d 22 D_{2d} 23 and C_{3v} 24 symmetries have been postulated [116] for a transition metal cluster complex of the type M_4H_4.

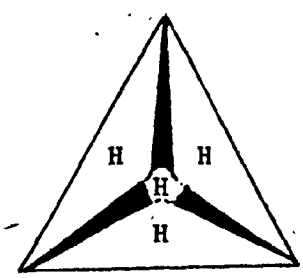

T_d

22

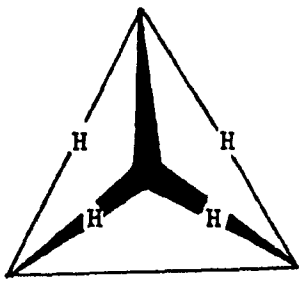

D_{2d}

23

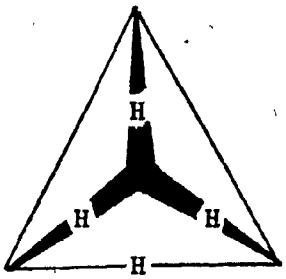

C_{3v}

24

At least four types of bonding modes [117], terminal (M-H), doubly bridged (H-M-H), triply bridged (M_3H) and hydrogen atoms embedded in the center of the polynuclear cluster have been established. The M-H-M bridge can be considered to be a electron deficient three center bond 26 similar to the hydrogen bridge found in boron hydride systems.

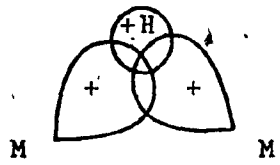

25

In the case of tetranuclear cluster complexes the metal-metal distances along a bridged edge of the terahedron formed by four metal atoms are found to be longer than similar non-bridged metal-metal distances. This criterion has been used [118-119] to locate the edge bridged hydrogen atoms in $(\mu_2\text{-H})Ru_4(CO)_{12}$ and similar complexes.

The variable temparature ^{13}C and ^{1}H solution NMR studies of transition metal carbonyl cluster hydride complexes have shown [120] that the structures are not static with respect to the position of ligands at various temperatures. The ligand migrations are explained in terms of the low energy bonding modes that can readily interconvert

terminal and bridging as shown below:

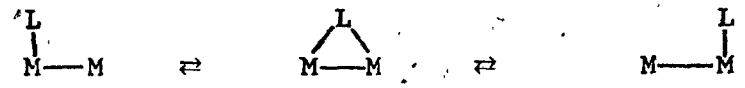

Thus it seems that the metal cluster complexes have easily available active sites for various substrates and low activation energies for the breaking up of the products formed. The fluxional behaviour of the cluster complexes also indicates the possibility of structural isomers.

The literature concerning the chemistry of transition metal hydrides including transition metal cluster hydrides has been reviewed up to 1971 by Saillant et al. [121] and up to 1979 by Bau et al. [122]. A number of polynuclear metal carbonyl hydrides have been reported in the literature and the hydrogen positions found in clusters such as $(\mu_2\text{-}H_4)Ru_4(CO)_9(C{\equiv}CMe)_3$ [123], $(\mu_2\text{-}H_2)Os_4(CO)_{10}$ [124], $(\mu_2\text{-}H)Fe_4(CO)_9[P(OMe)_3]_3$ [125], $[(\mu_2\text{-}H)Co_6(CO)_{15}]^-$ $[(Ph_3P)_2N]^+$ [126] and $[(\mu_2\text{-}H_2)Ni_{12}(CO)_{21}]^{-2}[(Ph_3P)_2N]^+$ [127] by neutron diffraction. The hydrogen positions in complexes such as $(\mu_2\text{-}H_4)Ru_4(CO)_{12}$ [117], $(\mu_2\text{-}H_4)Ru_4(CO)_{10}(Ph_3P)_2$ [117], $(\mu_2\text{-}H_4)Ru_4(CO)_9$(diphos) [128], $(\mu_2\text{-}H_4)Re_4(CO)_{12}$ [129] and $(\mu_2\text{-}H_4)Ru_4(CO)_{11}[P(OMe)_3]$ [130] have been determined by indirect and direct methods using X-ray diffraction. Two structural isomers have been found [131] for the complex $[(\mu_2\text{-}H_3)Ru_4(CO)_{12}]^-$ with M_4H_3 geometries C_2 and C_{3v}. In complexes,

$(\mu_2\text{-}H_4)Re_4(CO)_{12}$, $(\mu_2\text{-}H_4)Ru_4(CO)_{12}$[117] and $(\mu_2\text{-}H_4)Ru_4(CO)_{10}$(diphos) the geometries of the M_4H_4 core were T_d, D_{2d} and C_s, respectively. Monodentate phosphines such as PPh_3 in $(\mu_2\text{-}H_4)Ru_4(CO)_{10}(PPh_3)_2$ and bidentate phosphines such as $Ph_2P(CH_2)_2\ PPh_2$(diphos) in $(\mu_2\text{-}H_4)Ru_4(CO)_{10}$(diphos) are found attached to the metal atoms of tetranuclear clusters.

The complex, $(\mu_2\text{-}H_4)Ru_4(CO)_9$(tripod) - RUSH, was prepared [132] by the reaction between $(\mu_2\text{-}H_4)Ru_4(CO)_{12}$ and $(Ph_2P)_3CH$. The variable temperature ^1H NMR of the compound showed a single hydrogen peak at room temperature which split into a doublet and finally into four distinct peaks at low temperature indicating fluxional behaviour of the molecule. The X-ray crystallographic studies were undertaken to determine the nature of the bonding adopted by the tripod ligand and the approximate hydrogen positions on the tetrahedron formed by four ruthenium atoms to support the implications of the ^1H NMR, ^{31}P NMR and IR spectra.

2) RESULTS AND DISCUSSION

The molecular configuration and the numbering scheme of RUSH is shown in Figure IV-D-2-1. The principal molecular distances and angles are listed in Table IV-D-2-1. A packing diagram of the monclinic unit cell containing four RUSH molecules and four methylene chloride molecules are shown in Figure IV-D-2-2. The positional and thermal parameters of the non-hydrogen atoms are listed in Table A-4 of the Appendix A.

The molecule contains a tetrahedral cluster of four ruthenium atoms with four hydrogen atoms bridged to the Ru_1-Ru_2, Ru_1-Ru_3, Ru_2-Ru_4 and Ru_3-Ru_4 edges of the ruthenium tetrahedron, Figure IV-D-2-3. Each Ru_1, Ru_2 and Ru_3 atoms are linked to two carbonyl groups and a phosphine group of the tripod ligand. Thus, the tridentate tripod ligand is linked to the face formed by the Ru_1, Ru_2 and Ru_3 atoms of the tetrahedron. The ruthenium atom Ru_4 is bonded to three carbonyl groups, Figure IV-D-2-4.

Ruthenium-Tetrahedron

The coordination around each ruthenium atom of the tetrahedron is a distorted octahedron. Two types of Ru-Ru distances are observed in the tetrahedron with average longer and shorter distances 2.942 and 2.804Å, respectively. These Ru-Ru distances are

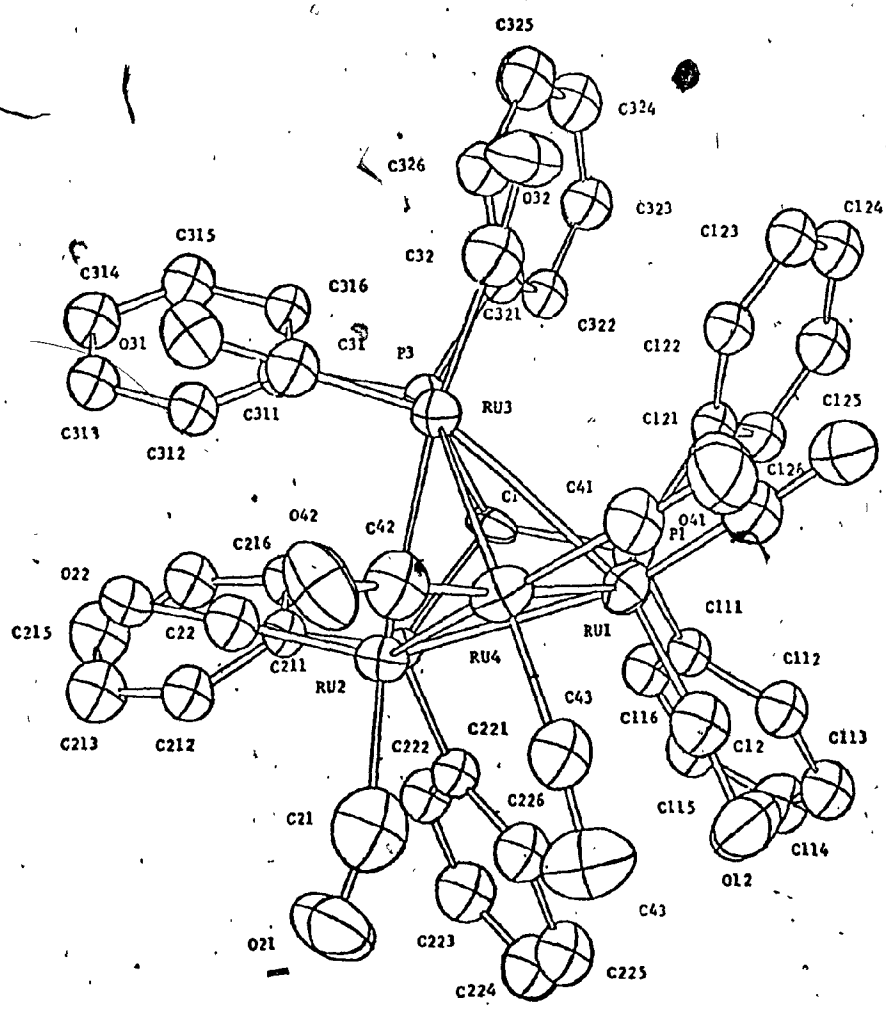

Figure IV-D-2-1. The molecular configuration and the numbering scheme for RUSH.

Table IV-D-2-1 The principal bond distances (Å) and angles(deg) in RUSH.

Bond Distances

Ru_1-Ru_2	2.960(2)	P_1-C_{111}	1.84 (2)	C_{124}-C_{125}	1.39 (2)
Ru_1-Ru_3	2.947(2)	P_1-C_{121}	1.88 (2)	C_{125}-C_{126}	1.42 (2)
Ru_1-Ru_4	2.768(2)	P_2-C_{211}	1.82 (1)	C_{126}-C_{121}	1.42 (2)
Ru_2-Ru_3	2.821(2)	P_2-C_{221}	1.86 (2)	C_{211}-C_{212}	1.41 (2)
Ru_2-Ru_4	2.908(2)	P_3-C_{311}	1.87 (1)	C_{212}-C_{213}	1.41 (2)
Ru_3-Ru_4	2.958(2)	P_3-C_{321}	1.86 (2)	C_{213}-C_{214}	1.37 (2)
				C_{214}-C_{215}	1.39 (2)
Ru_1-P_1	2.325(5)	C_{11}-O_{11}	1.21 (2)	C_{215}-C_{216}	1.45 (2)
Ru_2-P_2	2.314(5)	C_{12}-O_{12}	1.20 (2)	C_{216}-C_{211}	1.40 (2)
Ru_3-P_3	2.343(5)	C_{21}-O_{21}	1.14 (2)	C_{221}-C_{222}	1.41 (2)
		C_{22}-O_{22}	1.20 (2)	C_{222}-C_{223}	1.42 (2)
Ru_1-C_{11}	1.80 (2)	C_{31}-O_{31}	1.18 (2)	C_{223}-C_{224}	1.40 (2)
Ru_1-C_{12}	1.82 (2)	C_{32}-O_{32}	1.15 (2)	C_{224}-C_{225}	1.37 (2)
Ru_2-C_{21}	1.90 (2)	C_{41}-O_{41}	1.19 (2)	C_{225}-C_{226}	1.45 (2)
Ru_2-C_{22}	1.80 (1)	C_{42}-O_{42}	1.17 (2)	C_{226}-C_{221}	1.42 (2)
Ru_3-C_{31}	1.78 (1)	C_{43}-O_{43}	1.20 (2)	C_{311}-C_{312}	1.41 (2)
Ru_3-C_{32}	1.90 (2)			C_{312}-C_{313}	1.36 (2)
Ru_4-C_{41}	1.83 (2)	C_{111}-C_{112}	1.38 (2)	C_{313}-C_{314}	1.39 (2)
Ru_4-C_{42}	1.86 (2)	C_{112}-C_{113}	1.45 (2)	C_{314}-C_{315}	1.39 (2)
Ru_4-C_{43}	1.80 (2)	C_{113}-C_{114}	1.35 (2)	C_{315}-C_{316}	1.40 (2)
		C_{114}-C_{115}	1.37 (2)	C_{316}-C_{311}	1.41 (2)
CP-P_1	1.92 (1)	C_{115}-C_{116}	1.43 (2)	C_{321}-C_{322}	1.43 (2)
CP-P_2	1.91 (2)	C_{116}-C_{111}	1.41 (2)	C_{322}-C_{323}	1.45 (2)
CP-P_3	1.92 (1)	C_{121}-C_{122}	1.41 (2)	C_{323}-C_{324}	1.39 (2)
		C_{122}-C_{123}	1.41 (2)	C_{324}-C_{325}	1.41 (2)
C_1-Cl_1	1.72 (2)	C_{123}-C_{124}	1.38 (2)	C_{325}-C_{326}	1.41 (2)
C_1-Cl_2	1.78 (2)			C_{326}-C_{321}	1.41 (2)

Table IV-D-2-1 Cont'd.

Bond Angles

Ru_2-Ru_1-Ru_3	57.06 (5)	Ru_1-Ru_3-Ru_2	61.71 (5)
Ru_2-Ru_1-Ru_4	60.92 (5)	Ru_1-Ru_3-Ru_4	55.92 (5)
Ru_2-Ru_1-P_1	94.4 (1)	Ru_1-Ru_3-P_3	92.6 (1)
Ru_2-Ru_1-C_{12}	104.11 (5)	Ru_1-Ru_3-C_{32}	111.5 (5)
Ru_3-Ru_1-Ru_4	62.25 (5)	Ru_2-Ru_3-Ru_4	60.4 (5)
Ru_3-Ru_1-P_1	91.2 (1)	Ru_2-Ru_3-P_3	88.2 (1)
Ru_3-Ru_1-C_{11}	105.7 (5)	Ru_2-Ru_3-C_{31}	93.7 (5)
Ru_4-Ru_1-C_{11}	101.4 (5)	Ru_4-Ru_3-C_{31}	103.2 (5)
Ru_4-Ru_1-C_{12}	99.3 (5)	Ru_4-Ru_3-C_{32}	107.2 (5)
P_1-Ru_1-C_{11}	98.3 (5)	P_3-Ru_3-C_{31}	98.3 (5)
P_1-Ru_1-C_{12}	102.9 (5)	P_3-Ru_3-C_{32}	102.9 (5)
C_{11}-Ru_1-C_{12}	95.8 (7)	C_{31}-Ru_3-C_{32}	90.3 (7)
Ru_1-Ru_2-Ru_3	61.23 (5)	Ru_1-Ru_4-Ru_2	62.79 (5)
Ru_1-Ru_2-Ru_4	96.29 (5)	Ru_1-Ru_4-Ru_3	61.83 (5)
Ru_1-Ru_2-P_2	88.6 (1)	Ru_1-Ru_4-C_{41}	85.5 (5)
Ru_1-Ru_2-C_{21}	112.3 (3)	Ru_1-Ru_4-C_{43}	89.1 (5)
Ru_3-Ru_2-Ru_4	62.15 (5)	Ru_2-Ru_4-Ru_3	57.48 (5)
Ru_3-Ru_2-P_2	95.6 (1)	Ru_2-Ru_4-C_{42}	112.37 (5)
Ru_3-Ru_2-C_{22}	88.8 (5)	Ru_2-Ru_4-C_{43}	95.2 (6)
Ru_4-Ru_2-C_{21}	104.6 (6)	Ru_3-Ru_4-C_{41}	102.7 (7)
Ru_4-Ru_2-C_{22}	106.4 (5)	Ru_3-Ru_4-C_{42}	110.9 (5)
P_2-Ru_2-C_{21}	95.8 (6)	C_{41}-Ru_4-C_{42}	98.4 (7)
P_2-Ru_2-C_{22}	100.6 (5)	C_{41}-Ru_4-C_{43}	90.9 (8)
C_{21}-Ru_2-C_{22}	95.8 (7)	C_{42}-Ru_4-C_{43}	97.2 (8)

Table IV-D-2-1 Cont'd.

Bond Angles

Ru_1-P_1-CP	108.7	(4)	Ru_3-P_3-CP	110.6	(5)
Ru_1-P_1-C_{111}	119.4	(5)	Ru_3-P_3-C_{311}	117.9	(5)
Ru_1-P_1-C_{121}	116.1	(5)	Ru_3-P_3-C_{321}	118.0	(5)
CP-P_1-C_{111}	105.8	(6)	CP -P_3-C_{311}	108.2	(6)
CP-P_1-C_{121}	107.4	(7)	CP -P_3-C_{321}	104.1	(7)
C_{111}-P_1-C_{121}	98.3	(7)	C_{311}-P_3-C_{321}	96.3	(7)
Ru_2-P_2-CP	109.9	(5)	P_1-CP-P_2	110.6	(7)
Ru_2-P_2-C_{211}	120.2	(5)	P_1-CP-P_3	108.4	(7)
Ru_2-P_2-C_{221}	114.7	(5)	P_2-CP-P_3	102.6	(6)
CP-P_2-C_{211}	105.2	(7)			
CP-P_2-C_{221}	106.6	(7)	Cl_1-C_1-Cl_2	108.	(1)
C_{211}-P_2-C_{211}	98.9	(7)			

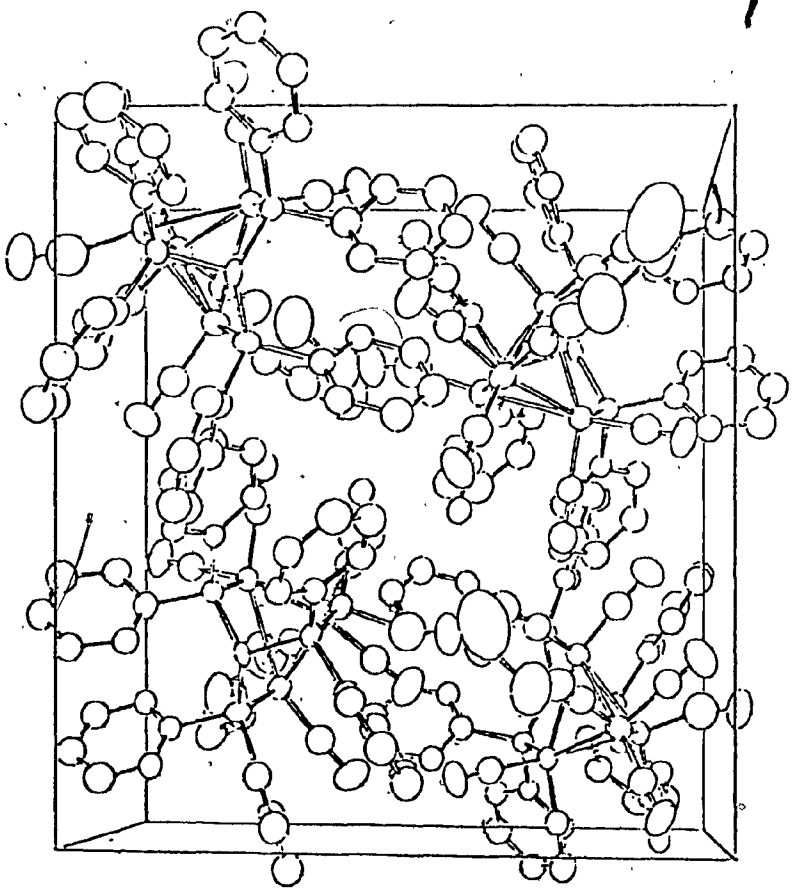

Figure IV-D-2-2. The unit cell packing diagram containing four molecules of RUSH and four methylene chloride molecules as viewed down the c axis.

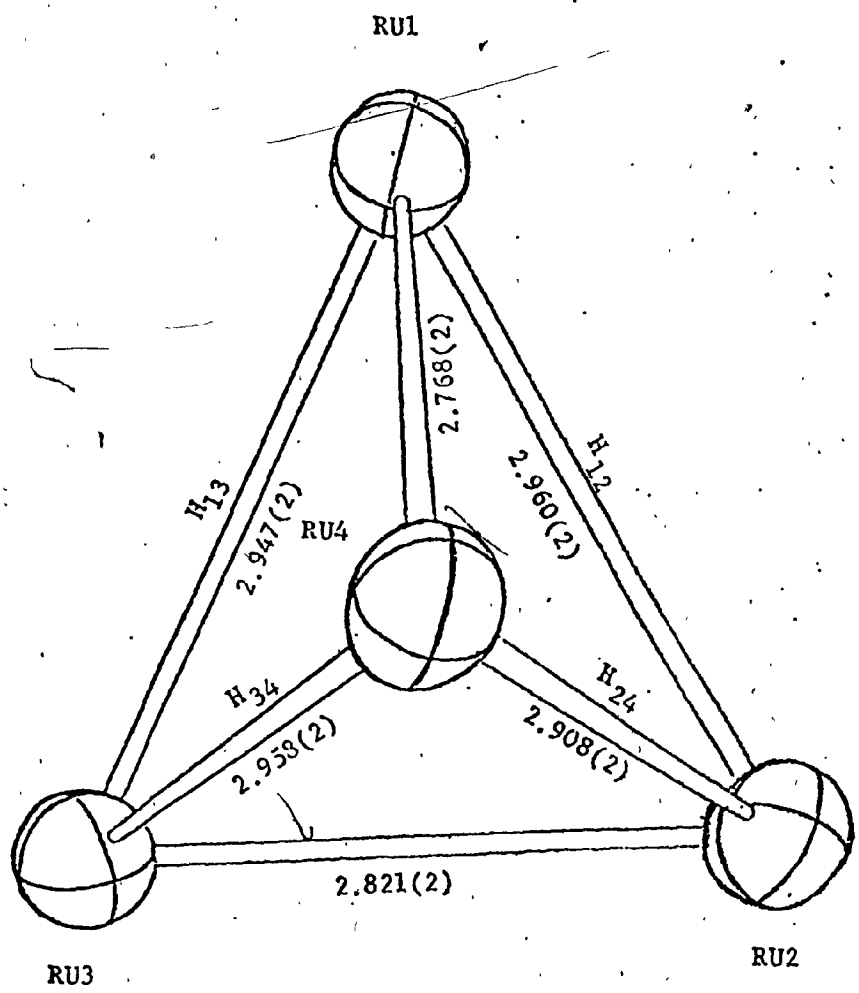

Figure IV-D-2-3. An illustration of ruthenium tetrahedron showing the Ru-Ru bond distances (Å).

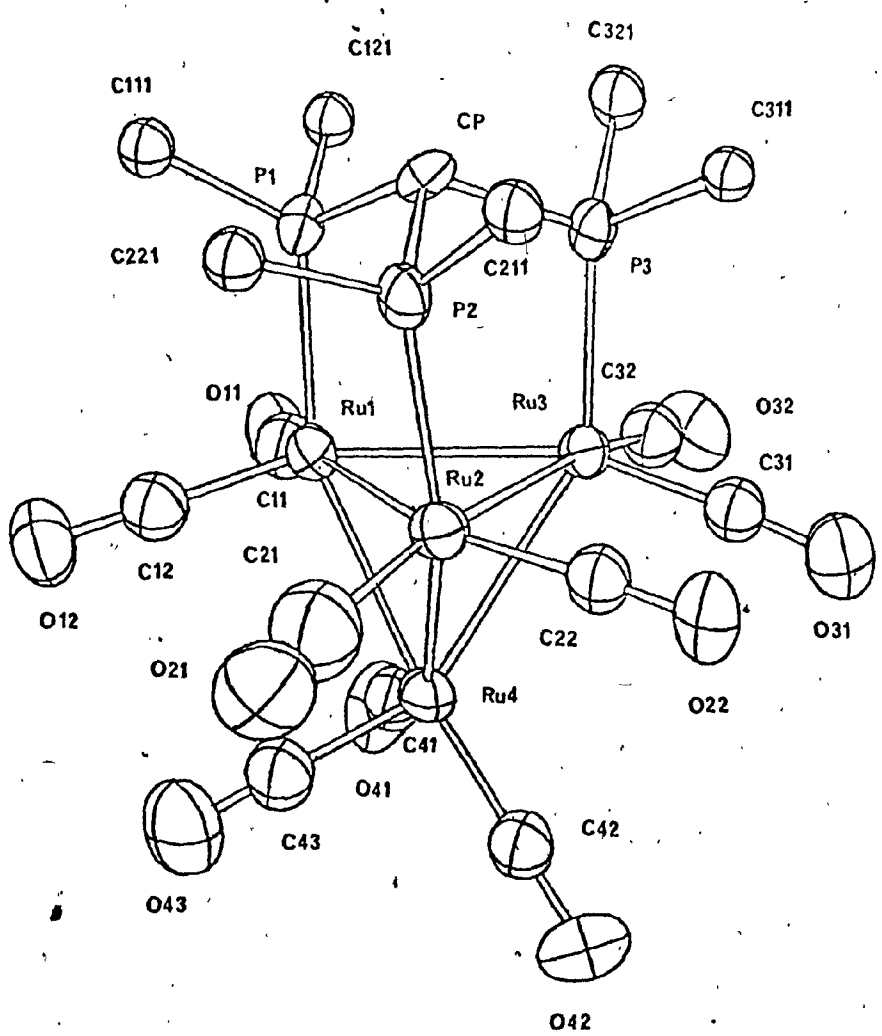

Figure IV-D-2-4. The configuration of RUSH molecule to illustrate the attachement of carbonyl and tripod ligand to the ruthenium tetrahedron.

comparable to those observed in $(\mu_2\text{-}H_4)Ru_4(CO)_{12}$, $(\mu_2\text{-}H_4)Ru_4(CO)_{10}[P(OMe)_3]$, $(\mu_2\text{-}H_4)Ru_4(CO)_{10}(PPh_3)_2$ and $(\mu_2\text{-}H_4)Ru_4(CO)_{10}(\mu_2\text{-diphos})$, Table IV-D-2-2. The average Ru-Ru-Ru angle of 56.9° formed by the longer Ru-Ru edges was smaller than the average angle of 61.66° formed by shorter Ru-Ru edges. These angles were comparable to those found in similar complexes, Table IV-D-2-2.

Ruthenium Tetrahedron and Carbonyl Groups

The ruthenium-carbonyl carbon distances and carbonyl C-O distances were comparable to those observed in ruthenium tetranuclear complexes of the type $(\mu_2\text{-}H_4)Ru_4(CO)_{12-n}L_n$, Table IV-D-2-3. Two types of principal Ru-Ru-carbonyl carbon angles formed by Ru-Ru distances involved in longer and shorter edges were observed. The average Ru-(long)-Ru-carbonyl carbon and Ru-(short)-Ru-carbonyl carbon angles, 106.35° and 92.95°, respectively, were similar to those found in similar complexes as shown in Table IV-D-2-3.

Positions of Hydrogens on the Tetrahedron

The presence of unequal Ru-Ru distances indicates the presence of four bridging hydrogen atoms (along the $Ru_1\text{-}Ru_2$, $Ru_1\text{-}Ru_3$, $Ru_2\text{-}Ru_4$ and $Ru_3\text{-}Ru_4$ edges of the ruthenium tetrahedron). The larger Ru-(long)-Ru-carbonyl carbon angles support this assumption since the larger angles indicate the displacement of the carbonyl groups from

Table IV-D-2-2. Dimensions of the Ru_4 core of $(\mu_2\text{-}H_4)Ru_4(CO)_{12-n}L_n$ complexes.

$(\mu_2\text{-}H_4)Ru_4(CO)_{12}$ [a]	$(\mu_2\text{-}H_4)Ru_4(CO)_{11}[P(OMe)_3]$ [b]	$(\mu_2\text{-}H_4)Ru_4(CO)_{10}(PPh_3)_2$ [c]	$(\mu_2\text{-}H_4)Ru_4(CO)_{10}$(diphos) [d]	RUSH
A. Longer Ru—Ru bond distances (Å).				
2.945(1)	2.94(1)	2.953(2)	2.931(1)	2.960(2)
2.948(1)	2.94(1)	2.956(2)	2.946(1)	2.947(2)
2.950(1)	2.92(1)	2.973(2)	2.988(1)	2.908(2)
2.956(1)	2.92(1)	2.938(2)	3.006(1)	2.958(2)
Av. 2.950	Av. 2.93	Av. 2.966	Av. 2.968	Av. 2.942
B. Shorter Ru—Ru bond distances (Å)				
2.784(1)	2.76(1)	2.770(2)	2.785(1)	2.768(2)
2.788(1)	2.76(1)	2.774(2)	2.796(1)	2.861(2)
Av. 2.786	Av. 2.76	Av. 2.772	Av. 2.791	Av. 2.804
C. Ru-(longer)-Ru-(longer)-Ru angles (deg).				
Av. 56.36	———	Av. 55.71	Av. 57.12	Av. 56.69
D. Ru-(long)-Ru-(short)-Ru angles (deg).				
Av. 61.82	———	Av. 62.14	Av. 61.498	Av. 61.66

a) Ref. [117]
b) Ref. [125]
c) Ref. [117]
d) Ref. [128]

Table IV-D-2-3. Comparison of Ru—C distances and the principle Ru—Ru—carbonyl carbon angles of $(\mu_2\text{-}H_4)Ru_4(CO)_{12-n}L_n$ complexes.

	$(\mu_2\text{-}H_4)Ru_4(CO)_{12}$ [a]	$(\mu_2\text{-}H_4)Ru_4(CO)_{10}(PPh_3)_2$ [b]	$(\mu_2\text{-}H_4)Ru_4(CO)_{10}(\mu_2\text{-diphos})$ [c]	RUSH
A. Ru carbonyl carbon distances (Å).				
	Av. 1.92	Av. 1.84	Av. 1.881	Av. 1.832
B. Carbonyl C O distances (Å).				
	Av. 1.131	Av. 1.18	Av. 1.138	Av. 1.18
C. Ru-(long)-Ru-carbonyl carbon angles (deg)				
	Av. 107.7	Av. 103.8	Av. 105.47	112.37(5), 105.70(5) 112.30(5), 104.60(5) 111.50(5), 104.11(5) 110.90(5), 103.20(5) 107.20(5), 102.95(5) 106.40(5), 95.20(6) Av. 106.35
D. Ru-(short)-Ru-carbonyl carbon angles (deg)				
	Av. 92.7	Av. 91.8	Av. 90.13	101.30(5) 99.30(5) 93.10(5) 89.10(5) 88.80(5) 85.50(5) Av. 92.95

a) Ref. [117]
b) Ref. [117]
c) Ref. [128]

the bridged edges to reduce the non-bonded interactions between bridged hydrogens and carbonyl groups, Figure IV-D-2-5. The angle between the planes through C_{41}, C_{42}, C_{43} and Ru_1, Ru_2, Ru_3 was 165° (deviation from the ideal 180°) showing the distortion of the molecule to accomodate the hydrogens H_{24} and H_{34}, Figure IV-D-2-6. The positions of the four hydrogens H_{12}, H_{13}, H_{24} and H_{34} were directly located from a difference fourier map calculated using low angle data. The bond distances of the hydrogens thus located bonded to ruthenium atoms are listed in Table IV-D-2-4 along with their positional parameters.

Ruthenium Tetrahedron and the Tripod Ligand

The Ru-P distances (av. 2.327Å) are within the range (2.359-2.335Å) observed in similar complexes as shown in Table IV-D-2-5. Two monodentate PPh_3, bidentate diphos and tridentate tripod ligands are found in complexes $(\mu_2\text{-}H_4)Ru_4(CO)_{10}(PPh_3)_2$, $(\mu_2\text{-}H_4)Ru(CO)_{10}(\mu_2\text{-diphos})$ and RUSH, respectively, Figure IV-D-2-7. The Ru-Ru-P angle decreased with the increasing chelation of the phosphine ligand as shown in Table IV-D-2-5. It is seen that the steric requirements for attachment of the multidentate phosphine ligands to the tetrahedron increase with their chelation. The strength of the link between tripod and the tetrahedron should be a balance between electronic stabilization resulting from the overlapping of the orbitals involved and the destabilization due to steric repulsion between the ligand and the carbonyl groups on the tetrahedron.

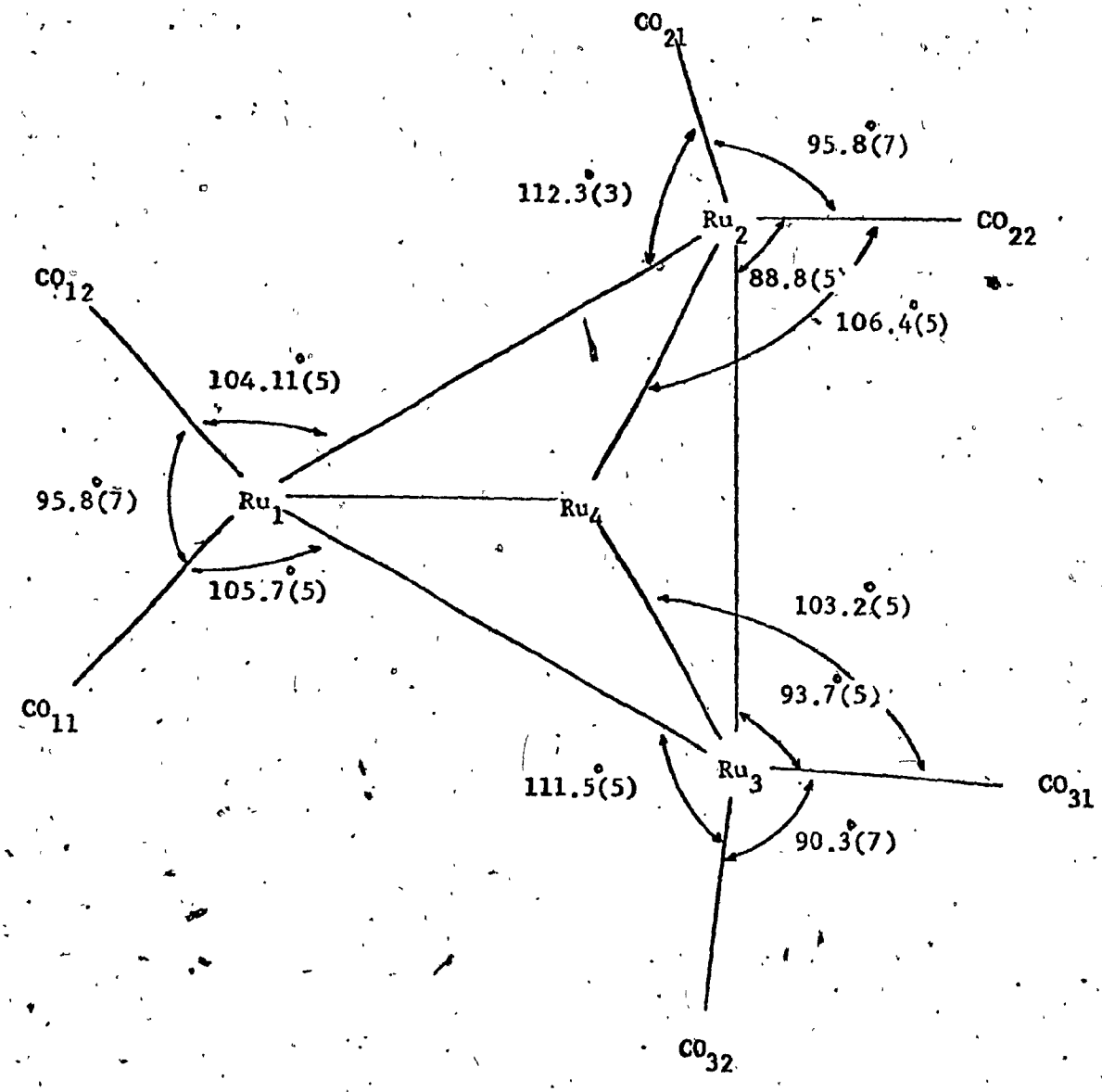

Figure IV-D-2-5. An illustration of Ru-Ru-carbonyl carbon angles in the ruthenium tetrahedron.

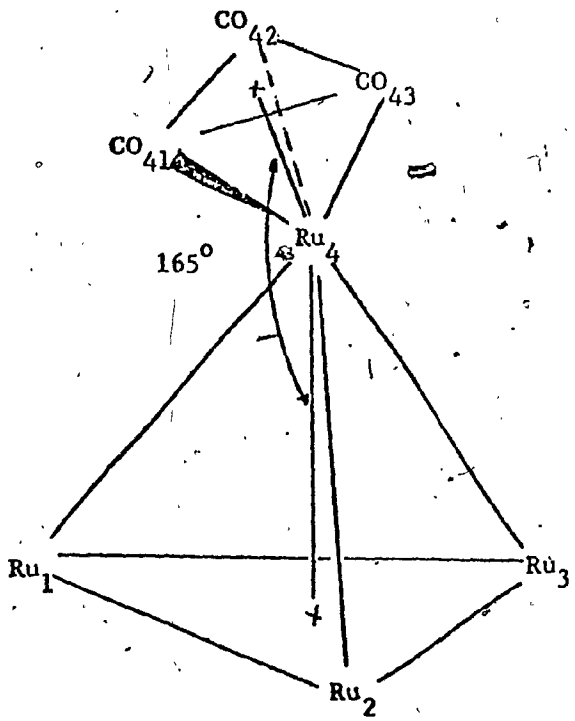

Figure IV-D-2-6. An illustration of the angle between the planes through Ru_1, Ru_2, Ru_3 and C_{41}, C_{42}, C_{43}.

Table IV-D-2-4. Ru-H bond distances (Å) and the positional parameters of the hydrogens bridged to ruthenium tetrahedron.

Ru-H distances

Ru_1-H_{12}	1.609(1)	Ru_2-H_{24}	1.836(1)
Ru_2-H_{12}	1.445(1)	Ru_4-H_{24}	1.528(1)
Ru_1-H_{13}	1.707(1)	Ru_3-H_{34}	1.585(1)
Ru_3-H_{13}	1.593(1)	Ru_4-H_{34}	1.846(1)

Positional parameters of the hydrogens

	X	Y	Z
H_{12}	.2294	.1531	.0824
H_{13}	.2031	.2948	.1117
H_{24}	.1292	.1019	.1611
H_{34}	.0971	.2341	.1873

Table IV-D-2-5. Comparison of Ru-P bond lengths and principle Ru-Ru-P angles in complexes, $(\mu_2\text{-}H_4)Ru_4(CO)_{12-n}L_n$ (L= PPh_3, diphos, tripod)

$(\mu_2\text{-}H_4)RU_4(CO)_{10}(PPh_3)_2$ [a]	$(\mu_2\text{-}H_4)Ru_4(CO)_{10}(\mu_2\text{-diphos})$ [b]	RUSH
A. Ru-P distances(Å)		
2.362(4)	2.356(4)	2.325(5)
2.356(4)	2.335(5)	2.314(5)
Av. 2.359	Av. 2.335	Av. 2.327
B. Ru-Ru-P angles(deg)		
108.94°(10)	99.7°(1)	94.4°(1)
110.19°(10)	104.3°(1)	92.6°(1)
Av. 109.565°	Av. 102.0°	88.6°(1)
		Av. 91.876°

a) Ref. [117]
b) Ref. [128]

Figure IV-D-2-7. Illustrations of a) Monodentate b) Bidentate c) Tridentate phosphine ligands attached to ruthenium tetrahedron.

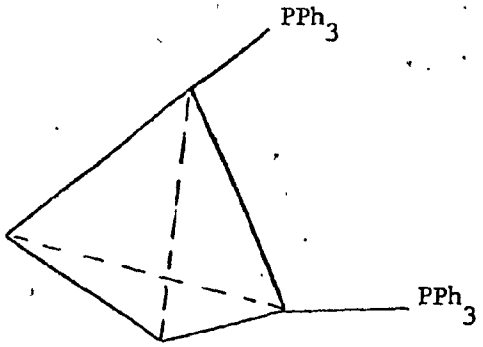

(a)

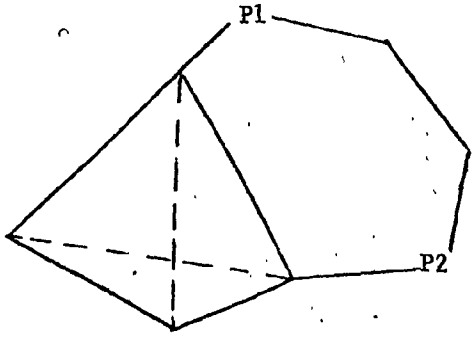

(b)

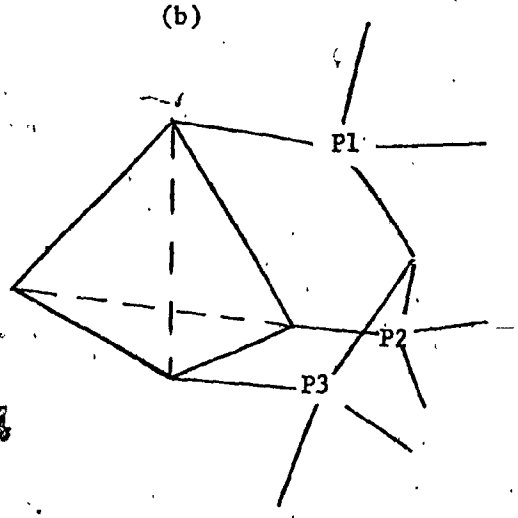

(c)

A comparison of these two factors was not possible since the ligands involved in the monodentate, bidentate and tridentate cases were sterically different.

Tripod Ligand

The phosphorus-carbon distances (see Table IV-D-2-6) of the tripod ligand found in $Fe(CO)_4$(tripod) [133], $Fe(CO)_3$(tripod) [134] and RUSH, Figure IV-D-2-8, were similar. The first complex contains a tripod ligand bound through only one phosphorus. The angles are within the ligand unconstrained. In the second case the tripod is bidentate and chelating the iron atom. The strain in the latter case is clearly shown by the relatively small Fe-P-Cp and P_1-Cp-P_3 angles in this complex (98.9°(av) and 89.2°, respectively). On this basis, the angles oberved in the third complex (RUSH) where the ligand is tridentate but not chelating, look relatively unstrained. The idea of using the ligand tripod to support triangular metal clusters is probably reasonable since the ligand is less strained in this situation than if it acts as a chelating group.

The tripod bonding to ruthenium tetrahedron in RUSH is interesting in the light of the recent efforts made [115] towards heterogenising the homogeneous catalysts. The ruthenium

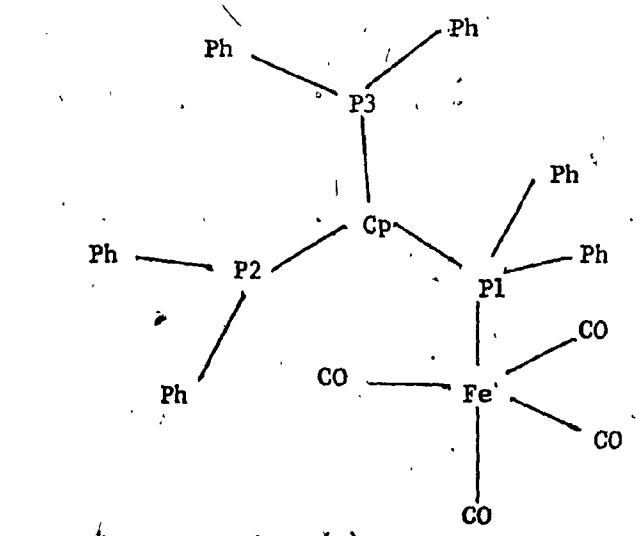

(a)

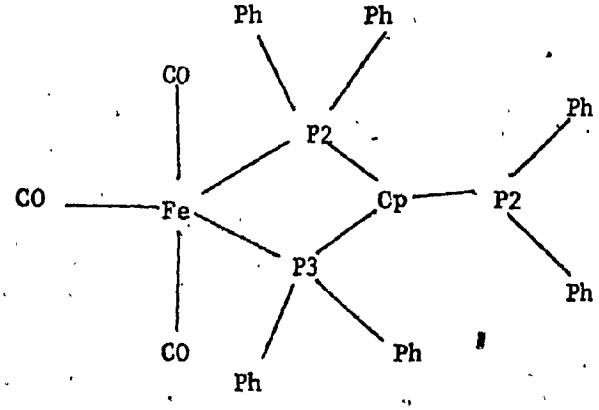

(b)

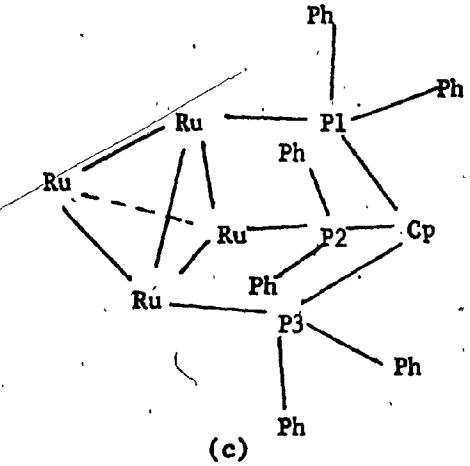

(c)

Figure IV-D-2-8. An illustration of bonding in a) Monodentate b) Bidentate c) Tridentate tripod ligand.

Table IV-D-2-6. Comparison of P-methane carbon lengths, metal-P-methane carbon, P-C-P and Ph-P-Ph angles in RUSH and some iron complexes containing tripod ligand.

	$Fe(CO)_4$(tripod) [a]	$Fe(CO)_3$(tripod) [b]	RUSH
A. P-methane carbon distances (Å).			
	P_1-Cp 1.86(1)	P_1-Cp 1.90(2)	P_1-Cp 1.92(1)
	P_2-Cp 1.91(1)	P_3^1-Cp 1.86(2)	P_1^2-Cp 1.91(2)
	P_3-Cp 1.90(1)	P_2-Cp 1.85(2)	P_3^2-Cp 1.92(1)
	Av. 1.89	Av. 1.87	Av. 1.92
B. Metal-P-methane carbon angles(deg).			
	Fe-P_1-Cp 114.1(4)	Fe-P_1-Cp 100.0(5)	Ru_1-P_1-Cp 108.7(4)
		Fe-P_2^1-Cp 97.7(5)	Ru_2-P_2^1-Cp 109.9(5)
			Ru_3-P_3^2-Cp 110.6(5)
	114.1	Av. 98.85	Av. 109.73
C. P-C-P angles(deg).			
	P_1-Cp-P_2 110.79(7)	P_1-Cp-P_3 89.2(7)	P_1-Cp-P_2 110.6(7)
	P_2^1-Cp-P_3^2 126.01(2)	P_1^1-Cp-P_3^2 116.2(8)	P_1^1-Cp-P_3^2 108.4(7)
	P_1^2-Cp-P_3 103.6 (9)	P_2^1-Cp-P_3 118.2(9)	P_2^1-Cp-P_3 102.6(6)
D. Ph-P-Ph angles(deg).			
	Ph-P_2-Ph 101.47(6)	Ph-P_1-Ph 106.4(5)	Ph-P_3-Ph 96.3(7)
	Ph-P_1^2-Ph 98.8 (6)	Ph-P_2^1-Ph 101.9(5)	Ph-P_3^1-Ph 98.3(7)
	Ph-P_3^1-Ph 104.7 (6)	Ph-P_3-Ph 102.4(6)	Ph-P_2^1-Ph 98.9(7)

a) Ref. [133]

b) Ref. [134]

tetrahedron will be in a position to participate in reactions with suitable substrates simulating a portion of the metal's surface of a heterogeneous catalyst, if the methane carbon of the tripod ligand in RUSH is bonded to a suitable polymer.

The variable temperature ^1H solution NMR spectra of RUSH is in contradiction with its solid state structure due to the appearence of four distinct peaks at very low temperature. According to the solid state structure the ^1H NMR should show only two peaks at very low temperature since there are only two sets of non-equivalent hydrogens. The molecule 26 has a mirror plane passing through H_{13},H_{34} and H_{12},H_{24} are equivalent with respect to this plane.

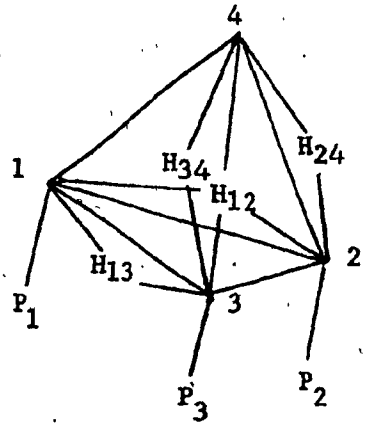

26

However, four peaks in ^1H solution NMR can be explained in terms of unsymmetrical bridging of hydrogens 27 in the solution state destroying the mirror plane in the solid state structure. The exchange between two base and edge bridged protons gives rise to two peaks at

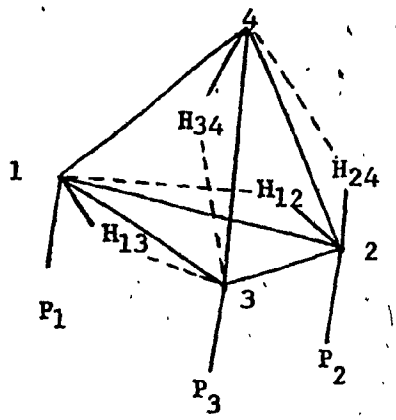

27

intermediate temperatures and finally, scrambling of all four protons at the room temperature will result only one peak for protons.

APPENDIX A.

Table A-1. The positional and thermal parameters for UNIQUE.

Table A-2. The positional and thermal parameters for FESCO.

Table A-3. The positional and thermal parameters for TICEP.

Table A-4. The positional and thermal parameters for RUSH.

Table A-1

PT1	0.12037	0.22096	0.38845	0.00930	0.00228	0.00613	-0.00086	0.00244	-0.00099
PT2	-0.03743	0.26765	0.11601	0.00832	0.00213	0.00633	-0.00025	0.00199	-0.00086
S1	0.07748	0.22885	0.56486	0.01571	0.00319	0.00753	-0.00099	0.00621	-0.00150
P1	0.23858	0.12695	0.45320	0.00879	0.00231	0.00657	-0.00064	0.00124	-0.00106
SB1	-0.00826	0.31516	0.29065	0.01052	0.00201	0.00734	-0.00078	0.00393	-0.00129
SB2	0.16506	0.22727	0.21158	0.00768	0.00262	0.00581	0.00008	0.00215	-0.00118
S2	-0.24594	0.30306	0.03605	0.00974	0.00296	0.01040	0.00104	0.00086	-0.00067
P2	-0.05580	0.22056	-0.04494	0.00851	0.00231	0.00581	-0.00004	0.00131	-0.00108
CB1	-0.15610	0.30655	0.33572	5.01500	—	—	—	—	—
CB2	0.27432	0.30151	0.22344	4.65084	—	—	—	—	—
CS1	0.15095	0.31355	0.59739	6.58913	—	—	—	—	—
CP1	0.29870	0.10510	0.60933	4.51303	—	—	—	—	—
CS2	-0.23522	0.39610	0.02620	6.71888	—	—	—	—	—
CP2	-0.06129	0.28487	-0.17281	4.82840	—	—	—	—	—
C11	0.29077	0.31666	0.59726	4.96426	—	—	—	—	—
C12	0.38106	0.28239	0.68758	7.13063	—	—	—	—	—
C13	0.50980	0.28727	0.68959	-7.36441	—	—	—	—	—
C14	0.54825	0.32644	0.60130	8.20462	—	—	—	—	—
C15	0.45796	0.36071	0.51098	6.82534	—	—	—	—	—
C16	0.32922	0.35583	0.50896	6.93698	—	—	—	—	—
C21	0.14904	0.05255	0.40280	-5.01112	—	—	—	—	—
C22	0.19195	-0.01238	0.44937	6.37730	—	—	—	—	—
C23	0.12366	-0.06833	0.40771	7.36341	—	—	—	—	—
C24	0.01247	-0.05935	0.31947	6.63447	—	—	—	—	—
C25	-0.03044	0.00559	0.27290	6.16648	—	—	—	—	—
C26	0.03785	0.06153	0.31456	6.16786	—	—	—	—	—
C31	0.38079	0.12975	0.40011	3.63029	—	—	—	—	—
C32	0.47445	0.17532	0.44633	6.26162	—	—	—	—	—
C33	0.58680	0.18230	0.41123	6.87494	—	—	—	—	—
C34	0.60549	0.14372	0.32990	7.52032	—	—	—	—	—
C35	0.51184	0.09815	0.28368	8.24134	—	—	—	—	—
C36	0.39949	0.09116	0.31878	5.27437	—	—	—	—	—

Table A-1 Con'd.

C41	0.30650	0.32478	0.11418	4.85876
C42	0.38848	0.28623	0.07763	6.31460
C43	0.42400	0.30866	-0.02259	5.52540
C44	0.37754	0.36964	-0.08626	6.57741
C45	0.29556	0.40819	-0.04971	7.88081
C46	0.26004	0.38576	0.05051	5.57637
C51	0.07281	0.16290	-0.04067	3.01157
C52	0.17138	0.18212	-0.09178	5.07328
C53	0.26865	0.13694	-0.08355	6.61536
C54	0.26735	0.07255	-0.02420	5.22596
C55	0.16878	0.05333	0.02691	4.86001
C56	0.07151	0.09851	0.01868	4.74861
C61	-0.19726	0.16639	0.91709	3.98667
C62	-0.26805	0.14733	0.99615	5.00042
C63	-0.37644	0.10701	0.96712	5.83955
C64	-0.41405	0.08575	0.85904	5.42689
C65	-0.34326	0.10482	0.77998	6.11703
C66	-0.23486	0.14514	0.80901	5.86582
C71	-0.20350	0.42778	0.92044	5.47306
C72	-0.07653	0.44188	0.92205	8.04205
C73	-0.04492	0.47083	0.82289	10.35302
C74	-0.14027	0.48569	0.72210	10.78575
C75	-0.26724	0.47160	0.72048	8.19227
C76	-0.29886	0.44264	0.81965	8.45545
C81	-0.22069	0.37396	0.33047	3.89589
C82	-0.16104	0.42406	0.39570	6.22924
C83	-0.22604	0.48307	0.39380	7.46519
C84	-0.35071	0.49198	0.32667	5.00667
C85	-0.41037	0.44187	0.26145	6.92904
C86	-0.34536	0.38286	0.26335	6.16114

Table A-2

ATOM	X	Y	Z	U11	U22	U33	U12	U13	U23
FE1	0.20587	0.20047	0.39145	0.03797	0.03578	0.04109	0.01056	-0.00726	-0.02385
FE2	0.69065	0.79987	0.41524	0.03788	0.03597	0.04590	0.01464	-0.01001	-0.02464
FE3	0.74898	0.42462	0.40262	0.04010	0.03484	0.04815	0.00917	-0.00269	-0.02615
FE4	0.89798	0.65096	0.32219	0.03326	0.03785	0.04432	0.01144	-0.00289	-0.02425
S1	0.35321	0.34618	0.28440	0.03858	0.03718	0.04573	0.01190	0.00081	-0.02131
S2	0.21159	0.31962	0.53286	0.03368	0.03130	0.03704	0.01103	-0.00346	-0.01948
S3	0.16613	0.58453	0.41848	0.04359	0.03682	0.04929	0.02041	-0.00604	-0.02043
O11	0.04830	0.93975	0.66707	0.06302	0.06243	0.08555	-0.00404	0.00652	-0.03971
O12	0.12517	0.37540	0.11381	0.08176	0.08036	0.05835	0.04569	-0.02772	-0.03167
O13	0.25075	0.01454	0.26859	0.08481	0.06368	0.09149	0.03192	-0.01804	-0.05707
O21	0.19864	0.94535	0.94047	0.10572	0.07150	0.07004	0.04230	0.00274	-0.01279
O22	0.38849	-0.00594	0.55575	0.07856	0.06435	0.09487	0.04567	-0.02476	-0.05005
O23	0.45304	0.35389	0.67981	0.06408	0.13010	0.15650	0.03298	-0.04721	-0.11228
O31	0.18680	0.72574	0.75432	0.09764	0.07378	0.11015	0.02206	0.00866	-0.06512
O32	0.29516	0.35181	0.90352	0.09128	0.08516	0.05600	0.03568	-0.01664	-0.03309
O33	0.43365	0.80473	0.43666	0.04741	0.08547	0.11321	-0.00594	0.00723	-0.06899
O41	0.04596	0.79700	0.42202	0.05540	0.07989	0.09247	0.02308	-0.03056	-0.05589
O42	-0.00559	0.45597	0.83309	0.07401	0.11619	0.10821	0.05344	-0.00638	-0.07657
O43	0.08929	0.09620	0.03539	0.08767	0.06440	0.04613	0.02059	-0.00669	-0.02383

Table A-2 Con'd.

ATOM	X	Y	Z	U11	U22	U33	U12	U13	U23
C1	0.25917	0.52449	0.40738	0.03365	0.04092	0.03926	0.02022	-0.01085	-0.02316
C2	0.32922	0.61500	0.23811	0.04433	0.03535	0.03666	0.01305	-0.00742	-0.01502
C3	0.37356	0.54806	0.17857	0.03799	0.04073	0.05372	0.01515	-0.00617	-0.02847
C4	0.44006	0.64067	0.01406	0.05541	0.05548	0.03961	0.01944	0.00640	-0.01537
C5	0.46144	0.79763	0.91657	0.06803	0.04422	0.04983	0.01123	0.00864	-0.01678
C6	0.41699	0.86806	0.97198	0.06899	0.04440	0.05125	0.01397	-0.00949	-0.02206
C7	0.35168	0.77624	0.13237	0.05146	0.02565	0.05175	0.00639	-0.01048	-0.01657
C11	0.10939	0.04372	0.55726	0.04279	0.05218	0.05755	0.02052	-0.01418	-0.03521
C12	0.15505	0.30702	0.22145	0.05567	0.04786	0.04448	0.02037	-0.01272	-0.02823
C13	0.23217	0.08631	0.31644	0.04516	0.03559	0.05252	0.00792	-0.00383	-0.02404
C21	0.24220	0.04726	0.80121	0.07016	0.04794	0.06102	0.02875	-0.01627	-0.02763
C22	0.35843	0.07211	0.56832	0.04642	0.04238	0.06672	0.00572	-0.00879	-0.03171
C23	0.39667	0.29875	0.64323	0.03879	0.07036	0.08583	0.02612	-0.01755	-0.04992
C31	0.21105	0.66479	0.69685	0.04545	0.05826	0.06686	0.01156	-0.00487	-0.04263
C32	0.27745	0.43843	0.77814	0.05179	0.05951	0.05419	0.00981	-0.00314	-0.04095
C33	0.36049	0.71888	0.49672	0.05121	0.04347	0.06890	0.00875	-0.00264	-0.03720
C41	0.01094	0.25832	0.61679	0.03323	0.05033	0.06812	0.00928	-0.00192	-0.03504
C42	0.03586	0.41593	0.77379	0.03753	0.05312	0.06802	0.01163	-0.00648	-0.03601
C43	0.09348	0.19589	0.89358	0.04289	0.05107	0.06388	0.00686	-0.00032	-0.04030

Table A-3

ATOM	X	Y	Z	U11	U22	U33	U12	U13	U23
TI1	0.34284	0.12944	0.05743	0.02915	0.06798	0.06279	-0.00222	0.03671	-0.00232
S2	0.11055	0.16451	0.14349	0.07205	0.11909	0.10986	0.02071	0.07486	0.02472
S1	0.37426	0.15368	0.33270	0.09174	0.10393	0.07433	-0.00007	0.05967	-0.01584
S3	0.03318	0.38419	0.46082	0.03614	0.11854	0.12089	-0.00093	0.05472	-0.01999
C11	0.55860	0.07597	0.29802	0.10266	0.10142	0.15356	-0.03578	0.13926	-0.03226
C12	0.38167	0.05895	0.19902	0.09265	0.02859	0.10270	0.02855	0.07471	0.00707
C13	0.30097	0.05114	0.00311	0.09168	0.03065	0.10563	0.01545	0.07979	-0.00236
C14	0.45018	0.06572	-0.01794	0.07502	0.04131	0.03168	0.00062	0.03229	-0.01100
C15	0.58027	0.07945	0.15449	0.03828	0.03401	0.07628	0.01745	0.01645	0.00492
C111	0.67591	0.41471	-0.01197	0.07477	0.16983	0.00483	0.00563	0.01866	0.01997
C122	0.28398	0.04452	0.30021	0.05777	0.11597	0.11362	0.01944	0.06544	0.07145
C133	0.13823	0.47190	0.35780	0.04683	0.07541	0.16492	0.05263	0.03525	0.04898
C144	0.44410	0.44769	0.31044	0.10023	0.07156	0.07520	0.00561	0.06471	0.02995
C155	0.79088	0.09005	0.21212	0.02850	0.09726	0.10596	-0.01623	0.04253	-0.00564
C21	0.24287	0.34035	0.25434	-0.02024	0.05812	0.08494	-0.01311	0.01948	-0.06205
C22	0.18769	0.30890	0.34420	0.07910	0.07728	0.09086	0.03979	0.07976	0.00082
C23	0.31841	0.21154	-0.00116	0.01793	0.08073	0.14064	0.02752	0.07064	0.06551
C24	0.48282	0.19295	0.03501	0.06955	0.03575	0.02367	-0.03886	0.01690	0.01888
C25	0.42641	0.33402	0.37829	0.15768	-0.00682	0.05343	-0.02894	0.09073	-0.03956
C211	0.14487	0.36135	0.09216	0.03679	0.08983	-0.00270	0.03105	-0.01528	0.03515
C222	0.99699	0.29344	0.24368	0.02503	0.14431	0.12047	-0.08561	0.05782	-0.10135
C233	0.32614	0.24795	0.11486	0.16763	0.00824	0.16802	-0.01607	0.14362	-0.06215
C244	0.68059	0.20744	0.19673	0.03189	0.06650	0.09085	-0.03382	0.02706	-0.02758
C255	0.58452	0.34680	0.33007	0.06225	0.12637	0.14216	-0.03337	0.09663	-0.04378
O1	0.45460	0.06628	0.12742						
O2	0.33283	0.18430	-0.09698						

Table A-4

ATOM	X	Y	Z	U11	U22	U33	U12	U13	U23
RU1	0.27891	0.22340	0.12152	0.03795	0.04718	0.03805	0.00282	-0.00281	0.00367
RU2	0.15608	0.11768	0.06134	0.04776	0.03322	0.04158	0.00383	0.00349	0.00237
RU3	0.11514	0.27727	0.10906	0.03900	0.03497	0.03871	0.00286	0.00097	-0.00049
RU4	0.16561	0.15593	0.21956	0.04836	0.05115	0.03923	0.00815	0.00389	0.00897
CL1	0.31348	0.37334	0.72835	0.29894	0.18018	0.12522	0.05062	0.05039	0.03932
CL2	0.22426	0.30208	0.61580	0.18260	0.11253	0.32570	-0.00987	0.02259	0.01961
P1	0.31521	0.28159	0.00613	0.03002	0.04777	0.03742	0.00230	0.00062	-0.00311
P2	0.20067	0.15521	0.94171	0.03972	0.03163	0.04587	0.00333	-0.00041	-0.00133
P3	0.13891	0.32105	0.98508	0.03466	0.03326	0.04456	-0.00178	-0.00127	-0.00396
O11	0.35227	0.34939	0.21908	0.09861	0.06165	0.08501	-0.00727	-0.02645	-0.00420
O12	0.41238	0.10534	0.14366	0.06603	0.08398	0.09215	0.02566	-0.01184	0.00822
O21	0.30359	0.43755	0.45270	0.13744	0.03770	0.15556	-0.01641	0.03024	-0.00402
O22	0.48562	0.41737	0.53964	0.05136	0.03245	0.09521	-0.00112	-0.01007	-0.01422
O31	0.44344	0.25032	0.61027	0.05393	0.07199	0.09625	0.00113	-0.00853	-0.01083
O32	0.09073	0.43581	0.19493	0.11307	0.04933	0.07713	0.01264	-0.01329	-0.02352
O41	0.23264	0.26032	0.34008	0.07562	0.10338	0.08773	-0.00513	-0.01416	-0.04182
O42	0.02848	0.08755	0.31448	0.09066	0.06872	0.06154	-0.02194	0.02436	0.00019
O43	0.27441	0.01567	0.24651	0.11150	0.08549	0.13195	0.04464	0.01714	0.03291
CP	0.23036	0.26815	0.94042	0.03027	0.01755	0.04450	-0.00410	0.01451	-0.00299
C1	0.29120	0.38130	0.63589	0.15690	0.06841	0.08392	0.00474	-0.00623	0.01633
C11	0.32331	0.29771	0.18081	0.04824	—	—	—	—	—
C12	0.35972	0.15343	0.13695	0.05064	—	—	—	—	—
C21	0.18837	0.00635	0.05297	0.08185	—	—	—	—	—
C22	0.05376	0.09855	0.04659	0.04330	—	—	—	—	—
C31	0.01244	0.25901	0.10595	0.04542	—	—	—	—	—
C32	0.09490	0.37701	0.16167	0.05752	—	—	—	—	—
C41	0.20828	0.22021	0.29078	0.05592	—	—	—	—	—
C42	0.07986	0.11612	0.27715	0.05459	—	—	—	—	—
C43	0.23293	0.07402	0.23842	0.06484	—	—	—	—	—
C111	0.40352	0.24424	0.95355	0.04201	—	—	—	—	—
C112	0.46706	0.22596	-0.00426	0.04990	—	—	—	—	—
C113	0.03852	0.30327	0.45700	0.06627	—	—	—	—	—
C114	0.03882	0.31077	0.38187	0.07039	—	—	—	—	—

Table A-4 Con'd.

ATOM	X	Y	Z	U11	U22	U33	U12	U13	U23
C115	0.47798	0.20659	0.83710	0.06325					
C116	0.40711	0.23559	0.87483	0.05105					
C121	0.34079	0.39349	0.00722	0.04011					
C122	0.39671	0.42376	0.95366	0.05225					
C123	0.41630	0.50759	0.95851	0.06769					
C124	0.11971	0.05945	0.48911	0.06220					
C125	0.17572	0.02856	0.43756	0.05699					
C126	0.30380	0.44433	0.06294	0.04092					
C211	0.13765	0.14314	0.86343	0.03665					
C212	0.08795	0.07362	0.86772	0.04234					
C213	0.04080	0.05767	0.80654	0.05821					
C214	0.03924	0.10728	0.74453	0.07163					
C215	0.08811	0.17536	0.74001	0.05795					
C216	0.13824	0.19431	0.80045	0.04655					
C221	0.28737	0.09693	0.90380	0.04189					
C222	0.33833	0.05681	0.95202	0.05360					
C223	0.40244	0.01045	0.92137	0.06432					
C224	0.41451	0.00050	0.84404	0.06762					
C225	0.36512	0.03924	0.79768	0.06794					
C226	0.29814	0.08772	0.82483	0.05404					
C311	0.05745	0.31095	0.91951	0.03296					
C312	0.50016	0.25016	0.43147	0.04276					
C313	0.43729	0.25219	0.38725	0.04324					
C314	0.42961	0.19692	0.32868	0.05370					
C315	0.48568	0.13557	0.31714	0.05864					
C316	0.05152	0.36874	0.86104	0.04202					
C321	0.15745	0.43199	0.96823	0.04754					
C322	0.21256	0.45659	0.90951	0.04799					
C323	0.27959	0.04312	0.60595	0.05592					
C324	0.33005	0.09515	0.56485	0.06186					
C325	0.38383	0.07012	0.50855	0.06730					
C326	0.10789	0.48636	0.01011	0.04990					

BIBILOGRAPHY

1. D.E. Sands, "Introduction to Crystallography", Benjamin Inc., 1969.

2. G.H. Stout and L.H. Jenson, "X-ray Structure Determination", McMillan, N.Y., 1968.

3. L.V. Azaroff, "Elements of Crystallography", McGraw-Hill, 1968.

4. M.J. Buerger,"X-ray Crystallogrphy", Wiley, N.Y., 1942.

5. M.J. Buerger, "The Precession Method in X-ray Crystallography", Wiley, N.Y., 1964.

6. M.J. Buerger, "Crystal Structure Analysis", Wiley, N.Y., 1960.

7. "The Optical Principles of the Diffraction of X-rays", Cornell University Press, Ithaca, N.Y., 1965, pp. 34-52.

8. G.H. Stout and L.H. Jenson, "X-ray Structure Determination", McMillan, N.Y., 1968, pp. 177-179.

9. E. Gabe,"The Data Collection Pakage", Crystallogrphic Division, National Research Council of Canada.

10. M.J. Buerger, "Crystal Structure Analysis", Wiley, N.Y., 1960, pp. 204-231.

11. J.W. Jeffery and K.M. Rose, Acta. Cryst., 10, 180 (1957).

12. W.R. Busing and H.A. Levy, Acta. Cryst., 10, 180 (1957); J. De Menlenaer and H. Tompa, Acta. Cryst., 19, 1014 (1965); P. Coppens, J. De Menlenaer and H. Tompa, Acta. Cryst., 22, 601 (1967); and references therein.

13. "The Optical Principles of X-ray Diffraction", Cornell University Press, Ithaca, N.Y.,1965, pp. 33-49.

14. M.J. Buerger, "Crystal Structure Analysis", Wiley, N.Y., 1960, pp. 231-237.

15. "The Optical Principles of the X-ray Diffraction", Cornell university Press, N.Y., 1965, pp. 193-267.

16. A.J.C. Wilson, Nature, 150, 151 (1942).

17. H. Lipson and W. Cochran, "The Determination of Crystal Structures", G. Bell, London, 1957, pp. 38-46.

18. M.J. Buerger, "Crystal Structure Analysis", Wiley, N.Y., 1960, pp. 259-282.

19. J.S. Rollett, Ed., "Computing Methods in Crystallography", Pregmon Press, Oxford, 1965, pp. 38-46.

20. H. Lipson and W. Cochran, "The Determination of Crystal structures" G. Bell, London, 1957, pp. 76-109.

21. G.H. Stout and L.H. Jenson, "X-ray Structure Determination", McMillan, N.Y., 1968, pp.267-269.

22. A.L. Patterson, Z. Krist., A90, 517 (1935).

23. H. Lipson and W. Cochran, "The Determination of Crystal structures", G. Bell, London, 1957, pp. 12-15.

24. M.J. Buerger, "Vector Space", Wiley, N.Y., 1954, pp. 41-64.

25. J Karle and I.L. Karle, Acta. Cryst., 21, 849 (1966).

26. J. Karle, "Advances in Structure Research by Diffraction Methods", R. Brill and B. Mason, Ed., Wiley-Interscience, N.Y., 1964, pp. 55-89.

27. D. Sayer, Acta. Cryst., 5, 60 (1952).

28. P. Main, M. Woolfson and G. Germain, Acta. Cryst., (1971).

29 E.T. Whittaker and H. Robinson, "The calculation of Observation" 4th ed., Blackie and Son., Glasgow, 1944, pp. 209-259..

30. E.W. Hughes, J. Am. Chem. Soc., 63, 1737 (1941).

31. W.C. Hamilton, "Statistics in Physical Science", Ronald Press, N.Y., 1964, pp. 124-577.

32. W.E. Deming, "Statistical Adjustment of Data", Wiley, N.Y., 1943, pp. 14-58.

33. "PREP" was written by P.H. Bird.

34. "GNABS" was a modified version of original program written by C.W. Burnam.(Am. Minerals, 51, 159 (1966).

35. "FORDAP" was written by A. Zalkin.

36. "SFLS" was written by C.T. Prewitt.

37. "RIGID" was written by P.H. Bird.

38. "NUCLS" was written by R.D. Dodens and J. Ibers.

39. "MULTAN" was written by P. Main, M. Woolfson and G. Germain.

40. "ORTEP" was written by C.R. Jhonson.

41. P.J. Vergamini and G.J. Kubas, Prog. Inorg. Chem., 21, 261 (1976).

42. J. Andrews, D. Coucouvanis and J.P. Feckler Jr., Inorg. Chem., 11, 493 (1972).

43. J.M. Coleman and L.F. Dhal, J. Am. Chem. Soc., 89, 543 (1967)

44. G. Ferguson, G. Hannaway and K.M.S. Islam, Chem. Comm., 1165 (1968).

45. D. Coucouvanis, S.J. Lippard and J.A. Zubieta, J. Am. Chem. Soc., 91, 761 (1969).

46. N.G. Connelly and L.F. Dhal, J Am. Chem. Soc., 92, 7470 (1970).

47. D.F. Lewis, S.J. Lippard and J.A Zubeita, J. Am. Chem. Soc., 94, 1563 (1972).

48. R.A. Winograd, D.F. Lewis and S.J. Lippard, Inorg. Chem., 14, 2601 (1975).

49. H. Vehrenkamp, Angew. Chem. Internat. Edit., 14, 322 (1975).

50. [illegible]. Mayer, Prog. Inorg. Chem., 19, 1 (1975).

51. H.N. Rabinowitzk, D. Karlin and S.J. Lippard, J. Am. Chem. Soc., 99, 1420 (1977).

52. W.E. Newton, J.W McDonald, K. Yamanouchi and J.H. Enemark, Inorg. Chem., 18, 1621 (1979).

53. J.C.T.R.B. Laurent, M.R. Caira, R.B. English, R.J. Haines and L.R. Nassinbeni, J. Chem. Soc. Dalt., 1077 (1977).

54. C. Mealli, S. Midollini and L. Sacconi, Inorg. Chem., 17, 632 (1978).

55. M. DiVaira, S. Midollini and L. Sacconi, Inorg. Chem., 16, 1518 (1977).

56. J. Chatt and F.A. Hart, Nature, 673, 2363 (1952).

57. J. Chatt and F.A.Hart, J. Chem. Soc., 2363 (1953).

58. M.P. Brown, R.J. Puddephatt and E.E. Upton, J. Chem. Soc. Dalt., 2490 (1976).

59. G.R. Clark, D. Hall and K. Marsden, J. Orgmetal. Chem., (1979).

60. J.J. Bonnet, P. Kalck and R. Poilblanc, Inorg. Chem., 16, 1514 (1977).

61. N.R. Kunchur, Acta. Cryst., B24, 1623 (1968).

62. R.O. Gould and M.M. Harding, J. Chem. Soc. (A), 2730 (1970).

63. P. Woodward, L.F. Dhal, E.C. Crosse and W. Abel, J. Am. Chem. Soc., 87, 5251 (1965).

64. J.J. Bonnet, Y. Jeannin, P. Kalck, A. Maisonnat and R. Poilblanc, Inorg. Chem., 14, 743 (1975).

65. E.L. Muetterties and L.J. Guggenberger, J. Am. Chem. Soc., 94, 8046 (1972).

66. T.G. Appleton, H.C. Clark and L.E. Manzer, Coor. Chem. Rev., 10, 335 (1973).

67. I.D. Brown, M.C. Brown and F.C. Hawthrone, BIDICS, 1977.

68. J. Chatt and F.A. Hart, J. Chem. Soc., 2807(1960).

69. S.F. Watkins, J. Chem. Soc. (A), 168 (1970).

70. M. Black, R.H.B. Mais and P.G. Owston, Acta. Cryst., B25, 1760 (1969).

71. J.A.J. Jarvis, B.T. Kilbourn, P.G. Owston and V.A. Raeburn, J. Chem. Soc. (A), 2770 (1970).

72. M.C. Hall, J.A.J. Jarvis, B.T. Kilbourn and P.G. Owston, J. Chem. Soc., 1544 (1972).

73. R. Lai and A. Shaver, McGill University, Montreal, Unpublished results.

74. ACS Advances in Chemistry Series 100, Bioorganic Chemistry.

75. S.J. Lippard, Acct. Chem. Res., 6, 282 (1973).

76. D. Coucouvanis, Prog. Inorg. Chem., 11, 233 (1970).

77. R.P. Burns, F.P. McCullough and C.A. McAuliffe, Adv. Inorg. Radiochem., 23, 211 (1980).

78. D. Coucouvanis and S.J. Lippard, J. Am. Chem. Soc., 90, 3281 (1968).

79. D. Coucouvanis and S.J. Lippard, J. Am. Chem. Soc., 91, 307 (1969).

80. J.M. Lisy, F.D. Dobrzynski, R.J. Angelici and J. Clardy, J. Am. Chem. Soc., 97, 656 (1975).

81. U. Oelimichen, T.G. Southern, H.Le Bozec and P. Dixneuf, J. Organometal. Chem., 156, C29 (1978).

82. G. Le Borgne, D. Grandjeau, R. Mathieu and R. Poilblanc, J. Organometal. Chem., 131, 429 (1977).

83. A. Shaver, P.J. Fitzpatrick, K. Stelion and I.S. Butler, J. Organometal. Chem., 172, C59 (1979).

84. J.A. De Beer and R.J. Haines, Chem. Comm., 288 (1970).

85. P.S. Battermann and R.J. Cross, Chem. Soc. Rev., 2, 271 (1973).

86. H. Patin, G. Magnani, C. Mane, J.Y. Le Maronille, T.G. Southern, A. Benoit and D. Grandjean, J. Organometal. Chem., 197, 315 (1980).

87. O. Lopez and A. Shaver, McGill University, Montreal, Unpublished results.

88. R. Eisenberg, Prog. Inorg. Chem., 12, 295 (1970).

89. M.J. Bonnett Jr., F.A. Cotton, A. Davidson, J.W. Faller, S.J. Lippard and S.M. Morenonse, J. Am. Chem. Soc., 88, 4371 (1966).

90. M. Schmidt, Angew. Chem. Internat. Edit., 12, 445 (1973).

91. M. Schmidt, NATO Conference Series, (1980).

92. R. Steudel and H.J. Mausle, Angew. Chem. Internat. Edit., 17, 57 (1978).

93. H.D. Block and R. Allmann, Cryst. Struc. Comm., 4, 53 (1975).

94. B.R. Davis, I. Bernal and H. Kopf, Angew. Chem. Internat. Edit., 10, 92 (1971).

95. P.E. Jones and L. Katz, Chem. Comm., 842 (1976).

96. J. Chatt and D.M.P. Mingos, J. Chem. Soc. (A), 1243 (1976).

97. E.G. Muller, J.L. Patterson and L.F. Dhal, J. Organometal. Chem., 111, 91 (1976).

98. H. Waner, Z. Anorg. Allg. Chem., 30, 464 (1980).

99. J.M. McCall and A. Shaver, McGill University, Montreal, Unpublished results.

100. J.W. Lauher and R. Hoffmann, J. Am. Chem. Soc., 98, 1731 (1976).

101. M.F. Rettig, "NMR of Paramagnetic Molecules, Principles and Applications", G.N. Lamar, W. De W. Horrocks Jr. and R.H. Holm, Ed., Academic Press, N.Y., 1973, pp. 217-242.

102. R. Hoffman, J. Chem. Phys., 39, 1397 (1963).

103. T.C. McKenzie, R.D. Sanner and J.E. Bercaw, J. Organometal. Chem., 102, 457 (1975).

104. E.L. Muetterties, Science, 196, 839 (1977).

105. R.M. Laine, R.G. Rinker and P.C. Ford, J. Am. Chem. Soc., 99, 252 (1977).

106. Z.M. Mithalska and D.E. Webster, Chem. Tech., 115, (1975).

107. T.L. Dabois, W.H. Mayers and D.W. Meek, J. Chem. Soc. Dalt., 1011, (1975).

108. R.B. King and J.C. Cloyed, J. Am. Chem. Soc., 97, 53 (1975).

109. R.B. King and P.N. Kapoor, J. Am. Chem. Soc., 93, 4158 (1971).

110. A.A. Arduini, A.A. Bahsoun, J.A. Osborn, C. Voelker, Angew. Chem., Int. Engl., 20, 0000, (1980).

111. C.A. McAuliffe and W. Levason, "Studies in Inorganic Chemistry 1", Elsevier, 1979, pp. 418-423.

112. S.J. LaPlace, W.C. Hamilton and J.A. Ibers, Inorg. Chem., 3, 1435 (1964).

113. M.R. Churchill, Adv. Chem. Ser., 167, 36 (1978).

114. J.A. Ibers, Adv. Chem. Ser., 167, 26 (1978).

115. R. Bau, W.E. Carrol, D.W. Hart, R.G. Teller and T.F. Kaetzle, Adv. Chem. Ser., 167, 73 (1978).

116. M.R. Churchill and R.A. Lashewyez, Inorg. Chem., 17, 1950 (1978).

117. R.D. Wilson, S.M. Wu, R.A. Love and R. Bau, Inorg. Chem., 17, 1271 (1978).

118. M.R. Churchill, P.H. Bird, H.D. Kaesz, R. Bau and B. Fontal, J. Am. Chem. Soc., 90, 7135 (1968).

119. M.R. Churchill and J. Wormald, J. Am. Chem. Soc., 93, 5670 (1971).

120. J.R. Shapley, S.I. Richter, M.R. Churchill and R.A. Lashewyez, J. Am. Chem. Soc., 99, 7384 (1977).

121. H.D. Kaesz and R.B. Saillant, Chem. Rev., 72, 231 (1972).

122. R. Bau, S.W. Kirtly and T.F. Koetzle, Acc. Chem. Res., 176, (1979).

123. M. Catti, G. Gervasio and S.A. Mason, J. Chem. Soc. Dalt., 2260 (1977).

124. R.W. Broach and J.M. Williams, Inorg. Chem. 18, 314 (1979).

125. R.G. Teller, R.D. Wilson, R.K. McMillan, T.F. Koetzel and R. Bau, J. Am. Chem. Soc., 100, 3071 (1978).

126. D.W. Hart, R.G. Teller, C.Y. Wei, R. Bau, G. Longoni, S. Campanella, P. Chini and T.F. Koetzel, Angew. Chem. Int. Ed. Engl., 18, 80 (1979).

127. R.W. Broach, L.F. Dhal, G. Longoni, P. Chini, A.J.Schultz and T.M. Williams, Adv. Chem. Ser., 167, 93 (1978).

128. M.R. Churchill, R.A. Lashewyez, J.R. Shapley and S.I. Richter, Inorg. Chem., 19, 1277 (1980).

129. R. Saillant, G. Barcelo and H.D. Kaesz, J. Am. Chem. Soc., 92, 5739 (1970).

130. R.D. Wilson and R. Bau, J. Am. Chem. Soc., 98, 4687 (1976).

131. P.F. Jackson, B.F.G. Johnson and J. Lewis, Chem. Comm., 920 (1978).

132. J.A. Osborn and A.A. Arduini, Institut Le Bel, Université Louis Pasteur, 4, rue Blaise Pascal, 67000 Strasbourg, France.

133. W.A. Wickramasinghe and P.H. Bird, Unpublished results.

134. D. Nucciarone and P.H. Bird, Unpublished results.